

# The CARMENES search for exoplanets around M dwarfs

## Stellar atmospheric parameters of target stars with STEPARSYN

E. Marfil<sup>1,2</sup>, H. M. Tabernero<sup>3,4</sup>, D. Montes<sup>1</sup>, J. A. Caballero<sup>2</sup>, F. J. Lázaro<sup>1</sup>, J. I. González Hernández<sup>5,6</sup>, E. Nagel<sup>7,8</sup>, V. M. Passegger<sup>7,9</sup>, A. Schweitzer<sup>7</sup>, I. Ribas<sup>10,11</sup>, A. Reiners<sup>12</sup>, A. Quirrenbach<sup>13</sup>, P. J. Amado<sup>14</sup>, C. Cifuentes<sup>2</sup>, M. Cortés-Contreras<sup>2</sup>, S. Dreizler<sup>12</sup>, C. Duque-Arribas<sup>1</sup>, D. Galadí-Enríquez<sup>15</sup>, Th. Henning<sup>16</sup>, S. V. Jeffers<sup>17,12</sup>, A. Kaminski<sup>13</sup>, M. Kürster<sup>16</sup>, M. Lafarga<sup>10,11,18</sup>, Á. López-Gallifa<sup>1</sup>, J. C. Morales<sup>10,11</sup>, Y. Shan<sup>12</sup>, and M. Zechmeister<sup>12</sup>

<sup>1</sup> Departamento de Física de la Tierra y Astrofísica & IPARCOS-UCM (Instituto de Física de Partículas y del Cosmos de la UCM), Facultad de Ciencias Físicas, Universidad Complutense de Madrid, 28040 Madrid, Spain  
e-mail: emigom01@ucm.es

<sup>2</sup> Centro de Astrobiología (CSIC-INTA), ESAC, Camino Bajo del Castillo s/n, 28691 Villanueva de la Cañada, Madrid, Spain

<sup>3</sup> Centro de Astrobiología (CSIC-INTA), Carretera a Ajalvir km 4, 28850 Torrejón de Ardoz, Madrid, Spain

<sup>4</sup> Instituto de Astrofísica e Ciências do Espaço, Universidade do Porto, CAUP, Rua das Estrelas, 4150-762 Porto, Portugal

<sup>5</sup> Instituto de Astrofísica de Canarias, c/ Vía Láctea s/n, 38205 La Laguna, Tenerife, Spain

<sup>6</sup> Universidad de La Laguna, Departamento de Astrofísica, 38206 La Laguna, Tenerife, Spain

<sup>7</sup> Hamburger Sternwarte, Gojenbergsweg 112, 21029 Hamburg, Germany

<sup>8</sup> Thüringer Landessternwarte Tautenburg, Sternwarte 5, 07778 Tautenburg, Germany

<sup>9</sup> Homer L. Dodge Department of Physics and Astronomy, University of Oklahoma, 440 West Brooks Street, Norman, OK-73019 Oklahoma, United States of America

<sup>10</sup> Institut de Ciències de l'Espai (CSIC), Campus UAB, c/ de Can Magrans s/n, 08193 Cerdanyola del Vallès, Spain

<sup>11</sup> Institut d'Estudis Espacials de Catalunya (IEEC), c/ Gran Capità 2-4, 08034 Barcelona, Spain

<sup>12</sup> Institut für Astrophysik, Georg-August-Universität-Göttingen, Friedrich-Hund-Platz 1, 37077 Göttingen, Germany

<sup>13</sup> Landessternwarte, Zentrum für Astronomie der Universität Heidelberg, Königstuhl 12, 69117 Heidelberg, Germany

<sup>14</sup> Instituto de Astrofísica de Andalucía (IAA-CSIC), Glorieta de la Astronomía s/n, 18008 Granada, Spain

<sup>15</sup> Observatorio de Calar Alto, Sierra de los Filabres, 04550 Gérgal, Almería, Spain

<sup>16</sup> Max-Planck-Institut für Astronomie, Königstuhl 17, 69117 Heidelberg, Germany

<sup>17</sup> Max-Planck-Institut für Sonnensystemforschung, Justus-von-Liebig-Weg 3, 37077 Göttingen, Germany

<sup>18</sup> Department of Physics, University of Warwick, Gibbet Hill Road, Coventry CV4 7AL, United Kingdom

Received 06 August 2021 / Accepted 7 October 2021

## ABSTRACT

We determined effective temperatures, surface gravities, and metallicities for a sample of 343 M dwarfs observed with CARMENES, the double-channel, high-resolution spectrograph installed at the 3.5 m telescope at Calar Alto Observatory. We employed STEPARSYN, a Bayesian spectral synthesis implementation particularly designed to infer the stellar atmospheric parameters of late-type stars following a Markov chain Monte Carlo approach. We made use of the BT-Settl model atmospheres and the radiative transfer code `turbospectrum` to compute a grid of synthetic spectra around 75 magnetically insensitive Fe I and Ti I lines plus the TiO  $\gamma$  and  $\epsilon$  bands. To avoid any potential degeneracy in the parameter space, we imposed Bayesian priors on  $T_{\text{eff}}$  and  $\log g$  based on the comprehensive, multi-band photometric data available for the sample. We find that this methodology is suitable down to M7.0 V, where refractory metals such as Ti are expected to condense in the stellar photospheres. The derived  $T_{\text{eff}}$ ,  $\log g$ , and [Fe/H] range from 3000 to 4200 K, 4.5 to 5.3 dex, and -0.7 to 0.2 dex, respectively. Although our  $T_{\text{eff}}$  scale is in good agreement with the literature, we report large discrepancies in the [Fe/H] scales, which might arise from the different methodologies and sets of lines considered. However, our [Fe/H] is in agreement with the metallicity distribution of FGK-type stars in the solar neighbourhood and correlates well with the kinematic membership of the targets in the Galactic populations. Lastly, excellent agreement in  $T_{\text{eff}}$  is found for M dwarfs with interferometric angular diameter measurements, as well as in the [Fe/H] between the components in the wide physical FGK+M and M+M systems included in our sample.

**Key words.** techniques: spectroscopic – stars: fundamental parameters – stars: late-type – stars: low-mass

## 1. Introduction

M dwarfs are cool and faint stars that comprise about two-thirds of the stellar population in the solar neighbourhood (Henry et al. 2018; Reylé et al. 2021). With main-sequence lifespans longer than the age of the Universe (Laughlin et al. 1997), these stars are not only an excellent record of the structure and evolution of

the Milky Way (Bochanski et al. 2007), but have also become prime targets for exoplanet surveys owing to their low mass, low temperature, and ubiquity (Bonfils et al. 2013; Dressing & Charbonneau 2013; Reiners et al. 2018); this combination favours detections of Earth-mass planets inside their habitable zone, where liquid water can be sustained (Scalo et al. 2007).

Installed at the 3.5 m telescope at the Calar Alto Observatory, the CARMENES instrument (Quirrenbach et al. 2020) is, along with SPIRou (Donati et al. 2020), NIRPS (Wildi et al. 2017), HPF (Mahadevan et al. 2012), IRD (Kotani et al. 2018), MAROON-X (Seifahrt et al. 2020), NEID (Schwab et al. 2016), and GIARPS (Claudi et al. 2018), a new-generation spectrograph designed to detect Earth-mass planets around M dwarfs by means of the radial velocity technique (Reiners et al. 2018). It consists of optical (hereafter VIS) and near-infrared (NIR) channels that cover the 5200–9600 Å and 9600–17100 Å wavelength regions with spectral resolutions of  $R = 94\,600$  and  $R = 80\,400$ , respectively. As of mid-2020, the CARMENES exoplanet survey had collected more than 18 500 VIS and 18 000 NIR spectra for a sample of 365 M dwarfs (Quirrenbach et al. 2020) obtained as part of its 750-night guaranteed time observations (GTO) programme. In addition to detecting and characterising the orbits of exoplanets (e.g. Trifonov et al. 2018, 2020; Luque et al. 2019; Zechmeister et al. 2019) and their atmospheres (Nortmann et al. 2018; Alonso-Floriano et al. 2019; Yan et al. 2019), the survey represents a unique opportunity to gain insights into the nature of M dwarfs (namely, their photospheric parameters, chemical compositions, magnetic fields, and chromospheric activity levels) in a statistically relevant way (Fuhrmeister et al. 2018, 2020; Passegger et al. 2018, 2019; Hintz et al. 2019, 2020; Schöfer et al. 2019; Schweitzer et al. 2019; Shulyak et al. 2019; Abia et al. 2020; Shan et al. 2021).

In the context of exoplanet research, a thorough account of the general properties of host stars directly affects the determination of the position of the habitable zone (Selsis et al. 2007; Kopparapu et al. 2013), the radius and mass of detected exoplanets, and their composition (Maldonado et al. 2020; Ishikawa et al. 2020). In addition, planet formation theories attempt to explain the observed occurrence rate of exoplanets (Johnson et al. 2010; Howard et al. 2012; Buchhave et al. 2012; Sabotta et al. 2021) and selection effects (Winn & Fabrycky 2015) in terms of the stellar parameters.

However, the computation of photospheric parameters for M dwarfs from stellar spectra, namely the effective temperature,  $T_{\text{eff}}$ , surface gravity,  $\log g$ , and stellar metallicity, [Fe/H], is an arduous challenge. The low photospheric temperatures give rise to pervasive molecular bands that severely distort the stellar continuum (Kirkpatrick et al. 1991; Tinney & Reid 1998; Reiners et al. 2018). This alone rules out classical techniques commonly adopted in the analysis of solar-type spectra, such as the equivalent width (EW) method (Marfil et al. 2020). Stellar convection in M dwarfs also calls into question some of the physical assumptions behind the model atmospheres of late-type stars, such as local thermodynamic equilibrium (LTE) and one-dimensional (1D) geometry for radiative transfer, which often represents a limitation to the interpretation at the resolution achieved by modern spectrographs (Bergemann et al. 2017; Olander et al. 2021). Furthermore, M dwarfs may exhibit strong magnetic fields that not only drive stellar activity (Delfosse et al. 1998; Donati et al. 2008), but may also distort magnetically sensitive lines via the Zeeman effect (Landi Degl'Innocenti & Landolfi 2004; Passegger et al. 2019). It is, therefore, difficult to choose a set of lines to disentangle the impact of the magnetic field and the photospheric parameters on the stellar spectra (Shulyak et al. 2019). To make matters worse, telluric absorption is ubiquitous in the NIR (Reiners et al. 2018; Nagel 2019), where the spectral energy distribution of M dwarfs peaks (Cifuentes et al. 2020).

Despite the above, several methods have proved fruitful for inferring  $T_{\text{eff}}$ ,  $\log g$ , and [Fe/H] in M dwarfs, including spectral synthesis (e.g. Passegger et al. 2018, 2019; Rajpurohit et al.

2018b; Souto et al. 2020; Hejazi et al. 2020), pseudo-EWs (e.g. Mann et al. 2013a, 2014; Neves et al. 2014; Maldonado et al. 2015, 2020), and spectral indices (e.g. Rojas-Ayala et al. 2012; Khata et al. 2020), all of which can be further investigated following a machine-learning approach (e.g. Sarro et al. 2018; Antoniadis-Karnavas et al. 2020; Passegger et al. 2020; Li et al. 2021). In general terms, spectral synthesis relies on a minimisation algorithm to find the synthetic spectrum that best matches the observed spectrum (Valenti & Fischer 2005; Brewer et al. 2016), while pseudo-EW and spectral index approaches draw on the sensitivity of certain features to  $T_{\text{eff}}$  and [Fe/H], as well as on calibrations with wide physical binaries harbouring an FGK-type primary with known metallicity (Casagrande et al. 2008; Neves et al. 2012; Montes et al. 2018, and references therein). Further studies have focused on ensuring consistency between these two approaches (Veyette et al. 2017).

Semi-empirically calibrated methods have been widely adopted in the literature. For example, based on observations in the photometric Y band (9470–11210 Å) with NIRSPEC on Keck II, Veyette et al. (2017) used a method to derive  $T_{\text{eff}}$ , [Fe/H], and [Ti/H] that rests on the approach described by Mann et al. (2013b) and a calibration sample of M dwarfs in common proper motion FGK+M binaries from Mann et al. (2013a). The method relies on the measured FeH index in the Wing-Ford band and on the EWs of seven Fe I and ten Ti I lines found in the Y band. More recently, Maldonado et al. (2020) derived  $T_{\text{eff}}$ ,  $\log g$ , and [Fe/H] for a sample of 204 stars with spectral types from K7 V to M4.0 V with HARPS and HARPS-N data, assuming the photometric  $M_K$ -[Fe/H] relationship from Neves et al. (2012) and the  $T_{\text{eff}}$  scale from Mann et al. (2013b).

M-dwarf studies based on spectral synthesis differ from one to another in terms of the synthetic grid employed, the spectral resolution of the data, and the features selected for comparison across different wavelength regions. For instance, Passegger et al. (2018) derived  $T_{\text{eff}}$ ,  $\log g$ , and [Fe/H] for 300 M dwarfs, 235 of which were observed with CARMENES. They adopted a  $\chi^2$  minimisation procedure based on the PHOENIX-ACES library of synthetic spectra (Husser et al. 2013) and several spectral features in the VIS wavelength region covered by CARMENES, namely the TiO γ band and several K I, Fe I, Ti I, and Mg I lines. To avoid unreliable values of  $\log g$  and [Fe/H] for some stars in the sample caused by degeneracies in the parameter space, they constrained  $\log g$  by using the evolutionary models of Baraffe et al. (1998). Passegger et al. (2019) expanded the analysis into the NIR wavelength region covered by CARMENES. For the first time, they directly compared the stellar parameters of 282 M dwarfs determined from simultaneous observations in the VIS and NIR wavelength regions. Despite some discrepancies, Passegger et al. (2019) conclude that it is best to consider both regions simultaneously to maximise the amount of spectral information and, thus, minimise the effects of imperfect modelling in M dwarfs. Furthermore, Passegger et al. (2019) lessened the impact of the Zeeman line broadening caused by the stellar magnetic field in the parameter computations in the NIR by selecting lines with low effective Landé factors. Adapting the method described by Rajpurohit et al. (2012, 2018b), Rajpurohit et al. (2018a) computed  $T_{\text{eff}}$ ,  $\log g$ , and [Fe/H] for 292 M dwarfs from the individual CARMENES spectra published by Reiners et al. (2018), using a grid of BT-Settl models (Allard et al. 2012), while keeping  $\log g$  free throughout the minimisation process. Hejazi et al. (2020) also employed BT-Settl models to derive the  $T_{\text{eff}}$ ,  $\log g$ , metallicity [M/H], and α element to iron abundance ratio, [α/Fe], of 1544 M dwarfs in the solar neighbourhood from low- and medium-resolution spectra collected

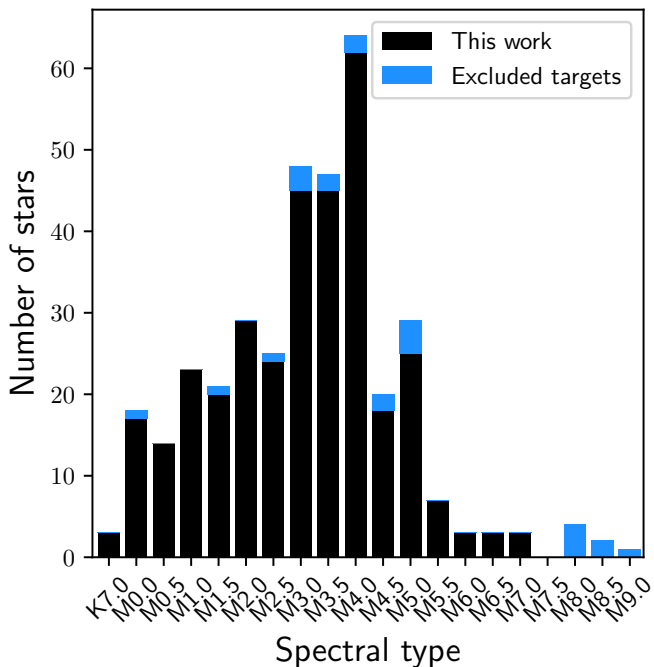


**Fig. 1.** Histogram of the M-dwarf sample analysed in this work (black) and the excluded CARMENES GTO targets (blue).

at the Michigan-Darmouth-MIT, Lick, Kitt Peak National, and Cerro-Tololo Inter-American observatories. Souto et al. (2020) computed  $T_{\text{eff}}$ ,  $\log g$ , and [Fe/H] for 21 M dwarfs from mid-resolution ( $R \approx 22\,500$ ) APOGEE  $H$ -band spectra (Wilson et al. 2010), a grid of MARCS models (Gustafsson et al. 2008), and the turbospectrum code (Plez 2012) through the bacchus wrapper (Masseron et al. 2016) and find excellent agreement in [Fe/H] between components in the wide physical binaries included in their sample. More recently, Sarmento et al. (2021) derived  $T_{\text{eff}}$ ,  $\log g$ , [M/H], and  $v_{\text{mic}}$  for a sample of 313 M dwarfs from APOGEE  $H$ -band spectra by means of a  $\chi^2$  minimisation against a synthetic grid generated with turbospectrum, ispec (Blanco-Cuaresma et al. 2014), and MARCS model atmospheres and find good agreement with the parameters obtained with the APOGEE Stellar Parameter and Chemical Abundances Pipeline (García Pérez et al. 2016).

In this work we derived the stellar atmospheric parameters ( $T_{\text{eff}}$ ,  $\log g$ , and [Fe/H]) for a sample of 343 M dwarfs observed with CARMENES (i.e. 5200–17100 Å at  $R \sim 90\,000$ ) by means of the STEPARSYN code (Tabernero et al. 2021), a Bayesian implementation of the spectral synthesis technique. This approach relied on the comparison of a synthetic grid against 75 magnetically insensitive Ti I and Fe I absorption lines along with the TiO  $\gamma$  and  $\epsilon$  bands. For the computation of the synthetic grid, we employed the turbospectrum code (Plez 2012) along with the BT-Settl model atmospheres (Allard et al. 2012). In contrast to other works that disregard stellar activity (Rajpurohit et al. 2018b; Sarmento et al. 2021), our methodology allowed us to expand the analysis to M dwarfs that are strongly active, fast-rotating, or late-type (down to M7.0 V), as a result of the careful selection of Ti I and Fe I lines according to their low sensitivity to chromospheric activity and the stellar magnetic field. In addition, the selected Ti I and Fe I lines are mostly free from non-LTE effects, which seem to affect lines of other elements widely used in other works (Passegger et al. 2018, 2019; Rajpurohit et al. 2018b), such as K I (Olander et al. 2021).

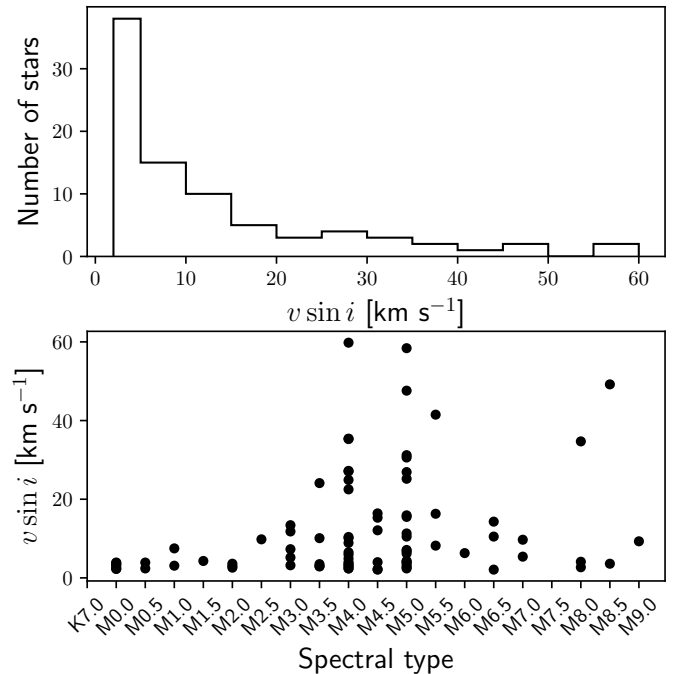


**Fig. 2.** Distribution of projected rotational velocities larger than 2 km s<sup>-1</sup> in the sample.

This study is structured as follows. In Sect. 2 we describe the CARMENES GTO sample. We explain the derivation of the stellar atmospheric parameters in Sect. 3. Finally, we discuss the results and highlight the main conclusions in Sects. 4 and 5, respectively.

## 2. Sample

Until mid-2020, the CARMENES M-dwarf radial velocity survey comprised 365 targets that cover the full M sequence from M0.0 V to M9.0 V (Quirrenbach et al. 2020). The sample also includes three K7 dwarfs. Spectra for all stars were collected as part of the GTO programme of the instrument consortium from January 2016 to March 2021, equivalent to more than 5 000 hours of observing time.

A histogram of the M-dwarf sample analysed in this work is shown in Fig. 1, while all targets excluded from further analysis are listed in Table 1. Among these targets are one eclipsing binary (CM Dra; Morales et al. 2009), ten double-line spectroscopic (SB2) binaries (Baroch et al. 2018, 2021), and two triple-line spectroscopic triple systems (Baroch et al. 2021), for which no reliable parameter determinations could be made. We also discarded three targets because of conspicuous artefacts over multiple orders of their CARMENES spectra. Lastly, after performing the spectral processing presented in Sect. 3.1, seven M dwarfs with spectral types M8.0 V or later were excluded due to limitations in our method. Altogether, our final sample includes 343 CARMENES GTO stars.

Table B.1 displays the CARMENES identifiers, common names, spectral types from the CARMENES Cool dwarf Information and daTa Archive (Carmencia; Alonso-Floriano et al. 2015; Caballero et al. 2016a), radial velocities ( $v_r$ ), projected rotational velocities ( $v \sin i$ ) adopted from Reiners et al. (2018) if available or computed following the same method otherwise, signal-to-noise ratios (S/N) over the entire spectra, and activity flags for the sample. Active stars are identified with an activity

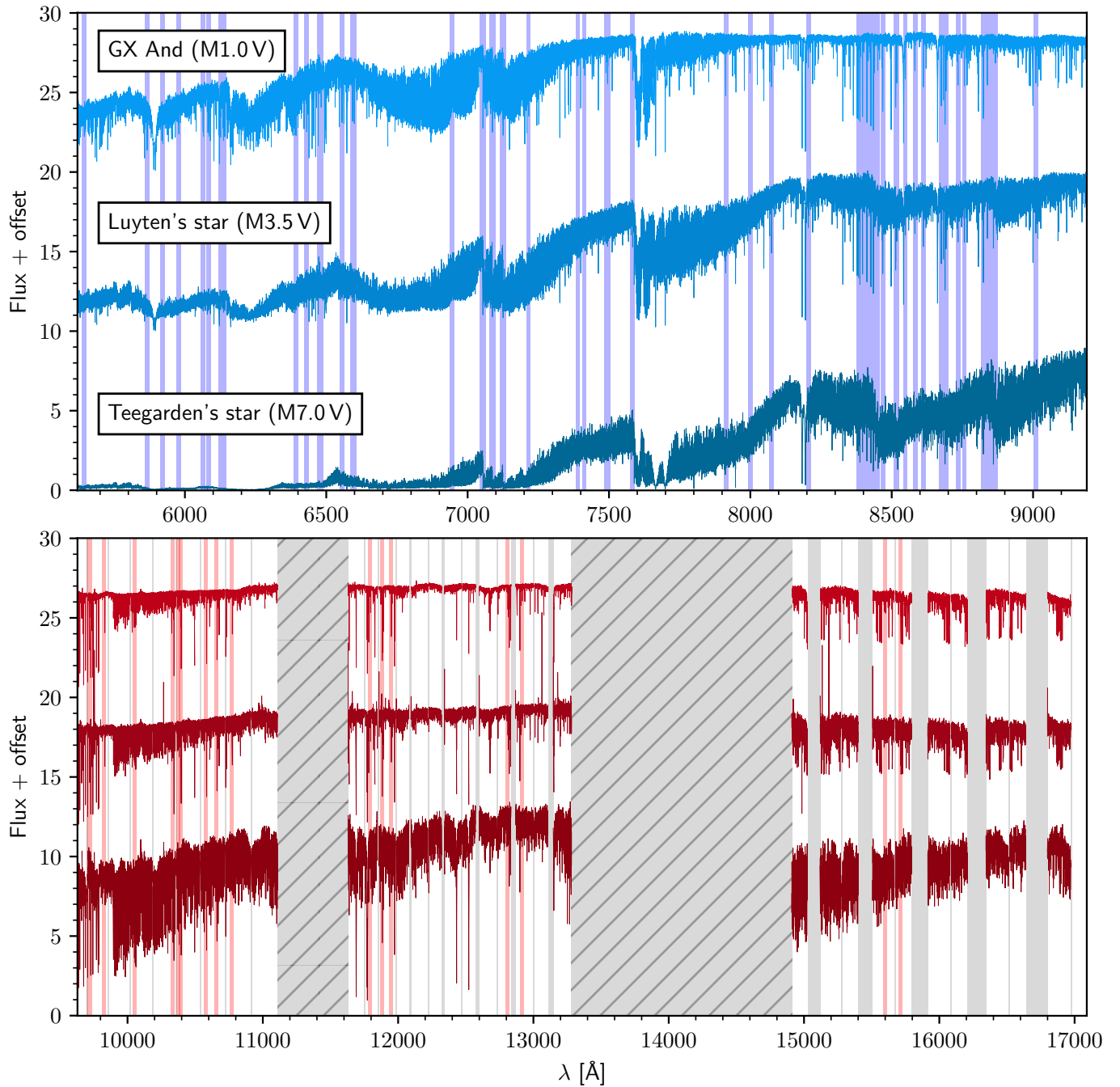


**Fig. 3.** CARMENES template spectra of GX And (M1.0 V, J00183+440), Luyten’s star (M3.5 V, J07274+052), and Teegarden’s star (M7.0 V, J02530+168) in the VIS channel (*top panel*) and the NIR channel (*bottom panel*). Blue and red shaded regions denote the ranges synthesised in this work. The two wide spectral gaps in the NIR channel shown as hatched rectangles correspond to regions severely affected by telluric absorption (Reiners et al. 2018). Inter- and intra-order gaps in the NIR channel are also shown, as grey shaded regions.

flag 1 if the pseudo-EW of the H $\alpha$  line satisfies  $p\text{EW}'(\text{H}\alpha) < -0.3 \text{ \AA}$ , following Schöfer et al. (2019). For most targets, radial velocities were adopted from Lafarga et al. (2020), who used cross-correlation with weighted binary masks. For targets that were not in Lafarga et al. (2020), we adopted the radial velocities provided by the CARMENES standard radial-velocity pipeline `serval`<sup>1</sup> (Zechmeister et al. 2018, 2020), based on least-squares fitting using high-S/N templates.

The distribution of  $v \sin i$  in the sample is shown in Fig. 2. Most targets in our sample (268 stars) do not exhibit significant rotation, that is,  $v \sin i < 2 \text{ km s}^{-1}$ , while targets with  $v \sin i$  values higher than this upper limit (74 stars) are typically mid-type M dwarfs (M4.0–5.0 V).

### 3. Analysis

In the following we describe the processing of the CARMENES observations, the selection of the spectral features to be compared with the synthetic spectra, the computation of the synthetic

<sup>1</sup> [www.github.com/mzechmeister/serval](https://github.com/mzechmeister/serval)

**Table 1.** GTO M dwarfs excluded from the analysis.

Karmn	Name	Reason
J00162+198W	EZ Psc AB	(1)
J01056+284	GJ 1029 AB	(1)
J02486+621	2MASS J02483695+6211228	(3)
J02573+765	G 245-61	(3)
J04198+425	LSR J0419+4233	(4)
J04219+213	K2-155	(3)
J05394+406	LSR J0539+4038	(4)
J05532+242	Ross 59 AB	(1)
J07001-190	2MASS J07000682-1901235 AB	(1)
J08536-034	LP 666-009	(4)
J10182-204	NLTT 23956 AB	(1)
J10354+694	LP 037-179 AB	(1)
J14155+046	GJ 1182 AB	(1)
J15412+759	UU UMi AB	(1)
J15474-108	LP 743-031 ABC	(2)
J16343+571	CM Dra Aab	(5)
J18356+329	LSR J1835+3259	(4)
J19169+051S	V1298 Aql	(4)
J19255+096	LSPM J1925+0938	(4)
J20198+229	LP 395-008 AB	(1)
J20556-140N	GJ 810 Aab	(1)
J23064-050	2MUCD 12171 (Trappist-1)	(4)
J23585+076	Wolf 1051 ABC	(2)

**Notes.** (1) Double-line spectroscopic (SB2) binary (Baroch et al. 2018, 2021). (2) Triple-line spectroscopic triple systems (Baroch et al. 2021). (3) Conspicuous artefacts in the CARMENES template spectra. (4) Spectral type M8.0 V or later. (5) Eclipsing binary (Morales et al. 2009).

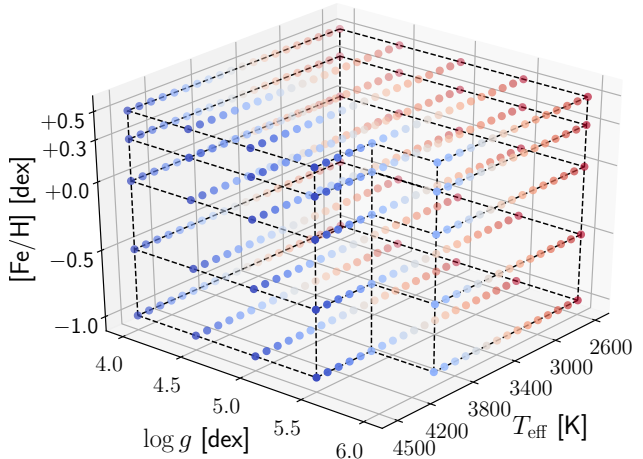
**Table 2.** Reference stars for the selection of Fe I and Ti I lines.

Reference star	SpT	$T_{\text{eff}}$ [K]
GX And	M1.0 V	~3700
Luyten's star	M3.5 V	~3400
Teegarden's star	M7.0 V	~2900

grid by means of the BT-Settl models and `turbospectrum`, and the analysis of the sample with the STEPARSYN code.

### 3.1. Spectral processing

All M dwarfs considered have been observed with CARMENES at several epochs since January 2016 (Reiners et al. 2018; Quirrenbach et al. 2020). The spectra were reduced following the standard CARMENES data flow. They were processed and calibrated in wavelength with the `caracal` pipeline (Caballero et al. 2016b). The wavelength calibration relies on a combination of hollow cathode lamps and two temperature- and pressure-stabilised Fabry-Pérot units that ensure median uncertainties of about  $1 \text{ m s}^{-1}$  in the VIS channel (Trifonov et al. 2018; Zechmeister et al. 2018). As an additional step in the data flow, individual spectra were corrected for telluric absorption before the co-addition into template spectra as a way to increase the S/N. The modelling of the telluric spectra was done with the software package `molecfit`<sup>2</sup> (Smette et al. 2015; Kausch et al. 2015), which incorporates the line-by-line radiative transfer code LBLRTM (Clough et al. 2005) and the HITRAN molecular line

**Fig. 4.** Coverage of our synthetic grid in  $T_{\text{eff}}$ ,  $\log g$ , and  $[\text{Fe}/\text{H}]$ .

list (Rothman et al. 2009). Further details on the removal of the telluric features can be found in Nagel (2019). The radial velocity pipeline `serval` (Zechmeister et al. 2018) co-adds all individual spectra and provides one high-S/N template spectrum per star and instrument channel. We transformed the wavelengths onto the air scale following the International Astronomical Union standard (Morton 2000) and corrected the spectra for the Doppler shift using the corresponding radial velocities of the targets.

### 3.2. Selection of spectral features and line masks

The selection of Fe I and Ti I lines employed in this work was the result of a careful inspection of the template spectra of three representative early-, mid-, and late-type M dwarfs, namely GX And, Luyten's star, and Teegarden's star (see Table 2). These M dwarfs show no significant rotation or activity, except for Teegarden's star, which shows relatively little activity for its spectral type (Zechmeister et al. 2019). In addition, their template spectra have a very high S/N. This choice of reference stars mirrors that of Reiners et al. (2018) for their spectral atlas.

For this purpose, we first requested several line lists from the Vienna Atomic Line Database<sup>3</sup> (VALD3; Ryabchikova et al. 2015) via the `extract_all` option, across the VIS and NIR wavelength regions covered by CARMENES. Following the prescriptions of Passegger et al. (2019), we excluded all Fe I and Ti I lines in the NIR channel ( $\lambda > 9600 \text{ \AA}$ ) with large Landé factors (i.e.  $g_{\text{eff}} > 1.5$ ) to alleviate the impact of the stellar magnetic field on the line profiles. The visual inspection was complemented by a literature search to include some of the Fe I and Ti I line selections of Tabernero et al. (2018) and Passegger et al. (2019). The final list of 75 Fe I and Ti I lines along with the synthesised wavelength ranges can be found in Table B.2. The ranges are wide enough (i.e. a few Å) to circumvent potential problems posed by convolution at the edges. We also included the TiO  $\gamma$  and  $\epsilon$  bands for the present analysis (see Table 3) given their high sensitivity to  $T_{\text{eff}}$  (Rajpurohit et al. 2014; Passegger et al. 2016). In Fig. 3 we show the template spectra of the three reference stars along with the selected wavelength ranges (see also Figs. 6 and 7). In contrast to some of the lines used in other works, such as K I

<sup>2</sup> <http://www.eso.org/sci/software/pipelines/skytools/molecfit>

<sup>3</sup> <http://vald.astro.uu.se>

**Table 3.** List of TiO bands and wavelength ranges synthesised.

TiO band	Range	Band head	
	$\lambda_{\min}$ [Å]	$\lambda_{\max}$ [Å]	$\lambda_{\text{head}}$ [Å]
$\gamma$ bands	7049.69	7058.85	~7054
	7082.49	7092.31	~7087
	7120.30	7129.69	~7125
$\epsilon$ bands	8436.60	8446.51	~8440
	8854.87	8864.58	~8859

(Passegger et al. 2018, 2019; Rajpurohit et al. 2018b), non-LTE effects are negligible for Fe I and Ti I lines (Olander et al. 2021).

We followed Tabernero et al. (2021) to define the wavelength regions around the observed Fe I and Ti I line profiles in the template spectra to be compared with the synthetic grid (i.e. the line masks). We first performed a preliminary Gaussian fit to the Ti I and Fe I lines by means of the Levenberg-Marquardt algorithm through the Python `scipy` package (Virtanen et al. 2020). Next, we adjusted the line profiles assuming an initial width of  $3\sigma$  around their centre, avoiding adjacent spectral features. For targets with  $v \sin i > 4 \text{ km s}^{-1}$  where the Gaussian approximation may no longer accurately reproduce the line profiles, we also broadened these line regions to account for rotation following the expression (Tabernero et al. 2021):

$$\Delta\lambda = 2\lambda_{\text{line}} \frac{v \sin i}{c}, \quad (1)$$

where  $\Delta\lambda$  is the broadening,  $\lambda_{\text{line}}$  is the central wavelength of the line, and  $c$  is the speed of light.

For active stars (as indicated by the H $\alpha$  flag), we specifically excluded some Fe I and Ti I lines that appear to be particularly sensitive to chromospheric activity and the stellar magnetic field. These lines are marked as magnetically sensitive in Table B.2 and will be discussed in a future publication (López-Gallifa et al., in prep.; for more details, see Montes et al. 2020). This additional consideration is particularly relevant for M dwarfs showing magnetic fields that can be as high as several kilogauss, such as EV Lac and YZ CMi (Shulyak et al. 2019). Overall, the line exclusion affected a total of 91 active stars in our sample and proved crucial in reaching convergence and, thus, avoiding getting unreliable parameters with STEPARSYN.

### 3.3. Synthetic grid

After the line selection step, we computed a coarse grid of synthetic spectra based on a set of BT-Settl model atmospheres (Allard et al. 2012) and the 1D LTE spectrum synthesis code `turbospectrum` (Alvarez & Plez 1998; Plez 2012). The grid is representative of the M-dwarf regime and ranges from 2600 K to 4500 K and 4.0 dex to 6.0 dex, when available (i.e. 5.5 dex instead for models with  $T_{\text{eff}} > 4000$  K) in steps of 100 K and 0.5 dex in  $T_{\text{eff}}$  and  $\log g$ , respectively (see Fig. 4). We set the metallicity, [Fe/H], to the following values: -1.0, -0.5, 0.0, +0.3, and +0.5 dex. For all models, we adopted the same micro-turbulence velocities as in the PHOENIX-ACES library of synthetic spectra<sup>4</sup> (Husser et al. 2013). We assumed the solar abundances as reported by Asplund et al. (2009) and scaled the abundances of the  $\alpha$  elements (O, Ne, Mg, Si, S, Ar, Ca, and Ti) following the discussion of Gustafsson et al. (2008) for the standard grid of MARCS models, so that  $[\alpha/\text{Fe}] = -0.4[\text{Fe}/\text{H}]$  for

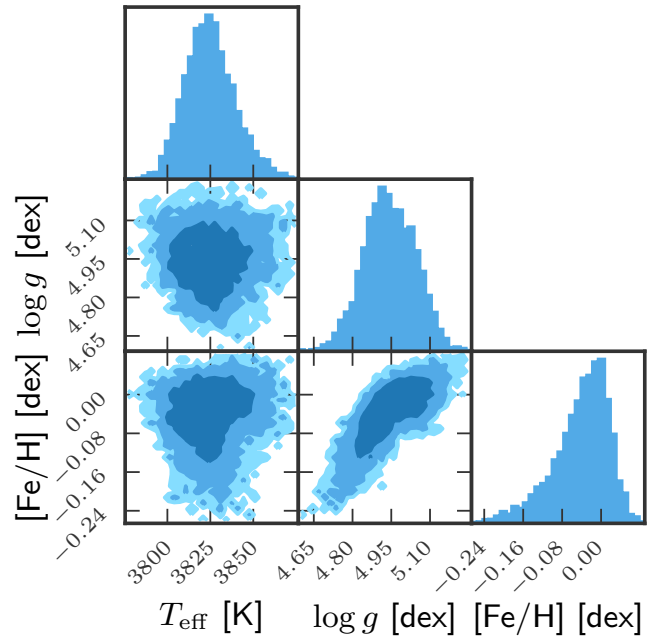


**Fig. 5.** Marginalised posterior distributions in  $T_{\text{eff}}$ ,  $\log g$ , and [Fe/H] for the M1.0 V star HD 233153 (J05415+534). The colour shades denote the  $1\sigma$ ,  $2\sigma$ , and  $3\sigma$  levels. The retrieved parameters are  $T_{\text{eff}} = 3825 \pm 14$  K,  $\log g = 4.94 \pm 0.10$  dex, and  $[\text{Fe}/\text{H}] = -0.04 \pm 0.06$  dex.

$-1.0 \leq [\text{Fe}/\text{H}] < 0.0$ , and  $[\alpha/\text{Fe}] = 0.0$  (i.e. no enhancement) for  $[\text{Fe}/\text{H}] \geq 0.0$ . The synthetic grid was finally stored in a binary file by means of the Python module `pickle` (Van Rossum 2020).

The atomic data were gathered via automatic email requests to the VALD3 database using the `extract_all` option for all the ranges listed in Tables 3 and B.2. The required molecular data were compiled from several sources and included H<sub>2</sub>O (Barber et al. 2006), FeH (Dulick et al. 2003), MgH (Kurucz 2014), CO (Goorvitch 1994), SiH (Kurucz 2014), OH (Kurucz 2014), VO (McKemmish et al. 2016), CaH, ZrO, and TiO (B. Plez priv. comm.; see Heiter et al. 2021). To reduce computation times, we only considered the most relevant transitions in each molecular line list by applying the following Boltzmann cut (Gray 2008):

$$\log(gf \cdot \lambda_i) - \chi_i \cdot \theta > \max_i[\log(gf \cdot \lambda_i) - \chi_i \cdot \theta] - 5, \quad (2)$$

where  $\lambda_i$  denotes the wavelength in Å of the transition  $i$ ,  $\log gf$  is the oscillator strength,  $\chi_i$  is the excitation potential in eV, and  $\theta = 5040 \text{ K}/T$ , with  $T = 3000$  K.

As discussed in Tabernero et al. (2021), the STEPARSYN code allows the synthetic grid to be sequentially convolved on the fly (i.e. prior to the comparison with the observed spectra) to account for both the stellar rotation and the instrumental profile as the main sources of spectral broadening. As for rotation, we assumed the rotational profile with a limb darkening coefficient of 0.6 from Gray (2008), and adopted the projected rotational velocities from Table B.1. Finally, to account for the instrumental profile, we convolved the spectra with a Voigt profile, assuming the corresponding median averaged Gaussian and Lorentzian components for the CARMENES VIS and NIR channels (Nagel 2019).

<sup>4</sup> <http://phoenix.astro.physik.uni-goettingen.de/>

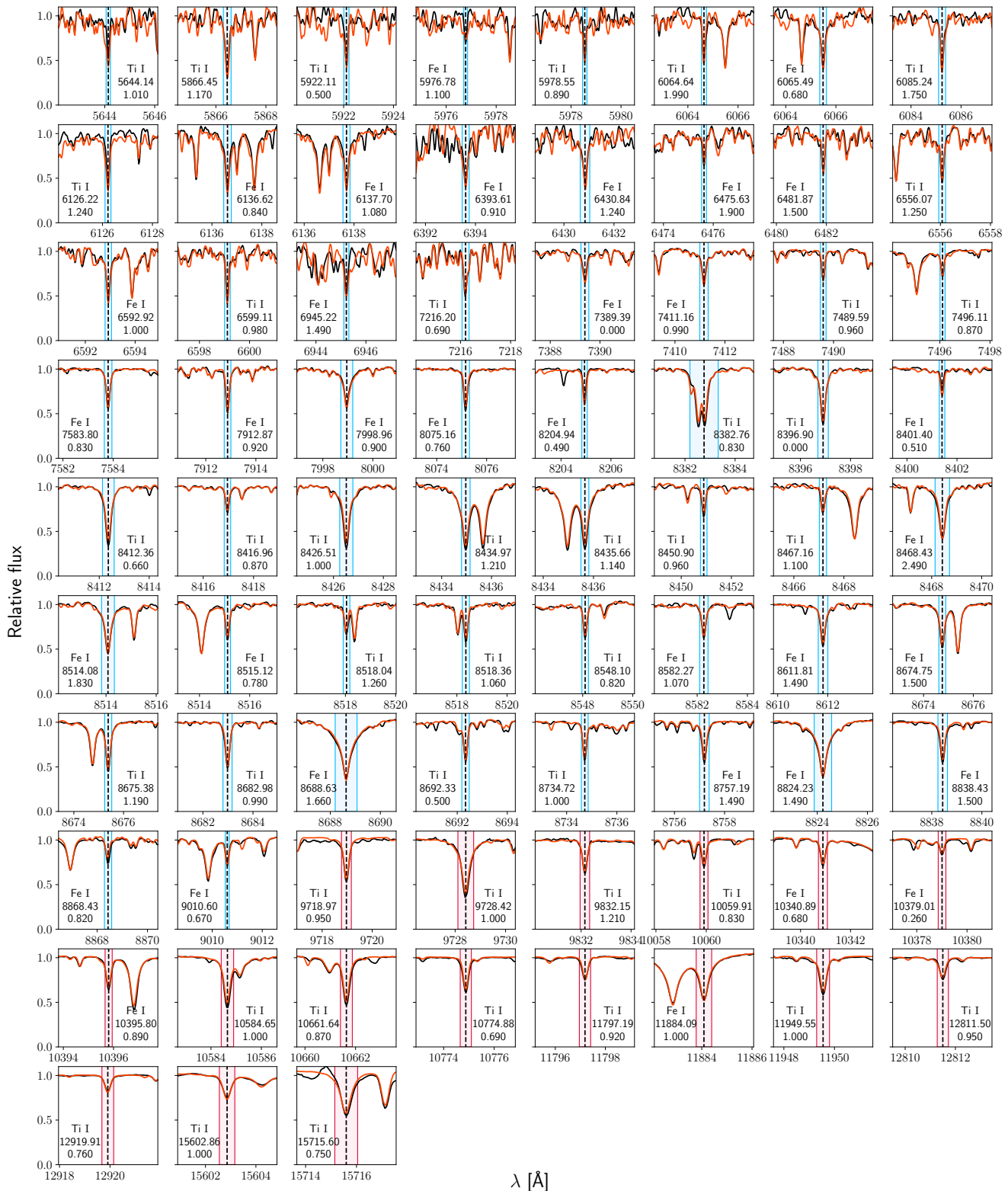


**Fig. 6.** Atomic line fits for the M1.0 V star HD 233153 (J05415+534). The solid black and orange lines are the observed and synthetic spectra, respectively. The blue and pink shaded areas are the regions of comparison between the observed and the synthetic spectra (i.e. line masks) for features in the VIS and NIR channels of CARMENES, respectively. The vertical dashed black lines mark the central wavelengths. The species, the central wavelength, and the effective Landé factor,  $g_{\text{eff}}$ , of the lines are indicated inside each box.

### 3.4. STEParSYN

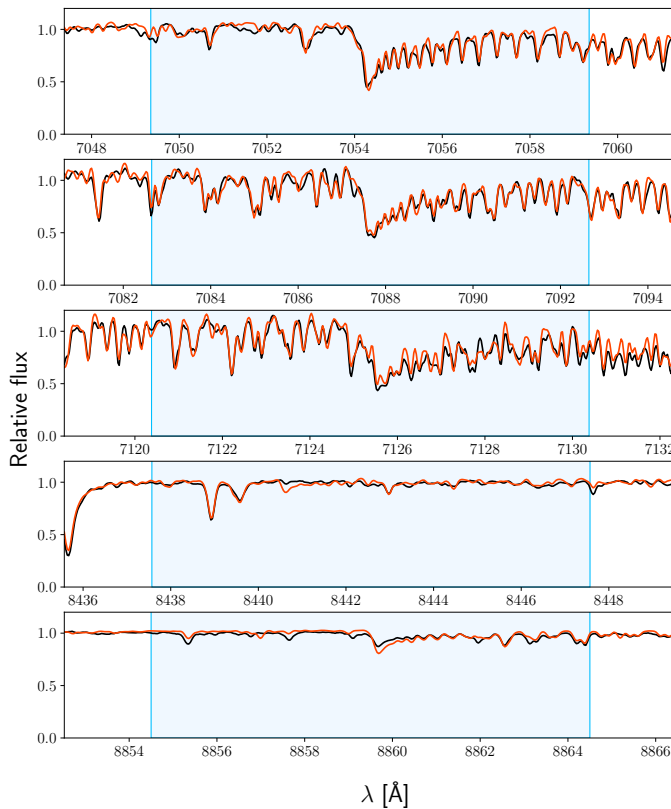
STEPARSYN is a Bayesian code written in Python 3 designed to map the probability distributions of the stellar atmospheric pa-

rameters ( $T_{\text{eff}}$ ,  $\log g$ , [Fe/H], and  $v \sin i$ ) from a given observed spectrum following an Markov chain Monte Carlo approach (Tabernero et al. 2021). It has already been employed in many astrophysical contexts, including the study of stars in open clusters

**Table 4.** List of outliers in  $\log g$ .

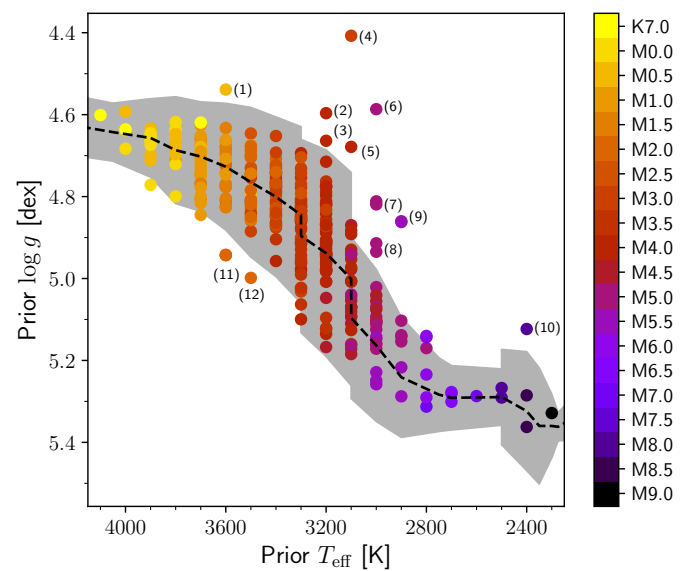
Name	Karmn	SpT	Prior $\log g$ [dex]	Label <sup>(a)</sup>	Remarks
Barta 161 12	J01352–072	M4.0 V	4.60	(2)	Member of $\beta$ Pictoris Moving Group
RX J0447.2+2038	J04472+206	M5.0 V	4.82	(7)	Member of IC 2391 Supercluster
1RXS J050156.7+010845	J05019+011	M4.0 V	4.66	(3)	Member of $\beta$ Pictoris Moving Group
RX J0506.2+0439	J05062+046	M4.0 V	4.68	(5)	Member of $\beta$ Pictoris Moving Group
2MASS J05082729–2101444	J05084–210	M5.0 V	4.59	(6)	Member of Local Association
LP 205–044	J06318+414	M5.0 V	4.81	(7)	Member of Local Association
1RXS J114728.8+664405	J11474+667	M5.0 V	4.91	(8)	Member of Castor Moving Group
K2-33	J16102–193	M3.0 V	4.41	(4)	Member of Local Association
1RXS J173353.5+165515	J17338+169	M5.5 V	4.86	(9)	Member of Local Association
LSPM J1925+0938	J19255+096	M8.0 V	5.12	(10)	Spectral type M8.0 V (see Table 2)
AU Mic	J20451–313	M1.0 V	4.54	(1)	Member of $\beta$ Pictoris Moving Group
Ross 695	J12248–182	M2.0 V	5.00	(12)	Behaviour akin to a subdwarf
GJ 625	J16254+543	M1.5 V	4.94	(11)	Behaviour akin to a subdwarf
Ross 730	J19070+208	M2.0 V	4.94	(11)	Behaviour akin to a subdwarf
HD 349726	J19072+208	M2.0 V	4.94	(11)	Behaviour akin to a subdwarf

**Notes.** Membership in young stellar kinematic groups following Cortés-Contreras et al. in prep. <sup>(a)</sup>Label column refers to Fig. 8. Two and three stars are superimposed under labels (7) and (11), respectively.

**Fig. 7.** Same as Fig. 6, but for the TiO  $\gamma$  and  $\epsilon$  bands.

(Lohr et al. 2018; Alonso-Santiago et al. 2019), stars in galaxies of the Local Group (Tabernero et al. 2018), and exoplanet host stars (Borsa et al. 2021; Demangeon et al. 2021).

In broad terms, the STEPARSYN code compares the observed spectrum with a grid of synthetic spectra computed around particular features. Prior decomposition of the synthetic grid following a principal component analysis (Francis & Wills 1999) helps to assess any given point of the parameter space in a

**Fig. 8.** Central prior  $T_{\text{eff}}$  and  $\log g$  values for the sample following Ci-fuentes et al. (2020). The spectral types are colour-coded. The dashed black line is the average  $T_{\text{eff}}$  and  $\log g$  for K7 V to M9.0 V objects, with the corresponding uncertainties shaded in grey. The 15 outliers discussed in Sect. 3.4 are labelled and listed in Table 4. Two and three stars are superimposed under labels (7) and (11), respectively.

computationally inexpensive way. STEPARSYN finally returns the marginalised posterior distributions in the stellar atmospheric parameters, as shown in Fig. 5 for a representative case (the M1.0 V star HD 233153), along with the best synthetic fits for the atomic lines and molecular bands, as shown in Figs. 6 and 7, respectively, for the same star (see Figs. A.1 to A.9 for the reference stars GX And, Luyten’s star, and Teegarden’s star). The corner plot showing the marginalised posterior distribution obtained with STEPARSYN was made with the Python pygtc package (Bocquet & Carter 2016). Further details about STEPARSYN can be found in Tabernero et al. (2021).

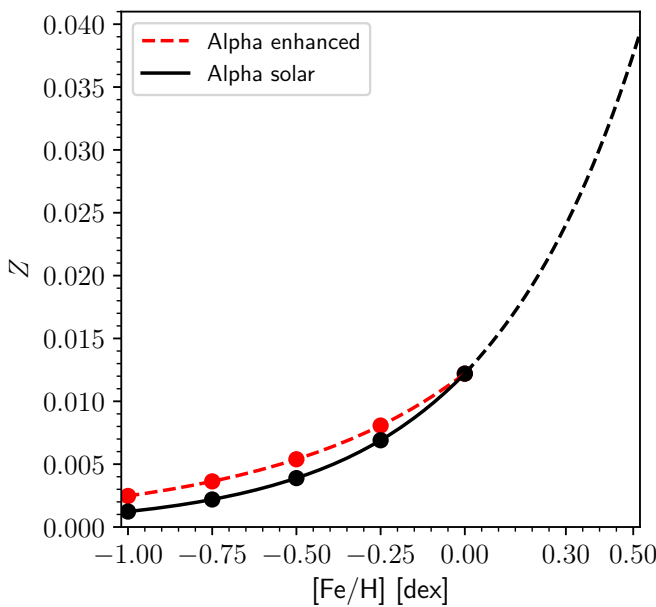


**Fig. 9.** Interpolation scheme between  $Z$  and  $[\text{Fe}/\text{H}]$  in alpha-enhanced (red) and alpha-solar (black) models.

To avoid degeneracies in the M-dwarf parameter space, particularly between  $\log g$  and  $[\text{Fe}/\text{H}]$ , we assumed Gaussian prior probability distributions in  $T_{\text{eff}}$  and  $\log g$  centred according to the  $T_{\text{eff}}$ , stellar mass, and radius reported by Cifuentes et al. (2020) for each target when available<sup>5</sup>, or otherwise the averaged parameters as listed in Table 6 in Cifuentes et al. (2020), with standard deviations of 200 K and 0.2 dex, respectively.  $T_{\text{eff}}$  and  $\log g$  prior distributions for our sample are included in Table B.3. These  $T_{\text{eff}}$  values were derived from a thorough multi-band photometric analysis carried out with the Virtual Observatory Spectral energy distribution Analyser (vosa; Bayo et al. 2008), whereas the stellar radii and masses were obtained from the Stefan-Boltzmann law and the mass-radius relation derived by Schweitzer et al. (2019).

In Fig. 8 we show a Kiel diagram (i.e.  $\log g$  versus  $T_{\text{eff}}$ ) of the prior  $T_{\text{eff}}$  and  $\log g$  values that we adopted for our sample. Some stars show low  $\log g$  values, which can be explained with stellar age. These stars were already identified as young stars by Schweitzer et al. (2019) on account of their membership in young stellar kinematic groups (Cortés-Contreras et al. in prep.). Among these are the Local Association,  $\beta$  Pictoris Moving Group, the IC 2391 Supercluster, and Castor Moving Group, with estimated ages of 10–150 Ma (Bell et al. 2015), 18.5 Ma (Miret-Roig et al. 2020), 50 Ma (Barrado y Navascués et al. 2004), and 440 Ma (Mamajek et al. 2013), respectively. On the contrary, a few additional targets exhibit a high  $\log g$ , probably due to their behaviour akin to subdwarfs, following the discussion by Schweitzer et al. (2019). All these outliers in  $\log g$  are listed in Table 4.

## 4. Results and discussion

The stellar atmospheric parameters of the sample computed with STEPARSYN ( $T_{\text{eff}}$ ,  $\log g$ ,  $[\text{Fe}/\text{H}]$ ) are given in Table B.3. Since some M-dwarf studies do not consider alpha enhancement in the computation of synthetic spectra (see e.g. Passegger et al. 2018),

we corrected our  $[\text{Fe}/\text{H}]$  scale into  $[\text{Fe}/\text{H}]_{\text{corr}}$  in order to compare our results more directly with that of the literature. We did this through a linear interpolation scheme via the `scipy` package between the mass fraction of elements heavier than helium ( $Z$ ) and the corresponding  $[\text{Fe}/\text{H}]$  value in alpha-enhanced and alpha-solar (i.e. no alpha enhancement) models, respectively, as shown in Fig. 9. The correspondence between  $Z$  and  $[\text{Fe}/\text{H}]$  was adopted from the MARCS atmosphere models with standard and alpha-poor compositions<sup>6</sup>. The interpolation scheme retrieves the  $[\text{Fe}/\text{H}]_{\text{corr}}$  value that corresponds to a given  $Z$  defined by the original  $[\text{Fe}/\text{H}]$  scale.

We note the limitations of our methodology with respect to the analysis of M dwarfs with spectral types M8.0 V or later due to the scarcity of useful  $\text{Fe I}$  and  $\text{Ti I}$  lines and the poor sensitivity of the  $\text{TiO}$  molecular bands to  $T_{\text{eff}}$  as a result of dust formation in the stellar photospheres (Tsuiji et al. 1996; Allard et al. 2001). Furthermore, the version of the BT-Settl models used in this work does not allow for the formation of enough dust in very late M dwarfs (Allard et al. 2012). However, we note that this limit in spectral type is similar to other studies based on spectral synthesis in M dwarfs (Rajpurohit et al. 2018b; Schweitzer et al. 2019).

We compared our results against some recent M-dwarf studies, including Passegger et al. (2019, Fig. 10), Rojas-Ayala et al. (2012, Fig. A.10), Gaidos & Mann (2014, Fig. A.11), Maldonado et al. (2015, Fig. A.12), Mann et al. (2015, Fig. A.13), Passegger et al. (2018, Fig. A.14), Rajpurohit et al. (2018b, Fig. A.15), Schweitzer et al. (2019, Fig. A.16), Maldonado et al. (2020, Fig. A.17), and Passegger et al. (2020, Fig. A.18). The approaches to the computation of stellar parameters in the M-dwarf regime are manifold and generally dependent on the covered wavelength region  $\Delta\lambda$ , the spectral resolution  $R$ , and the S/N of the spectra. For instance,  $T_{\text{eff}}$  can be derived from the  $\text{H}_2\text{O-K2}$  index (Rojas-Ayala et al. 2012), the pseudo-EW of spectral features (Maldonado et al. 2015, 2020), and spectral fitting to a variety of synthetic grids, including PHOENIX-ACES (Passegger et al. 2018; Schweitzer et al. 2019), PHOENIX-SESAM (Passegger et al. 2019), and grids based on BT-Settl models (Gaidos & Mann 2014; Mann et al. 2015; Rajpurohit et al. 2018b). As for  $\log g$ , in some studies it is left as a free parameter in the fitting procedure (Rajpurohit et al. 2018b), while in others  $\log g$  is kept fixed instead based on evolutionary models to break the observed degeneracy in the M-dwarf parameter space (Rojas-Ayala et al. 2012; Passegger et al. 2018, 2019). In other cases,  $\log g$  is derived indirectly from the stellar masses and radii obtained from different approaches, primarily semi-empirical calibrations (Gaidos & Mann 2014; Mann et al. 2015; Maldonado et al. 2015, 2020; Schweitzer et al. 2019). Lastly, stellar metallicity is usually derived from semi-empirically calibrated relations established between the spectral features of M dwarfs that are companions of FGK-type stars with known metallicities (Terrien et al. 2012; Mann et al. 2013a, 2014, 2015; Newton et al. 2014; Neves et al. 2014; Maldonado et al. 2015, 2020), and the use of weights in the spectral fitting for spectral features that appear to be more sensitive to metallicity variations (Passegger et al. 2016, 2018, 2019).

To explore possible sources of systematic trends or offsets, we followed the same Monte Carlo method as in Tabernero et al. (2018). We generated 10 000 artificial samples based on the stellar atmospheric parameters derived with STEPARSYN by assuming a normal distribution centred at the original measurements, and widths equal to the uncertainties in the parameters. The sum-

<sup>5</sup> <https://github.com/ccifuentesr/CARMENES-V>

<sup>6</sup> <https://marcs.astro.uu.se/>

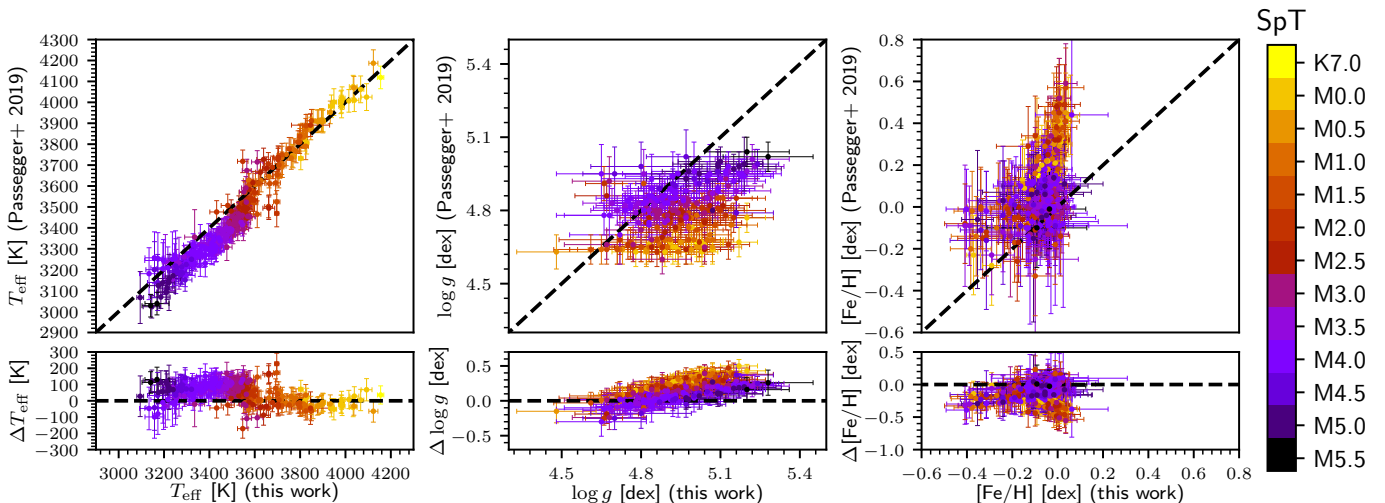


**Fig. 10.** Comparison between this work and the VIS+NIR analysis done by Passegger et al. (2019). Spectral types are colour-coded. The dashed black lines indicate the 1:1 relationship.

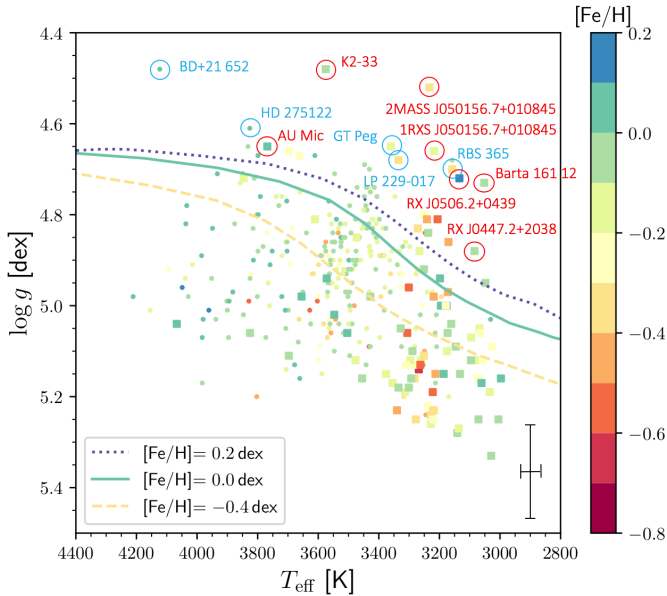


**Fig. 11.** Kiel diagram of the sample showing the parameters computed with SteParSyn. Squares depict H $\alpha$ -active stars. The metallicity  $[Fe/H]_{corr}$  is colour-coded. Lines correspond to 5-Ga PARSEC isochrones with  $[Fe/H] = -0.4, 0.0$ , and  $0.2$  dex (Bressan et al. 2012). Typical uncertainties in  $\log g$  and  $T_{\text{eff}}$  are shown in the bottom-right corner. Outliers in  $\log g$  are marked with red and blue circles (see Sect. 4 for details).

many of these Monte Carlo simulations can be found in Table 5. We computed the Pearson ( $r_p$ ) and the Spearman ( $r_s$ ) correlation coefficients, which quantify the degree of correlation between any two given variables. Our temperature scale appears to have an intrinsic systematic offset relative to the literature values in the range from 4 K to 85 K. The offset is smallest for Gaidos & Mann (2014) and largest for Mann et al. (2015). In other words, all literature sources report on average slightly lower effective temperatures. However, we note that the offsets are compatible with zero in all instances but Mann et al. (2015). Regarding  $\log g$ , our values appear to be higher (between 0.02 and 0.17 dex on average with respect to the literature), except for Rajpurohit et al.

(2018b), although even in that case the discrepancies are compatible with zero. As to metallicity, our  $[Fe/H]$  scale seems to agree best with the results by Rojas-Ayala et al. (2012), Mann et al. (2015), and Maldonado et al. (2015, 2020). In contrast, large discrepancies in metallicity can be seen when comparing our results with Passegger et al. (2018, 2019), and Schweitzer et al. (2019). Among the plausible explanations are the use of different synthetic models, minimisation algorithms, and sets of lines in their analyses, especially K I lines, which have been shown to be affected by non-LTE effects that can translate into metallicity corrections of the order of 0.2 dex (Olander et al. 2021).

Regarding the comparison between our results and the prior distributions, we find that the spectroscopic  $T_{\text{eff}}$  values are higher by  $136 \pm 88$  K, which is in agreement with the findings of Ciolfu et al. (2020) when comparing their estimations using photometry and vosa to spectroscopic studies, namely Passegger et al. (2019) and Rajpurohit et al. (2018b). This difference is in turn more noticeable towards the mid-type and late M dwarfs, probably due to missing opacity sources. Regarding  $\log g$ , it also seems to be higher by  $0.08 \pm 0.14$  dex with respect to the prior values.

Similarly to Fig. 8, Fig. 11 is a Kiel diagram of our sample showing the results obtained with SteParSyn along with theoretical isochrones from the PAdova and TRieste Stellar Evolution Code (PARSEC; Bressan et al. 2012). Since M dwarfs evolve very slowly once they reach the main sequence (Burrows et al. 1997), we selected a set of isochrones with an age of 5 Ga and different compositions, namely  $[Fe/H] = -0.4, 0.0$ , and  $0.2$  dex. Active and inactive stars in Fig 11 are shown with different symbols. First, we note that the fraction of active stars increases towards the late M-dwarf regime, as discussed by Tal-Or et al. (2018) and Reiners et al. (2018). While some stars fall inside the region encompassed by the isochrones, we note that most of them deviate towards higher values of  $\log g$ . However, the trend established by the isochrones is preserved in the retrieved  $\log g$  values throughout the diagram. Additionally, conspicuous outliers have been labelled and marked with red and blue circles. Red circles denote seven of the ten targets identified as young according to Table 4, whereas blue circles indicate other stars that also correspond to higher  $\log g$  values. We note that most of

**Table 5.** Summary of the Monte Carlo simulations on  $T_{\text{eff}}$ ,  $\log g$ , and [Fe/H] between different comparison samples.

Sample	Size	Parameter	Difference	$r_p \pm \sigma_p$	$r_s \pm \sigma_s$
Rajpurohit et al. (2018b)	292	$T_{\text{eff}}$	$64 \pm 95$ K	$0.807 \pm 0.016$	$0.824 \pm 0.013$
		$\log g$	$-0.23 \pm 0.30$ dex	$0.069 \pm 0.054$	$0.051 \pm 0.054$
		[Fe/H]	$-0.25 \pm 0.28$ dex	$0.079 \pm 0.054$	$0.084 \pm 0.053$
Schweitzer et al. (2019)	287	$T_{\text{eff}}$	$25 \pm 53$ K	$0.937 \pm 0.006$	$0.940 \pm 0.005$
		$\log g$	$0.03 \pm 0.20$ dex	$0.253 \pm 0.040$	$0.288 \pm 0.039$
		[Fe/H]	$-0.19 \pm 0.17$ dex	$0.397 \pm 0.018$	$0.467 \pm 0.013$
Passegger et al. (2019)	282	$T_{\text{eff}}$	$48 \pm 61$ K	$0.931 \pm 0.007$	$0.930 \pm 0.006$
		$\log g$	$0.13 \pm 0.14$ dex	$0.223 \pm 0.041$	$0.259 \pm 0.042$
		[Fe/H]	$-0.20 \pm 0.15$ dex	$0.275 \pm 0.051$	$0.288 \pm 0.049$
Passegger et al. (2018)	235	$T_{\text{eff}}$	$29 \pm 44$ K	$0.932 \pm 0.008$	$0.945 \pm 0.005$
		$\log g$	$0.02 \pm 0.15$ dex	$0.182 \pm 0.045$	$0.241 \pm 0.045$
		[Fe/H]	$-0.10 \pm 0.12$ dex	$0.288 \pm 0.051$	$0.350 \pm 0.048$
Maldonado et al. (2020)	102	$T_{\text{eff}}$	$29 \pm 80$ K	$0.883 \pm 0.014$	$0.877 \pm 0.015$
		$\log g$	$0.08 \pm 0.15$ dex	$0.249 \pm 0.071$	$0.285 \pm 0.072$
		[Fe/H]	$-0.06 \pm 0.15$ dex	$0.312 \pm 0.063$	$0.364 \pm 0.065$
Mann et al. (2015)	86	$T_{\text{eff}}$	$85 \pm 63$ K	$0.928 \pm 0.011$	$0.924 \pm 0.011$
		$\log g$	$0.11 \pm 0.13$ dex	$0.355 \pm 0.063$	$0.427 \pm 0.060$
		[Fe/H]	$-0.13 \pm 0.13$ dex	$0.611 \pm 0.057$	$0.648 \pm 0.046$
Gaidos & Mann (2014)	63	$T_{\text{eff}}$	$4 \pm 76$ K	$0.850 \pm 0.030$	$0.860 \pm 0.023$
		$\log g$	$0.09 \pm 0.15$ dex	$0.088 \pm 0.084$	$0.156 \pm 0.083$
		[Fe/H]	$-0.12 \pm 0.11$ dex	$0.643 \pm 0.064$	$0.665 \pm 0.051$
Passegger et al. (2020)	50	$T_{\text{eff}}$	$23 \pm 107$ K	$0.917 \pm 0.017$	$0.911 \pm 0.015$
		$\log g$	$0.17 \pm 0.16$ dex	$0.341 \pm 0.088$	$0.398 \pm 0.098$
		[Fe/H]	$-0.32 \pm 0.12$ dex	$0.264 \pm 0.122$	$0.245 \pm 0.138$
Rojas-Ayala et al. (2012)	40	$T_{\text{eff}}$	$41 \pm 124$ K	$0.915 \pm 0.019$	$0.886 \pm 0.021$
		$\log g^{(a)}$	...	...	...
		[Fe/H]	$-0.15 \pm 0.13$ dex	$0.513 \pm 0.103$	$0.533 \pm 0.099$
Maldonado et al. (2015)	21	$T_{\text{eff}}$	$39 \pm 42$ K	$0.884 \pm 0.040$	$0.883 \pm 0.037$
		$\log g$	$0.12 \pm 0.13$ dex	$0.213 \pm 0.169$	$0.210 \pm 0.171$
		[Fe/H]	$-0.07 \pm 0.14$ dex	$0.576 \pm 0.116$	$0.581 \pm 0.100$

**Notes.** We give the average difference on each parameter and the Pearson ( $r_p$ ) and the Spearman ( $r_s$ ) correlation coefficients (see Sect. 4 for details).

<sup>(a)</sup>Rojas-Ayala et al. (2012) fixed  $\log g$  to 5.0 dex.

them are active stars, with the exception of the early M dwarfs BD+21 652 and HD 275122.

In light of such a large dispersion in  $\log g$ , we performed an additional run by fixing  $\log g$  to the prior values. The results of this run ( $T_{\text{eff}}$ ,  $[\text{Fe}/\text{H}]_{\text{fixed}}$ , and  $[\text{Fe}/\text{H}]_{\text{corr, fixed}}$ ) can also be found in Table B.3. In Fig. 12 we show the differences in  $T_{\text{eff}}$  and [Fe/H] between these two runs. The impact of fixing  $\log g$  on  $T_{\text{eff}}$  is well below 100 K for most targets, whereas the impact on [Fe/H] is between 0.1 and 0.2 dex in most cases. In general terms, the larger the difference in  $\log g$  between the runs, the larger the change in [Fe/H], as expected.

To check our metallicity scale, in Fig. 13 we compare the M-dwarf metallicity distribution presented in this work to that from the Geneva-Copenhagen survey (Nordström et al. 2004), which comprises around 14 000 F- and G-type dwarfs in the solar neighbourhood, and is volume-complete to a distance of  $\sim 40$  pc. We note that the two distributions are very similar in the low-metallicity regime, whereas high-metallicity stars appear to be marginally underrepresented. There appears to be an excess of M dwarfs with solar metallicity and we retrieve no metallicity higher than 0.25 dex. The scarcity of high-metallicity values is also noticeable when comparing our determinations with the lit-

erature, as shown in Figs. A.10 (Rojas-Ayala et al. 2012), A.11 (Gaidos & Mann 2014), and Fig. A.13 (Mann et al. 2015).

We also investigated the M-dwarf metallicity distribution in terms of the kinematic membership of the stars in the Galactic populations, namely the thick disc (TD), the thick disc-thin disc transition (TD-D), the thin disc (D), and the young disc (YD) (Montes et al. 2001, Cortés-Contreras et al. in prep.), as shown in Fig. 14. It can be seen that the mean metallicity of M dwarfs belonging to the TD is lower than that of those belonging to the D, in accordance with the results presented by Bensby et al. (2003, 2005).

#### 4.1. M dwarfs with interferometric angular measurements

In Table 6 we compile the 18 M dwarfs in our sample with interferometrically measured radii from Boyajian et al. (2012) and von Braun et al. (2014), which may be used along with other information (e.g. trigonometric parallax, bolometric flux, isochrone fitting, and mass-luminosity relations) to derive  $T_{\text{eff}}$  and  $\log g$  independently from spectroscopy. For this reason, this set of stars is particularly helpful as a benchmark test for any method aimed at determining stellar atmospheric parameters (Casagrande et al. 2008; Mann et al. 2015; Birkby et al. 2020).

**Table 6.** M dwarfs with interferometric angular diameter measurements in common with the CARMENES GTO survey.

Name	Karmn	SpT	$R$ [ $R_{\odot}$ ]	$T_{\text{eff}}$ [K]	$L_{\text{bol}}$ [ $10^{-4} L_{\odot}$ ]	$M$ [ $M_{\odot}$ ]	Ref. <sup>(a)</sup>	$T_{\text{eff}}^{(b)}$ [K]	$\log g^{(b)}$ [dex]	[Fe/H] <sub>corr</sub> [dex]
HD 79210	J09143+526	M0.0 V	$0.5773 \pm 0.0131$	$3907 \pm 35$	$697 \pm 21$	0.622	B12	$4015 \pm 16$	$4.91 \pm 0.08$	$-0.12 \pm 0.05$
HD 79211	J09144+526	M0.0 V	$0.5673 \pm 0.0137$	$3867 \pm 37$	$647 \pm 19$	0.600	B12	$3983 \pm 17$	$5.17 \pm 0.07$	$-0.03 \pm 0.04$
GX And	J00183+440	M1.0 V	$0.3874 \pm 0.0023$	$3563 \pm 11$	$217.3 \pm 2.1$	0.423	B12	$3603 \pm 24$	$4.99 \pm 0.14$	$-0.52 \pm 0.11$
BD+44 2051 A	J11054+435	M1.0 V	$0.3982 \pm 0.0091$	$3497 \pm 39$	$212.9 \pm 2.6$	0.403	B12	$3628 \pm 19$	$5.01 \pm 0.13$	$-0.56 \pm 0.09$
BD+25 3173	J16581+257	M1.0 V	$0.5387 \pm 0.0157$	$3590 \pm 45$	$432 \pm 13$	0.54	v14	$3782 \pm 17$	$4.87 \pm 0.09$	$-0.05 \pm 0.05$
HD 199305	J20533+621	M1.0 V	$0.5472 \pm 0.0067$	$3692 \pm 22$	$499.0 \pm 6.2$	0.573	B12	$3815 \pm 16$	$4.83 \pm 0.14$	$-0.10 \pm 0.08$
HD 36395	J05314-036	M1.5 V	$0.5735 \pm 0.0044$	$3801 \pm 9$	$616.3 \pm 8.8$	0.615	B12	$3850 \pm 27$	$4.71 \pm 0.18$	$0.05 \pm 0.08$
Lalande 21185	J11033+359	M1.5 V	$0.3921 \pm 0.0037$	$3465 \pm 17$	$198.9 \pm 1.2$	0.403	B12	$3557 \pm 26$	$4.95 \pm 0.14$	$-0.49 \pm 0.10$
HD 119850	J13457+148	M1.5 V	$0.4840 \pm 0.0084$	$3618 \pm 31$	$360 \pm 5$	0.520	B12	$3620 \pm 24$	$4.93 \pm 0.12$	$-0.34 \pm 0.07$
HD 216899	J22565+165	M1.5 V	$0.5477 \pm 0.0048$	$3713 \pm 11$	$511.2 \pm 7.4$	0.569	B12	$3798 \pm 21$	$4.80 \pm 0.12$	$0.03 \pm 0.06$
HD 285968	J04429+189	M2.0 V	$0.4525 \pm 0.0221$	$3679 \pm 77$	$337 \pm 18$	0.45	v14	$3678 \pm 16$	$5.13 \pm 0.08$	$0.00 \pm 0.03$
Ross 905	J11421+267	M2.5 V	$0.4546 \pm 0.0182$	$3416 \pm 53$	$252.5 \pm 1.2$	0.472	B12	$3533 \pm 26$	$4.83 \pm 0.11$	$-0.12 \pm 0.10$
HO Lib	J15194-077	M3.0 V	$0.2990 \pm 0.0100$	$3442 \pm 54$	$113 \pm 8$	0.297	B12	$3500 \pm 26$	$4.97 \pm 0.11$	$-0.08 \pm 0.07$
BD+68 946	J17364+683	M3.0 V	$0.4183 \pm 0.0070$	$3413 \pm 28$	$212.8 \pm 2.3$	0.413	B12	$3389 \pm 81$	$4.89 \pm 0.15$	$-0.06 \pm 0.13$
HD 173739	J18427+526N	M3.0 V	$0.3561 \pm 0.0039$	$3407 \pm 15$	$153.1 \pm 1.8$	0.318	B12	$3473 \pm 34$	$4.90 \pm 0.11$	$-0.31 \pm 0.12$
Barnard's star	J17578+046	M3.5 V	$0.1867 \pm 0.0012$	$3224 \pm 10$	$33.8 \pm 0.2$	0.150	B12	$3254 \pm 32$	$5.13 \pm 0.12$	$-0.57 \pm 0.10$
HD 173740	J18427+596S	M3.5 V	$0.3232 \pm 0.0061$	$3104 \pm 28$	$87.1 \pm 1.2$	0.235	B12	$3393 \pm 48$	$4.98 \pm 0.12$	$-0.38 \pm 0.18$
IL Aqr	J22532-142	M4.0 V	$0.3761 \pm 0.0059$	$3129 \pm 19$	$122 \pm 2$	0.37	v14	$3421 \pm 40$	$4.83 \pm 0.10$	$-0.06 \pm 0.10$

**Notes.** <sup>(a)</sup>Stellar radii, effective temperatures, luminosities, and stellar masses from Boyajian et al. (2012, B12) and von Braun et al. (2014, v14). The estimates of the stellar mass from these works conservatively assume 10% and 5% uncertainties, respectively. <sup>(b)</sup>This work.

Figure 15 shows the comparison in  $T_{\text{eff}}$  and  $\log g$  for these M dwarfs between Boyajian et al. (2012), von Braun et al. (2014), and this work. The  $\log g$  value was computed from the stellar mass and radius using the standard definition (i.e.  $g = GM/R^2$ , where  $G$  is the gravitational constant). In general, we find good agreement, with systematic offsets of  $72 \pm 67$  K in  $T_{\text{eff}}$ , and  $0.10 \pm 0.09$  dex in  $\log g$ . However, we note two outliers in  $T_{\text{eff}}$ , namely IL Aqr and HD 173740, which show a difference around 300 K between the interferometric and the spectroscopic approaches. Interestingly enough, HD 173740 also belongs to a wide binary system together with HD 173739, as discussed in Sect. 4.3. Although they exhibit similar chemical compositions and differ by only one spectral subtype, the  $T_{\text{eff}}$  derived from interferometry appears to be irreconcilable between the two components. In contrast, we derived very similar  $T_{\text{eff}}$  with STEPARSYN for both components. However, accounting for this difference is beyond the scope of this paper.

#### 4.2. M dwarfs in FGK+M systems

The study of multi-star systems serves as a benchmark test for [Fe/H] given that all components are thought to be formed from the same molecular cloud, be coeval, and have roughly similar chemical compositions (Desidera et al. 2006; Önehag et al. 2012; Souto et al. 2020; Ishikawa et al. 2020). In Table 7 we compile all M dwarfs in our sample that are bound in wide physical binaries with an FGK-type primary (Montes et al. 2018). For the FGK-type primaries, we adopted the metallicities from Montes et al. (2018), who employed the STEPAR code (Tabernero et al. 2019) as the preferred implementation of the EW method. For the fast-rotating F7 V star  $\theta$  Boo A ( $v \sin i = 30.4$  km s $^{-1}$ , Luck 2017), we adopted the metallicity from Tabernero et al. (2021).

In Fig. 16 we show the comparison in [Fe/H] between the components in these FGK+M systems. We find good agreement between our [Fe/H] determinations for the M-dwarf secondaries, with an internal scatter of  $-0.01 \pm 0.19$  dex, which is similar to what is found in other works (Souto et al. 2020; Antoniadis-Karnavas et al. 2020). The largest discrepancy in metallicity between components is found for  $\rho$  Cnc B. If we assume a homogeneous chemical composition in FGK+M systems, this star also

exhibits a C/O ratio that is larger than expected for an M dwarf, since C/O = 1.12 for the primary star (Delgado Mena et al. 2010). We note that the pseudo-continuum level is very sensitive to C/O and alterations in C/O can explain a large fraction of the variation in the strength of the atomic metal lines in M-dwarf spectra (Veyette et al. 2016; Souto et al. 2020). However, disentangling the effect of C/O on [Fe/H] computations is beyond the scope of this paper.

#### 4.3. M dwarfs in M+M systems

Similarly to FGK+M systems, wide physical M+M binaries can also prove useful as a benchmark test for [Fe/H]. In this case, both components are analysed with the same methodology (i.e. spectral synthesis). In Table 9 we list the astrometric parameters (parallax  $\pi$ , proper motion  $\mu$ , and radial velocity  $v_r$ ) along with the stellar atmospheric parameters ( $T_{\text{eff}}$ ,  $\log g$ , and [Fe/H]) of the 32 M dwarfs in our sample bound in M+M systems. These include two SB2 systems (EZ Psc and GJ 810) and the M8.0 V star V1298 Aql (vB 10), for which no reliable parameter determinations could be made (see Table 1). Parallaxes and proper motions were compiled from the *Gaia* DR2 and EDR3 releases (Gaia Collaboration et al. 2018, 2021).

In Fig. 16 we compare the metallicity computed in this work for both components, in the same way as for the FGK+M wide binaries. The mean difference in [Fe/H] between components is  $0.10 \pm 0.08$  dex, which is in agreement with other works ( $0.06 \pm 0.07$  dex, Antoniadis-Karnavas et al. 2020). However, we note that the differences become larger (i.e. up to  $\sim 0.2$  dex) in cases where the components differ by more than one spectral type.

#### 4.4. Choice of model atmospheres

Recent studies have shown that different parameter determination methods can lead to significant variations in the results for the same stars (Blanco-Cuaresma 2019; Passegger et al. 2021). These differences can be attributed to a number of factors, including the choice of model atmospheres, atomic and molecular data, and radiative transfer code. For this reason, we performed a test on the reference stars (i.e. GX And, Luyten's star, and Tee-

**Table 7.** M dwarfs in wide physical binaries with FGK-type primaries in common with the CARMENES GTO survey.

Primary			Secondary					
Name	SpT	[Fe/H] [dex]	Name	Karmn	SpT	$T_{\text{eff}}$ [K]	$\log g$ [dex]	[Fe/H] <sub>corr</sub> [dex]
V538 Aur	K1 V	0.04 ± 0.02	HD 233153	J05415+534	M1.0 V	3825 ± 14	4.94 ± 0.10	-0.02 ± 0.06
V869 Mon	K0/2 V	-0.11 ± 0.03	GJ 282 C	J07361-031	M1.0 V	3825 ± 12	5.06 ± 0.08	-0.04 ± 0.06
HD 154363	K5 V	-0.62 ± 0.05	HD 154363 B	J17052-050	M1.5 V	3587 ± 14	4.89 ± 0.10	-0.39 ± 0.07
$\theta$ Boo A	F7 V	-0.09 ± 0.01	$\theta$ Boo B	J14251+518	M2.5 V	3551 ± 22	4.90 ± 0.10	-0.14 ± 0.06
HD 16160	K3 V	-0.20 ± 0.02	BX Cet	J02362+068	M4.0 V	3335 ± 45	4.91 ± 0.10	-0.24 ± 0.12
$\sigma^2$ Eri A	K0.5 V	-0.37 ± 0.02	$\sigma^2$ Eri C	J04153-076	M4.5 V	3179 ± 61	5.00 ± 0.18	-0.30 ± 0.17
$\rho$ Cnc	G8 V	0.29 ± 0.04	$\rho$ Cnc B	J08526+283	M4.5 V	3321 ± 37	4.87 ± 0.08	-0.10 ± 0.11

**Notes.** Metallicities of the FGK-type primary stars from Montes et al. (2018), except for  $\theta$  Boo A, which is from Tabernero et al. (2021). Stellar atmospheric parameters of the M-dwarf secondaries ( $T_{\text{eff}}$ ,  $\log g$ , and [Fe/H]) as computed in this work.

**Table 8.** Parameters derived for the reference stars with different synthetic grids.

Reference star	Grid	$T_{\text{eff}}$ [K]	$\log g$ [dex]	[Fe/H] <sub>corr</sub> [dex]
GX And	BT-Settl	3603 ± 24	4.99 ± 0.14	-0.52 ± 0.11
	MARCS	3675 ± 30	4.90 ± 0.10	-0.45 ± 0.08
	PHOENIX-ACES	3664 ± 37	4.84 ± 0.12	-0.54 ± 0.13
Luyten's star	BT-Settl	3380 ± 43	4.96 ± 0.11	-0.11 ± 0.11
	MARCS	3429 ± 38	4.88 ± 0.10	-0.08 ± 0.09
	PHOENIX-ACES	3412 ± 50	4.81 ± 0.14	-0.19 ± 0.12
Teegarden's star	BT-Settl	3034 ± 45	5.19 ± 0.20	-0.11 ± 0.28
	MARCS	3072 ± 51	5.08 ± 0.16	-0.13 ± 0.24
	PHOENIX-ACES	3081 ± 57	5.10 ± 0.17	-0.24 ± 0.25

garden's star) with the aim of evaluating the impact of different sets of models on our parameter computations with STEPARSYN.

We first computed a synthetic grid based on MARCS models by following the same procedure as described in Sect. 3.3. We set the MARCS grid from 2500 K to 3900 K, 4.0 dex to 5.5 dex, and -1.0 dex to +1.0 dex, in steps of 100 K, 0.5 dex, and 0.25 dex in  $T_{\text{eff}}$ ,  $\log g$ , and [Fe/H], respectively. Similarly, we adopted the PHOENIX-ACES grid used by Passegger et al. (2021), which ranges from 2700 K to 4500 K, 4.2 dex to 5.5 dex, and -1.0 dex to +0.8 dex, in steps of 100 K, 0.1 dex, and 0.1 dex in  $T_{\text{eff}}$ ,  $\log g$ , and [Fe/H], respectively. While the MARCS grid is based on atmosphere models with standard composition and, thus, follows the same scaled  $[\alpha/\text{Fe}]$  pattern as the BT-Settl grid, the PHOENIX-ACES grid has  $[\alpha/\text{Fe}] = 0$  since models with  $[\alpha/\text{Fe}] \neq 0$  are only available for  $T_{\text{eff}} > 3500$  K (Husser et al. 2013; Passegger et al. 2018). Therefore, metallicities derived with the PHOENIX-ACES grid do not need to be corrected with the interpolation scheme described in Sect. 4.

In Table 8 we list the parameters obtained for the reference stars and the considered grids (i.e. BT-Settl, MARCS, and PHOENIX-ACES). The derived  $\log g$  and [Fe/H] values agree within the uncertainties for all models, while the average differences in  $T_{\text{eff}}$ ,  $\log g$ , and [Fe/H] between models are around 32 K, 0.11 dex, and 0.06 dex, respectively. In addition, the derived  $T_{\text{eff}}$  values appear to be slightly higher when using MARCS and PHOENIX-ACES models. In contrast,  $\log g$  values are slightly lower. The differences in these results might arise from the synthetic gap (Passegger et al. 2020), that is, the fact that synthetic spectra do not perfectly match the observed spectra as a result of the underlying chemo-physical assumptions (e.g. different equations of state). However, a more detailed study is required to further explore the origin of these small discrepancies.

## 5. Summary and conclusions

We have computed the stellar atmospheric parameters ( $T_{\text{eff}}$ ,  $\log g$ , [Fe/H], and [Fe/H]<sub>corr</sub>) of 343 M dwarfs observed with CARMENES with the STEPARSYN code as a Bayesian implementation of the spectral synthesis technique, along with a grid of BT-Settl models, and the radiative transfer code turbospectrum. We excluded one eclipsing binary, ten SB2 binaries, two triple-line spectroscopic triple systems, and three targets with low-quality spectra to prevent unreliable parameter determinations. To avoid any potential degeneracy in the M-dwarf parameter space, we imposed prior probability distributions in  $T_{\text{eff}}$  and  $\log g$  based on the comprehensive, multi-band photometric data available for the sample (Cifuentes et al. 2020). Our method is suited for the M sequence from M0.0 V to M7.0 V, but not beyond, due to the scarcity of Ti I and Fe I lines at M8.0 V and later spectral types, as well as the insensitivity of TiO bands to  $T_{\text{eff}}$  as a result of dust formation (Tsuiji et al. 1996; Allard et al. 2001).

We selected 75 Fe I and Ti I lines in the VIS and NIR wavelength regions covered by CARMENES. Following the prescriptions of Passegger et al. (2019), NIR lines with low Landé factors (i.e.  $g_{\text{eff}} < 1.5$ ) were selected to minimise the impact of the stellar magnetic field on parameter computations. Even so, some Fe I and Ti I lines appear to be highly sensitive to chromospheric activity and the stellar magnetic field and were excluded in the analysis of the active stars in our sample based on the H $\alpha$  flag. Such lines will be discussed in a future publication (López-Gallifa et al. in prep.).

We also compared our derived parameters with some recent M-dwarf studies in the literature (Rojas-Ayala et al. 2012; Maldonado et al. 2015, 2020; Mann et al. 2015; Rajpurohit et al.

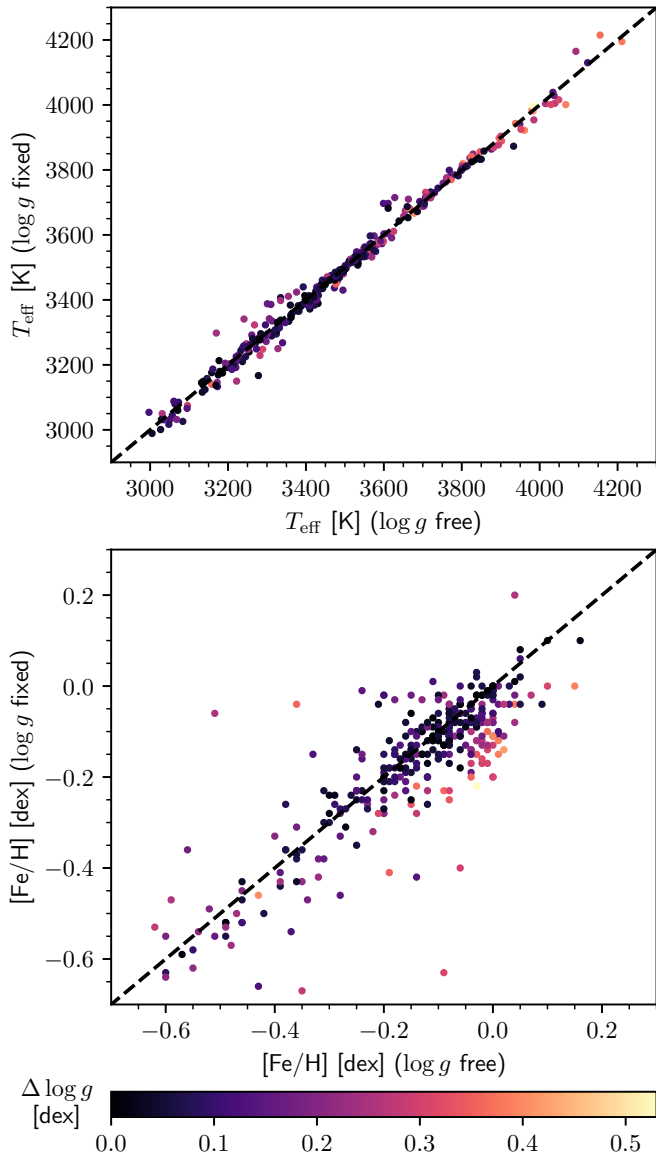


**Fig. 12.** Comparison of  $T_{\text{eff}}$  (top panel) and  $[\text{Fe}/\text{H}]$  (bottom panel) between the runs with free and fixed  $\log g$ . The quantity  $\Delta \log g$  is calculated as  $\log g$  (prior) –  $\log g$  (free).

2018b; Schweitzer et al. 2019; Passegger et al. 2018, 2019, 2020), finding similar  $T_{\text{eff}}$  but disparate metallicity scales. The metallicity determinations that correlate best with the literature are the  $[\text{Fe}/\text{H}]_{\text{corr}}$  values since they are corrected from the  $\alpha$  enhancement of the synthetic grid. The best agreement in metallicity is found when comparing with Mann et al. (2015), Gaidos & Mann (2014), and Rojas-Ayala et al. (2012). The M-dwarf metallicity distribution for our sample is also in agreement with both the Geneva-Copenhagen survey of FG-type stars in the solar neighbourhood (Nordström et al. 2004) and the kinematic membership of the targets in the Galactic populations (Cortés-Contreras et al. in prep.). Regarding  $\log g$ , we find larger values than the ones reported in the literature, although fixing  $\log g$  to the prior values does not have a strong impact on either the derived  $T_{\text{eff}}$  or the  $[\text{Fe}/\text{H}]$  scales. As a benchmark test, we placed special emphasis on the M dwarfs with interferometrically measured radii (Boyajian et al. 2012; von Braun et al. 2014), wide physical FGK+M binaries (Montes et al. 2018), and M+M sys-

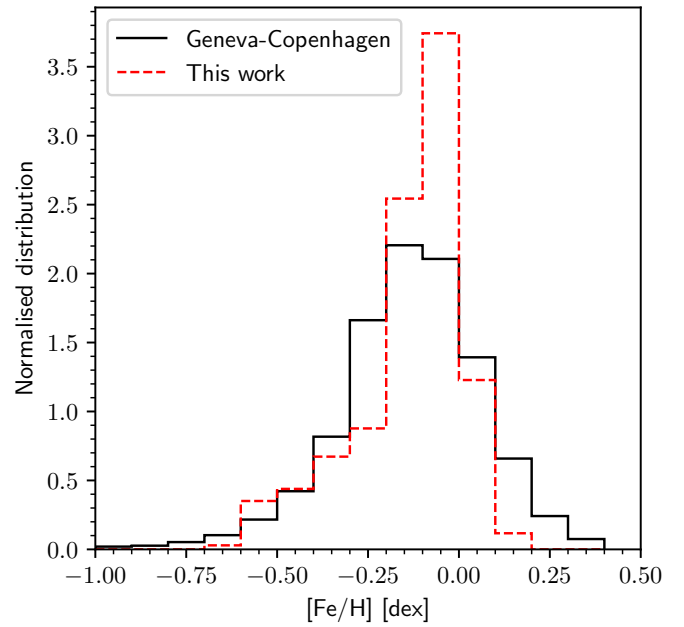


**Fig. 13.** Metallicity distribution in this work and in the Geneva-Copenhagen survey (Nordström et al. 2004).

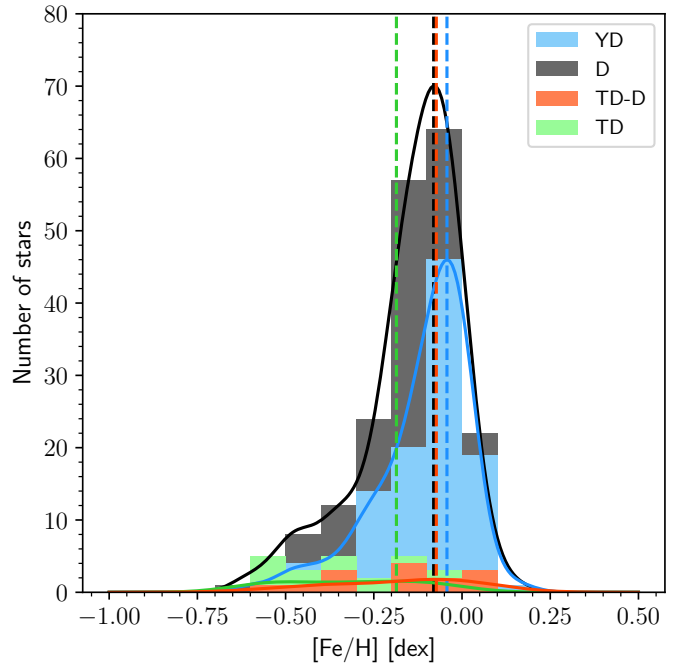


**Fig. 14.** M-dwarf metallicity distributions separated by the kinematic membership of the targets in the thick disc (TD), the thick disc-thin disc transition (TD-D), the thin disc (D), and the young disc (YD), following Cortés-Contreras et al. in prep. The vertical dashed lines indicate the peak of the distributions.

tems. Despite systematic offsets that are inherent to any methodology, we find that our parameter determinations are fairly consistent with the literature values in all these cases.

*Acknowledgements.* We thank the anonymous referee for the insightful comments and suggestions that improved the manuscript of the paper. CARMENES is an instrument for the Centro Astronómico Hispano en Andalucía at Calar Alto (CAHA). CARMENES is funded by the German Max-Plank Gesellschaft (MPG), the Spanish Consejo Superior de Investigaciones Científicas (CSIC),

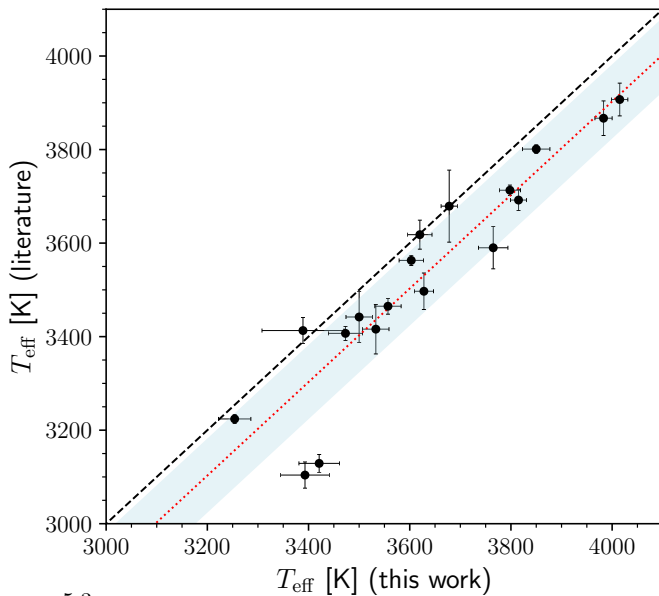


**Fig. 15.** Comparison in  $T_{\text{eff}}$  (upper panel) and  $\log g$  (bottom panel) for M dwarfs with interferometric angular measurements (see Table 6). The dashed black lines indicate the 1:1 relationship, whereas the dotted red lines show the 1:1 relationship, shifted following the average differences in each parameter. The blue shaded region denotes the  $1\sigma$  level.

the European Union through FEDER/ERF FICTS-2011-02 funds, and the members of the CARMENES Consortium (Max-Plank-Institut für Astronomie, Instituto de Astrofísica de Andalucía, Landessternwarte Königstuhl, Institut de Ciències de l'Espai, Institut für Astrophysik Göttingen, Universidad Complutense de Madrid, Thüringer Landessternwarte Tautenburg, Instituto de Astrofísica de Canarias, Hamburger Sternwarte, Centro de Astrobiología and Centro Astronómico Hispano-Andaluz), with additional contributions by the Spanish Ministry of Economy, the German Science Foundation through the Major Research Instrumentation Programme and DFG Research Unit FOR2544 "Blue Planets around Red Stars", the Klaus Tschira Stiftung, the states of Baden-Württemberg and Niedersachsen, and by the Junta de Andalucía. The authors acknowledge financial support from the Fundação para a Ciéncia e a Tecnologia (FCT) through the research grants UID/FIS/04434/2019, UIDB/04434/2020 and UIDP/04434/2020, national funds PTDC/FIS-AST/28953/2017, by FEDER (Fundo Europeu de Desenvolvimento Regional) through COMPETE2020 - Programa Operacional Competitividade e Internacionalização (POCI-01-0145-FEDER-028953), and the Spanish Ministerio de Ciencia, Innovación y Universidades, Ministerio de Economía y Competitividad, the Universidad Complutense de Madrid, and the Fondo Europeo de Desarrollo Regional (FEDER/ERF)

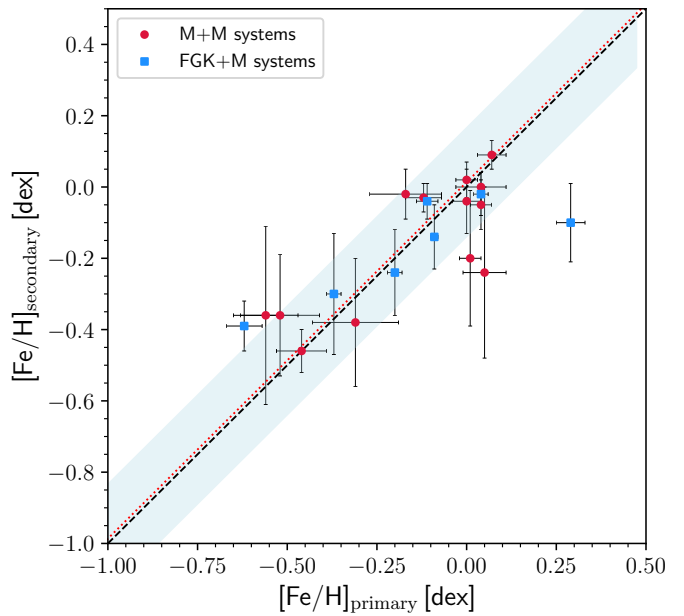


**Fig. 16.** Same as Fig. 15, but for the comparison in  $[{\text{Fe}}/{\text{H}}]$  between the components in FGK+M (blue) and M+M (red) systems (see Tables 7 and 9).

through fellowship FPU15/01476, and projects AYA2016-79425-C3-1/2/3-P, PID2019-109522GB-C5[1:4]/AEI/10.13039/501100011033, AYA2014-56359-P, BES-2017-080769, and RYC-2013-14875. The authors also acknowledge financial support from the Centre of Excellence "Severo Ochoa" and "María de Maeztu" awards to the Instituto de Astrofísica de Canarias (SEV-2015-0548), Instituto de Astrofísica de Andalucía (SEV-2017-0709), and Centro de Astrobiología (MDM-2017-0737), and the Generalitat de Catalunya/CERCA programme. This work has made use of the VALD database, operated at Uppsala University, the Institute of Astronomy RAS in Moscow, and the University of Vienna, and of data from the European Space Agency (ESA) mission *Gaia* (<https://www.cosmos.esa.int/gaia>), processed by the *Gaia* Data Processing and Analysis Consortium (DPAC, <https://www.cosmos.esa.int/web/gaia/dpac/consortium>). Funding for the DPAC has been provided by national institutions, in particular the institutions participating in the *Gaia* Multilateral Agreement. V. M. P. acknowledges financial support from NASA through grant NNX17AG24G. S. V. J. acknowledges the support of the DFG priority program SPP 1992 "Exploring the Diversity of Extrasolar Planets" (JE 701/5-1). E. M. would also like to warmly thank the staff at the Hamburger Sternwarte for their hospitality during his stay funded by project EST18/00162. Based on data from the CARMENES data archive at CAB (INTA-CSIC).

## References

- Abia, C., Tabernero, H. M., Korotin, S. A., et al. 2020, *A&A*, **642**, A227
- Allard, F., Hauschildt, P. H., Alexander, D. R., Tamanai, A., & Schweitzer, A. 2001, *ApJ*, **556**, 357
- Allard, F., Homeier, D., & Freytag, B. 2012, *Philosophical Transactions of the Royal Society of London Series A*, **370**, 2765
- Alonso-Floriano, F. J., Morales, J. C., Caballero, J. A., et al. 2015, *A&A*, **577**, A128
- Alonso-Floriano, F. J., Sánchez-López, A., Snellen, I. A. G., et al. 2019, *A&A*, **621**, A74
- Alonso-Santiago, J., Negueruela, I., Marco, A., et al. 2019, *A&A*, **631**, A124
- Alvarez, R. & Plez, B. 1998, *A&A*, **330**, 1109
- Antoniadis-Karnavas, A., Sousa, S. G., Delgado-Mena, E., et al. 2020, *A&A*, **636**, A9
- Asplund, M., Grevesse, N., Sauval, A. J., & Scott, P. 2009, *ARA&A*, **47**, 481
- Baraffe, I., Chabrier, G., Allard, F., & Hauschildt, P. H. 1998, *A&A*, **337**, 403
- Barber, R. J., Tennyson, J., Harris, G. J., & Tolchenov, R. N. 2006, *MNRAS*, **368**, 1087
- Baroch, D., Morales, J. C., Ribas, I., et al. 2021, *A&A*, **653**, A49
- Baroch, D., Morales, J. C., Ribas, I., et al. 2018, *A&A*, **619**, A32
- Barrado y Navascués, D., Stauffer, J. R., & Jayawardhana, R. 2004, *ApJ*, **614**, 386

**Table 9.** Astrometric and stellar atmospheric parameters of the M dwarfs bound in M+M systems in the CARMENES GTO sample.

Karmn	Name	SptT	$\pi$ [mas]	$\mu_\alpha \cos\delta$ [mas a <sup>-1</sup> ]	$\mu_\delta$ [mas a <sup>-1</sup> ]	$v_r$ [km s <sup>-1</sup> ]	$T_{\text{eff}}$ [K]	$\log g$ [dex]	[Fe/H] <sub>corr</sub> [dex]
J001622+198E	LP 404–062	M4.0 V	65.05 ± 0.04	708.14 ± 0.05	-748.88 ± 0.04	-1.62 ± 0.02	3329 ± 30	4.93 ± 0.07	-0.11 ± 0.09
J001622+198W	EZ Psc AB <sup>(a)</sup>	M4.0 V	65.11 ± 0.04	714.64 ± 0.05	-761.97 ± 0.04	-0.50 ± 0.04	...	...	...
J00183+440	GX And	M1.0 V	280.71 ± 0.02	2891.52 ± 0.02	411.83 ± 0.01	+11.48 ± 0.02	3603 ± 24	4.99 ± 0.14	-0.52 ± 0.11
J00184+440	GQ And	M3.5 V	280.69 ± 0.03	2862.80 ± 0.02	336.43 ± 0.02	+10.68 ± 0.03	3318 ± 53	5.20 ± 0.11	-0.36 ± 0.17
J01026+623	BD+61 195	M1.5 V	101.42 ± 0.02	731.09 ± 0.01	90.53 ± 0.02	-6.30 ± 0.02	3791 ± 19	4.76 ± 0.11	0.05 ± 0.06
J01033+623	V388 Cas	M5.0 V	101.37 ± 0.05	730.40 ± 0.04	85.97 ± 0.05	-6.52 ± 0.08	3057 ± 49	5.12 ± 0.18	-0.24 ± 0.24
J02489–145W	PM J02489–1432W	M2.0 V	26.57 ± 0.02	164.07 ± 0.03	46.55 ± 0.03	+32.27 ± 0.06	3655 ± 25	4.98 ± 0.10	0.04 ± 0.05
J02489–145E	PM J02489–1432E	M2.5 V	26.54 ± 0.02	174.43 ± 0.03	45.47 ± 0.03	+32.40 ± 0.06	3572 ± 27	4.94 ± 0.12	0.00 ± 0.04
J05365+113	V2689 Ori	M0.0 V	87.53 ± 0.02	-2.82 ± 0.03	-56.35 ± 0.02	+21.51 ± 0.02	4067 ± 14	5.04 ± 0.07	0.01 ± 0.03
J05366+112	PM J05366+1117	M4.0 V	87.35 ± 0.03	-3.32 ± 0.04	-60.84 ± 0.03	+21.53 ± 0.02	3355 ± 23	5.17 ± 0.16	-0.20 ± 0.10
J09143+526	HD 79210	M0.0 V	157.89 ± 0.02	-1545.79 ± 0.02	-569.05 ± 0.02	+10.69 ± 0.02	4015 ± 16	4.91 ± 0.08	-0.12 ± 0.05
J09144+526	HD 79211	M0.0 V	157.88 ± 0.02	-1573.04 ± 0.02	-659.91 ± 0.02	+11.90 ± 0.02	3983 ± 12	5.17 ± 0.07	-0.03 ± 0.04
J09425+700	GJ 360	M2.0 V	84.33 ± 0.02	-671.78 ± 0.02	-271.16 ± 0.02	+6.70 ± 0.02	3547 ± 23	5.02 ± 0.12	0.00 ± 0.03
J09428+700	GJ 362	M3.0 V	84.30 ± 0.02	-670.96 ± 0.02	-265.46 ± 0.02	+6.35 ± 0.03	3504 ± 30	5.06 ± 0.12	0.02 ± 0.05
J11054+435	BD+44 2051 A	M1.0 V	203.89 ± 0.03	-4406.47 ± 0.03	938.53 ± 0.03	+68.58 ± 0.02	3628 ± 19	5.01 ± 0.13	-0.56 ± 0.09
J11055+435	WX UMa	M5.5 V	203.83 ± 0.05	-4339.85 ± 0.05	960.70 ± 0.04	+69.16 ± 0.02	3278 ± 86	5.25 ± 0.20	-0.36 ± 0.25
J11110+304E	HD 97101 A	K7.0 V	84.18 ± 0.03	591.60 ± 0.02	-197.12 ± 0.03	-16.00 ± 0.03	4211 ± 13	4.98 ± 0.07	0.04 ± 0.03
J11110+304W	HD 97101 B	M2.0 V	84.16 ± 0.02	604.91 ± 0.02	-206.05 ± 0.02	-15.69 ± 0.02	3730 ± 20	4.78 ± 0.13	-0.05 ± 0.07
J14257+236W	BD+24 2733 A	M0.0 V	61.24 ± 0.02	792.55 ± 0.01	-1116.41 ± 0.02	+8.88 ± 0.02	3985 ± 13	4.89 ± 0.08	0.07 ± 0.04
J14257+236E	BD+24 2733 B	M0.5 V	61.20 ± 0.02	793.44 ± 0.01	-1118.91 ± 0.02	+7.96 ± 0.02	3933 ± 12	4.71 ± 0.11	0.09 ± 0.04
J16167+672S	HD 147379	M0.0 V	92.88 ± 0.01	-497.92 ± 0.02	84.05 ± 0.02	-19.36 ± 0.02	4034 ± 17	4.78 ± 0.09	0.00 ± 0.04
J16167+672N	EW Dra	M3.0 V	92.90 ± 0.02	-483.01 ± 0.02	89.05 ± 0.02	-18.78 ± 0.03	3569 ± 32	4.97 ± 0.11	-0.02 ± 0.06
J16554–083N	GJ 643	M3.5 V	153.88 ± 0.05	-817.58 ± 0.05	-898.60 ± 0.04	+15.50 ± 0.03	3397 ± 33	5.07 ± 0.12	-0.17 ± 0.10
J16555–083	vB 8	M7.0 V	153.97 ± 0.06	-813.04 ± 0.06	-870.61 ± 0.04	+14.41 ± 0.03	3005 ± 21	5.25 ± 0.18	-0.04 ± 0.09
J18427+596N	HD 173739	M3.0 V	283.84 ± 0.02	-1311.68 ± 0.03	1792.33 ± 0.03	-0.75 ± 0.08	3473 ± 34	4.90 ± 0.11	-0.31 ± 0.12
J18427+596S	HD 173740	M3.5 V	283.84 ± 0.03	-1400.26 ± 0.04	1862.53 ± 0.03	+1.02 ± 0.08	3493 ± 48	4.98 ± 0.12	-0.38 ± 0.18
J19070+208	Ross 730	M2.0 V	113.25 ± 0.03	-478.27 ± 0.02	-349.09 ± 0.03	+32.06 ± 0.02	3543 ± 21	5.03 ± 0.12	-0.46 ± 0.07
J19072+208	HD 349726	M2.0 V	113.22 ± 0.02	-480.75 ± 0.02	-332.50 ± 0.02	+31.83 ± 0.02	3558 ± 19	5.06 ± 0.10	-0.46 ± 0.06
J19169+051N	V1428 Aql <sup>(b)</sup>	M2.5 V	169.06 ± 0.02	-579.08 ± 0.03	-1332.87 ± 0.02	+35.61 ± 0.03	3575 ± 25	4.88 ± 0.12	-0.08 ± 0.08
J19169+051S	V1298 Aql <sup>(b)</sup>	M8.0 V	168.95 ± 0.07	-598.76 ± 0.07	-1366.06 ± 0.07	+35.73 ± 0.03	...	...	...
J20556–140N	GJ 810 Ab <sup>(a)</sup>	M4.0 V	84.86 ± 0.47	1416.62 ± 0.44	-472.38 ± 0.33	-142.10 ± 0.02	3193 ± 23	4.98 ...	-0.36 ± 0.11
J20556–140S	GJ 810 B	M5.0 V	80.20 ± 0.04	1420.76 ± 0.04	-472.27 ± 0.03	-142.04 ± 0.02	3193 ± 23	4.98 ± 0.10	-0.36 ± 0.11

**Notes.** Parallaxes ( $\pi$ ) and proper motions ( $\mu_\alpha \cos\delta, \mu_\delta$ ) from *Gaia* DR2 and DR3 (Gaia Collaboration et al. 2018, 2021). Radial velocities ( $v_r$ ) from Lafarga et al. (2020), except for J00162+198W and J20556–140N, which are from Baroch et al. (2018), and J02489–145E, J02489–145W, J11110+304E, and J18427+596S, which were computed with serval (Zechmeister et al. 2018, 2020).

<sup>(a)</sup>Double-line spectroscopic (SB2) binary (Baroch et al. 2018), <sup>(b)</sup>Spectral type M8.0 V or later.

- Bayo, A., Rodrigo, C., Barrado Y Navascués, D., et al. 2008, [A&A](#), **492**, 277
- Bell, C. P. M., Mamajek, E. E., & Naylor, T. 2015, [MNRAS](#), **454**, 593
- Bensby, T., Feltzing, S., & Lundström, I. 2003, [A&A](#), **410**, 527
- Bensby, T., Feltzing, S., Lundström, I., & Ilyin, I. 2005, [A&A](#), **433**, 185
- Bergemann, M., Collet, R., Schönrich, R., et al. 2017, [ApJ](#), **847**, 16
- Birky, J., Hogg, D. W., Mann, A. W., & Burgasser, A. 2020, [ApJ](#), **892**, 31
- Blanco-Cuaresma, S. 2019, [MNRAS](#), **486**, 2075
- Blanco-Cuaresma, S., Sobiran, C., Heiter, U., & Jofré, P. 2014, iSpec: Stellar atmospheric parameters and chemical abundances, Astrophysics Source Code Library
- Bochanski, J. J., Munn, J. A., Hawley, S. L., et al. 2007, [AJ](#), **134**, 2418
- Bocquet, S. & Carter, F. W. 2016, [The Journal of Open Source Software](#), **1**, 1
- Bonfils, X., Delfosse, X., Udry, S., et al. 2013, [A&A](#), **549**, A109
- Borsa, F., Allart, R., Casasayas-Barris, N., et al. 2021, [A&A](#), **645**, A24
- Boyajian, T. S., von Braun, K., van Belle, G., et al. 2012, [ApJ](#), **757**, 112
- Bressan, A., Marigo, P., Girardi, L., et al. 2012, [MNRAS](#), **427**, 127
- Brewer, J. M., Fischer, D. A., Valenti, J. A., & Piskunov, N. 2016, [ApJS](#), **225**, 32
- Buchhave, L. A., Latham, D. W., Johansen, A., et al. 2012, [Nature](#), **486**, 375
- Burrows, A., Marley, M., Hubbard, W. B., et al. 1997, [ApJ](#), **491**, 856
- Caballero, J. A., Cortés-Contreras, M., Alonso-Floriano, F. J., et al. 2016a, in 19th Cambridge Workshop on Cool Stars, Stellar Systems, and the Sun (CS19), **148**
- Caballero, J. A., Guàrdia, J., López del Fresno, M., et al. 2016b, in Society of Photo-Optical Instrumentation Engineers (SPIE) Conference Series, Vol. 9910, **9910-0E**
- Casagrande, L., Flynn, C., & Bessell, M. 2008, [MNRAS](#), **389**, 585
- Cifuentes, C., Caballero, J. A., Cortés-Contreras, M., et al. 2020, [A&A](#), **642**, A115
- Claudi, R., Benatti, S., Carleo, I., et al. 2018, in Society of Photo-Optical Instrumentation Engineers (SPIE) Conference Series, Vol. 10702, **107020Z**
- Clough, S. A., Shephard, M. W., Mlawer, E. J., et al. 2005, [J. Quant. Spectr. Rad. Transf.](#), **91**, 233
- Delfosse, X., Forveille, T., Perrier, C., & Mayor, M. 1998, [A&A](#), **331**, 581
- Delgado Mena, E., Israeli, G., González Hernández, J. I., et al. 2010, [ApJ](#), **725**, 2349
- Demangeon, O. D. S., Zapatero Osorio, M. R., Alibert, Y., et al. 2021, [A&A](#)
- Desidera, S., Gratton, R. G., Lucatello, S., & Claudi, R. U. 2006, [A&A](#), **454**, 581
- Donati, J. F., Kouach, D., Moutou, C., et al. 2020, [MNRAS](#), **498**, 5684
- Donati, J. F., Morin, J., Petit, P., et al. 2008, [MNRAS](#), **390**, 545
- Dressing, C. D. & Charbonneau, D. 2013, [ApJ](#), **767**, 95
- Dulick, M., Bauschlicher, C. W., Jr., Burrows, A., et al. 2003, [ApJ](#), **594**, 651
- Francis, P. J. & Wills, B. J. 1999, in Astronomical Society of the Pacific Conference Series, Vol. 162, Quasars and Cosmology, ed. G. Ferland & J. Baldwin, **363**
- Führmeister, B., Czesla, S., Hildebrandt, L., et al. 2020, [A&A](#), **640**, A52
- Führmeister, B., Czesla, S., Schmitt, J. H. M. M., et al. 2018, [A&A](#), **615**, A14
- Gaia Collaboration, Brown, A. G. A., Vallenari, A., et al. 2018, [A&A](#), **616**, A1
- Gaia Collaboration, Brown, A. G. A., Vallenari, A., et al. 2021, [A&A](#), **649**, A1
- Gaidos, E. & Mann, A. W. 2014, [ApJ](#), **791**, 54
- García Pérez, A. E., Allende Prieto, C., Holtzman, J. A., et al. 2016, [AJ](#), **151**, 144
- Goorvitch, D. 1994, [ApJS](#), **95**, 535
- Gray, D. F. 2008, The Observation and Analysis of Stellar Photospheres (Cambridge University Press)
- Gustafsson, B., Edvardsson, B., Eriksson, K., et al. 2008, [A&A](#), **486**, 951
- Heiter, U., Lind, K., Bergemann, M., et al. 2021, [A&A](#), **645**, A106
- Hejazi, N., Lépine, S., Homeier, D., Rich, R. M., & Shara, M. M. 2020, [AJ](#), **159**, 30
- Henry, T. J., Jao, W.-C., Winters, J. G., et al. 2018, [AJ](#), **155**, 265
- Hintz, D., Führmeister, B., Czesla, S., et al. 2019, [A&A](#), **623**, A136
- Hintz, D., Führmeister, B., Czesla, S., et al. 2020, [A&A](#), **638**, A115
- Howard, A. W., Marcy, G. W., Bryson, S. T., et al. 2012, [ApJS](#), **201**, 15
- Husser, T.-O., Wende-von Berg, S., Dreizler, S., et al. 2013, [A&A](#), **553**, A6
- Ishikawa, H. T., Aoki, W., Kotani, T., et al. 2020, [PASJ](#), **72**, 102
- Johnson, J. A., Aller, K. M., Howard, A. W., & Crepp, J. R. 2010, [PASP](#), **122**, 905
- Kausch, W., Noll, S., Smette, A., et al. 2015, [A&A](#), **576**, A78
- Khata, D., Mondal, S., Das, R., Ghosh, S., & Ghosh, S. 2020, [MNRAS](#), **493**, 4533
- Kirkpatrick, J. D., Henry, T. J., & McCarthy, Donald W. J. 1991, [ApJS](#), **77**, 417
- Kopparapu, R. K., Ramirez, R., Kasting, J. F., et al. 2013, [ApJ](#), **765**, 131
- Kotani, T., Tamura, M., Nishikawa, J., et al. 2018, in Society of Photo-Optical Instrumentation Engineers (SPIE) Conference Series, Vol. 10702, **1070211**
- Kurucz, R. L. 2014, Problems with Atomic and Molecular Data: Including All the Lines (Springer, Cham), 63–73
- Lafarga, M., Ribas, I., Lovis, C., et al. 2020, [A&A](#), **636**, A36
- Landi Degl'Innocenti, E. & Landolfi, M. 2004, Polarization in Spectral Lines, Vol. 307 (Springer Netherlands)
- Laughlin, G., Bodenheimer, P., & Adams, F. C. 1997, [ApJ](#), **482**, 420
- Li, J., Liu, C., Zhang, B., et al. 2021, [ApJS](#), **253**, 45
- Lohr, M. E., Negueruela, I., Tabernero, H. M., et al. 2018, [MNRAS](#), **478**, 3825
- Luck, R. E. 2017, [AJ](#), **153**, 21
- Luque, R., Pallé, E., Kossakowski, D., et al. 2019, [A&A](#), **628**, A39
- Mahadevan, S., Ramsey, L., Bender, C., et al. 2012, in Society of Photo-Optical Instrumentation Engineers (SPIE) Conference Series, Vol. 8446, **84461S**
- Maldonado, J., Affer, L., Micela, G., et al. 2015, [A&A](#), **577**, A132
- Maldonado, J., Micela, G., Baratella, M., et al. 2020, [A&A](#), **644**, A68
- Mamajek, E. E., Bartlett, J. L., Seifahrt, A., et al. 2013, [AJ](#), **146**, 154
- Mann, A. W., Brewer, J. M., Gaidos, E., Lépine, S., & Hilton, E. J. 2013a, [AJ](#), **145**, 52
- Mann, A. W., Deacon, N. R., Gaidos, E., et al. 2014, [AJ](#), **147**, 160
- Mann, A. W., Feiden, G. A., Gaidos, E., Boyajian, T., & von Braun, K. 2015, [ApJ](#), **804**, 64
- Mann, A. W., Gaidos, E., & Ansdel, M. 2013b, [ApJ](#), **779**, 188
- Marfil, E., Tabernero, H. M., Montes, D., et al. 2020, [MNRAS](#), **492**, 5470
- Masseron, T., Merle, T., & Hawkins, K. 2016, BACCHUS: Brussels Automatic Code for Characterizing High accuracy Spectra, Astrophysics Source Code Library
- McKemmish, L. K., Yurchenko, S. N., & Tennyson, J. 2016, [MNRAS](#), **463**, 771
- Miret-Roig, N., Galli, P. A. B., Brandner, W., et al. 2020, [A&A](#), **642**, A179
- Montes, D., González-Peinado, R., Tabernero, H. M., et al. 2018, [MNRAS](#), **479**, 1332
- Montes, D., López-Gallifa, A., Labarga, F., et al. 2020, in Contributions to the XIV.0 Scientific Meeting (virtual) of the Spanish Astronomical Society, **168**
- Montes, D., López-Santiago, J., Gálvez, M. C., et al. 2001, [MNRAS](#), **328**, 45
- Morales, J. C., Ribas, I., Jordi, C., et al. 2009, [ApJ](#), **691**, 1400
- Morton, D. C. 2000, [ApJS](#), **130**, 403
- Nagel, E. 2019, PhD thesis, Universität Hamburg
- Neves, V., Bonfils, X., Santos, N. C., et al. 2012, [A&A](#), **538**, A25
- Neves, V., Bonfils, X., Santos, N. C., et al. 2014, [A&A](#), **568**, A121
- Newton, E. R., Charbonneau, D., Irwin, J., et al. 2014, [AJ](#), **147**, 20
- Nordström, B., Mayor, M., Andersen, J., et al. 2004, [A&A](#), **418**, 989
- Nortmann, L., Pallé, E., Salz, M., et al. 2018, [Science](#), **362**, 1388
- Olander, T., Heiter, U., & Kochukhov, O. 2021, [A&A](#), **649**, A103
- Önehag, A., Heiter, U., Gustafsson, B., et al. 2012, [A&A](#), **542**, A33
- Passegger, V. M., Bello-García, A., Ordieres-Meré, J., et al. 2021, [A&A](#), submitted
- Passegger, V. M., Bello-García, A., Ordieres-Meré, J., et al. 2020, [A&A](#), **642**, A22
- Passegger, V. M., Reiners, A., Jeffers, S. V., et al. 2018, [A&A](#), **615**, A6
- Passegger, V. M., Schweitzer, A., Shulyak, D., et al. 2019, [A&A](#), **627**, A161
- Passegger, V. M., Wende-von Berg, S., & Reiners, A. 2016, [A&A](#), **587**, A19
- Plez, B. 2012, Turbospectrum: Code for spectral synthesis, Astrophysics Source Code Library
- Quirrenbach, A., Amado, P. J., et al. 2020, in Society of Photo-Optical Instrumentation Engineers (SPIE) Conference Series, Vol. 11447, **114473C**
- Rajpurohit, A. S., Allard, F., Rajpurohit, S., et al. 2018a, [A&A](#), **620**, A180
- Rajpurohit, A. S., Allard, F., Teixeira, G. D. C., et al. 2018b, [A&A](#), **610**, A19
- Rajpurohit, A. S., Reyé, C., Allard, F., et al. 2014, [A&A](#), **564**, A90
- Rajpurohit, A. S., Reyé, C., Schultheis, M., et al. 2012, [A&A](#), **545**, A85
- Reiners, A., Zechmeister, M., Caballero, J. A., et al. 2018, [A&A](#), **612**, A49
- Reylé, C., Jardine, K., Fouqué, P., et al. 2021, [A&A](#), **650**, A201
- Rojas-Ayala, B., Covey, K. R., Muirhead, P. S., & Lloyd, J. P. 2012, [ApJ](#), **748**, 93
- Rothman, L. S., Gordon, I. E., Barbe, A., et al. 2009, [J. Quant. Spectr. Rad. Transf.](#), **110**, 533
- Rybchikova, T., Piskunov, N., Kurucz, R. L., et al. 2015, [Phys. Scr](#), **90**, 054005
- Sabotta, S., Schlecker, M., Chaturvedi, P., et al. 2021, [A&A](#), **653**, A114
- Sarmiento, P., Rojas-Ayala, B., Delgado Mena, E., & Blanco-Cuaresma, S. 2021, [A&A](#), **649**, A147
- Sarro, L. M., Ordieres-Meré, J., Bello-García, A., González-Marcos, A., & Solano, E. 2018, [MNRAS](#), **476**, 1120
- Scalo, J., Kaltenegger, L., Segura, A. G., et al. 2007, [Astrobiology](#), **7**, 85
- Schöfer, P., Jeffers, S. V., Reiners, A., et al. 2019, [A&A](#), **623**, A44
- Schwab, C., Rakich, A., Gong, Q., et al. 2016, in Ground-based and Airborne Instrumentation for Astronomy VI, Vol. 9908, **99087H**
- Schweitzer, A., Passegger, V. M., Cifuentes, C., et al. 2019, [A&A](#), **625**, A68
- Seifahrt, A., Bean, J. L., Stürmer, J., et al. 2020, in Society of Photo-Optical Instrumentation Engineers (SPIE) Conference Series, Vol. 11447, **114471F**
- Selsis, F., Kasting, J. F., Levrard, B., et al. 2007, [A&A](#), **476**, 1373
- Shan, Y., Reiners, A., Fabbian, D., et al. 2021, [A&A](#), in press
- Shulyak, D., Reiners, A., Nagel, E., et al. 2019, [A&A](#), **626**, A86
- Smette, A., Sana, H., Noll, S., et al. 2015, [A&A](#), **576**, A77
- Souto, D., Cunha, K., Smith, V. V., et al. 2020, [ApJ](#), **890**, 133
- Tabernero, H. M., Dorda, R., Negueruela, I., & González-Fernández, C. 2018, [MNRAS](#), **476**, 3106
- Tabernero, H. M., Marfil, E., Montes, D., & González Hernández, J. I. 2019, [A&A](#), **628**, A131
- Tabernero, H. M., Marfil, E., Montes, D., & González Hernández, J. I. 2021, arXiv e-prints, arXiv:2110.00444

- Tal-Or, L., Zechmeister, M., Reiners, A., et al. 2018, [A&A](#), **614**, A122  
Terrien, R. C., Mahadevan, S., Bender, C. F., et al. 2012, [ApJ](#), **747**, L38  
Tinney, C. G. & Reid, I. N. 1998, [MNRAS](#), **301**, 1031  
Trifonov, T., Kürster, M., Zechmeister, M., et al. 2018, [A&A](#), **609**, A117  
Trifonov, T., Lee, M. H., Kürster, M., et al. 2020, [A&A](#), **638**, A16  
Tsuji, T., Ohnaka, K., & Aoki, W. 1996, [A&A](#), **305**, L1  
Valenti, J. A. & Fischer, D. A. 2005, [ApJS](#), **159**, 141  
Van Rossum, G. 2020, The Python Library Reference, release 3.8.2 (Python Software Foundation)  
Veyette, M. J., Muirhead, P. S., Mann, A. W., & Allard, F. 2016, [ApJ](#), **828**, 95  
Veyette, M. J., Muirhead, P. S., Mann, A. W., et al. 2017, [ApJ](#), **851**, 26  
Virtanen, P., Gommers, R., Oliphant, T. E., et al. 2020, [Nature Methods](#), **17**, 261  
von Braun, K., Boyajian, T. S., van Belle, G. T., et al. 2014, [MNRAS](#), **438**, 2413  
Wildi, F., Blind, N., Reshetov, V., et al. 2017, in Society of Photo-Optical Instrumentation Engineers (SPIE) Conference Series, Vol. 10400, [1040018](#)  
Wilson, J. C., Hearty, F., Skrutskie, M. F., et al. 2010, in Society of Photo-Optical Instrumentation Engineers (SPIE) Conference Series, Vol. 7735, [77351C](#)  
Winn, J. N. & Fabrycky, D. C. 2015, [ARA&A](#), **53**, 409  
Yan, F., Casasayas-Barris, N., Molaverdikhani, K., et al. 2019, [A&A](#), **632**, A69  
Zechmeister, M., Dreizler, S., Ribas, I., et al. 2019, [A&A](#), **627**, A49  
Zechmeister, M., Reiners, A., Amado, P. J., et al. 2018, [A&A](#), **609**, A12  
Zechmeister, M., Reiners, A., Amado, P. J., et al. 2020, SERVAL: SpEctrum Radial Velocity AnaLyser, Astrophysics Source Code Library

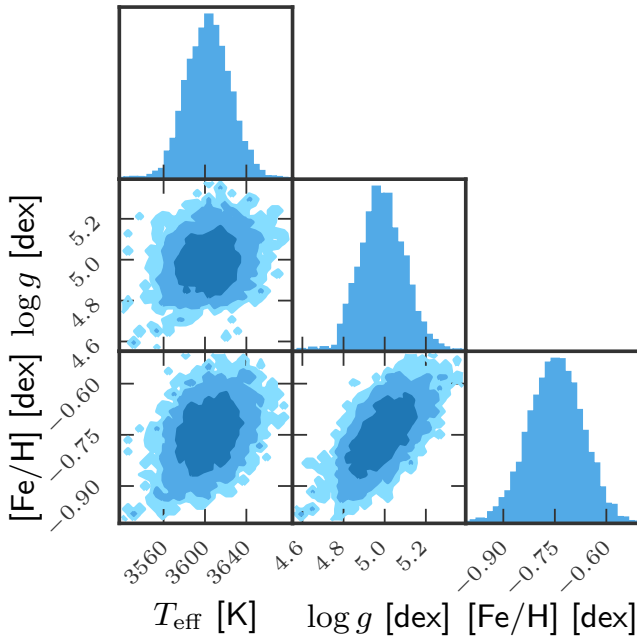


**Fig. A.1.** Same as Fig. 5, but for GX And (M1.0 V, J00183+440). The retrieved parameters are  $T_{\text{eff}} = 3603 \pm 24$  K,  $\log g = 4.99 \pm 0.14$  dex, and  $[\text{Fe}/\text{H}] = -0.75 \pm 0.11$  dex.

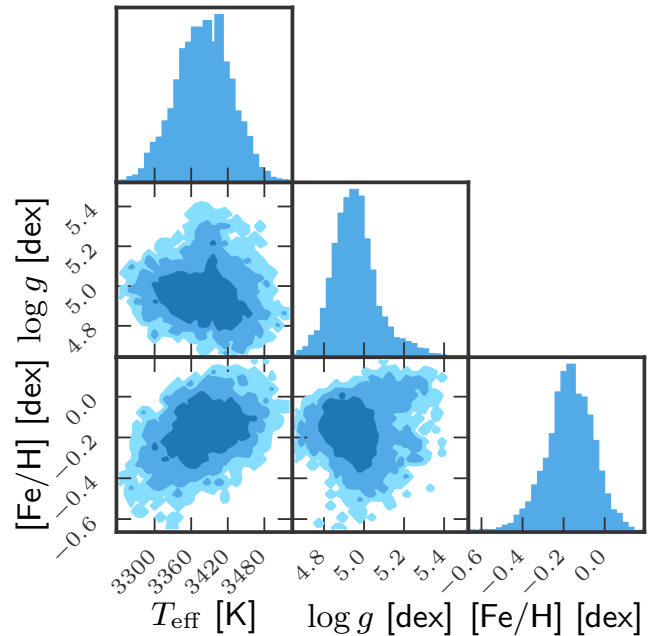
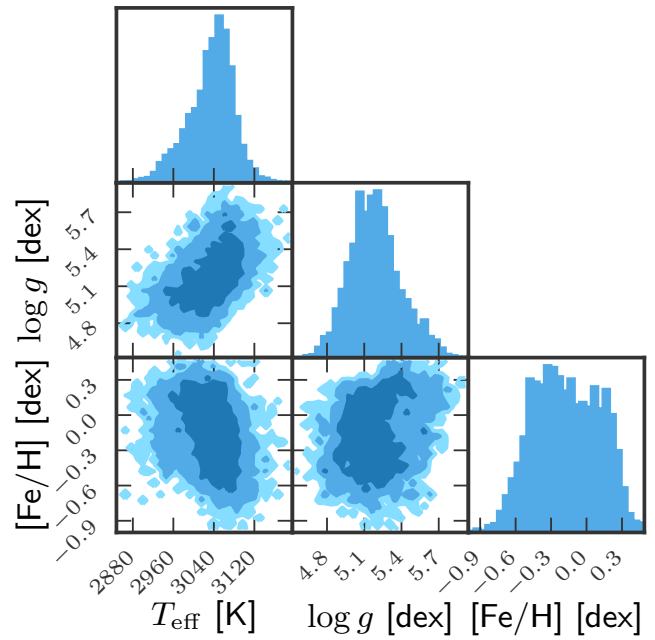


**Fig. A.2.** Same as Fig. 5, but for Luyten's star (M3.5 V, J07274+052). The retrieved parameters are  $T_{\text{eff}} = 3380 \pm 43$  K,  $\log g = 4.96 \pm 0.11$  dex, and  $[\text{Fe}/\text{H}] = -0.17 \pm 0.11$  dex.

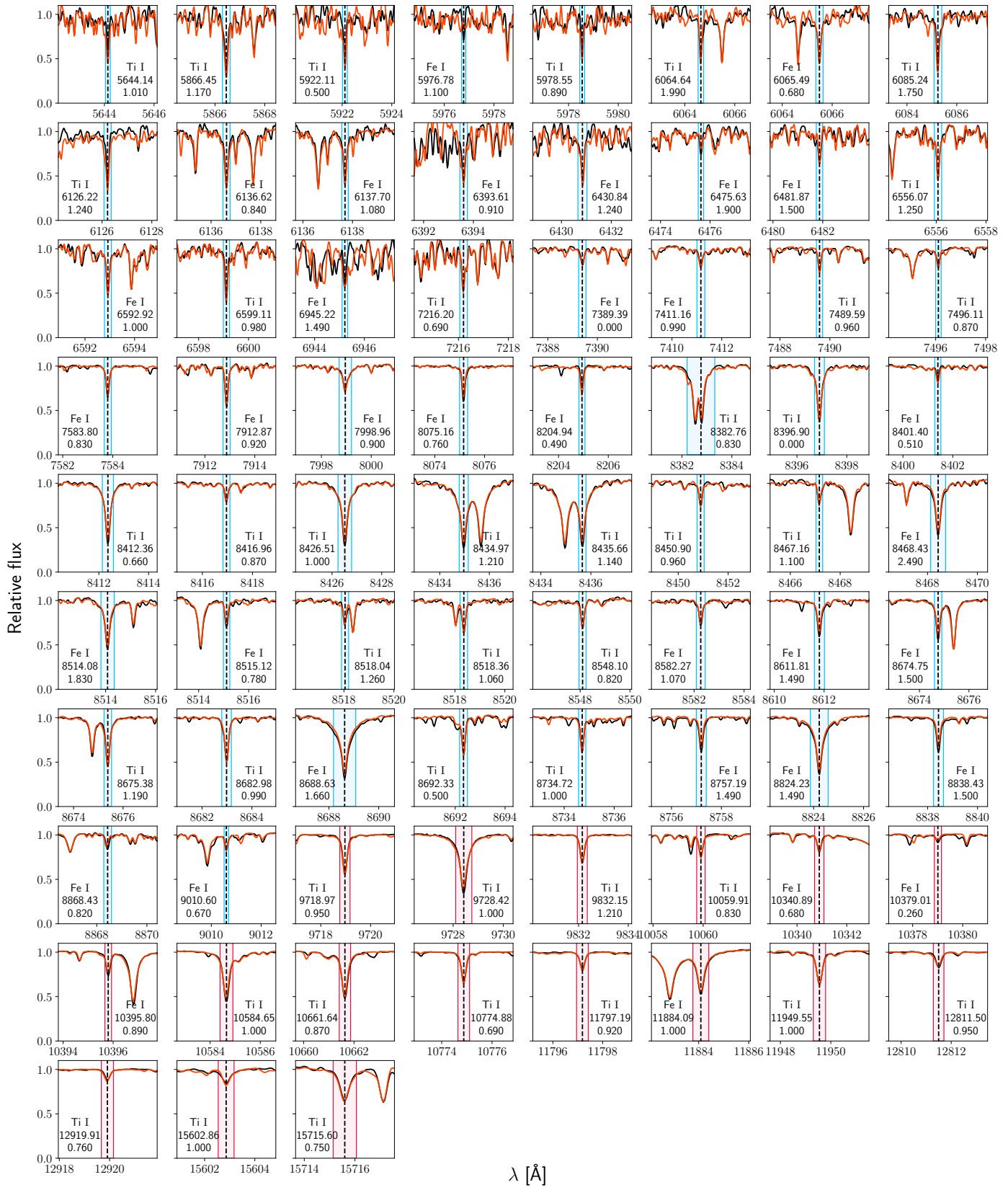
## Appendix A: Additional figures

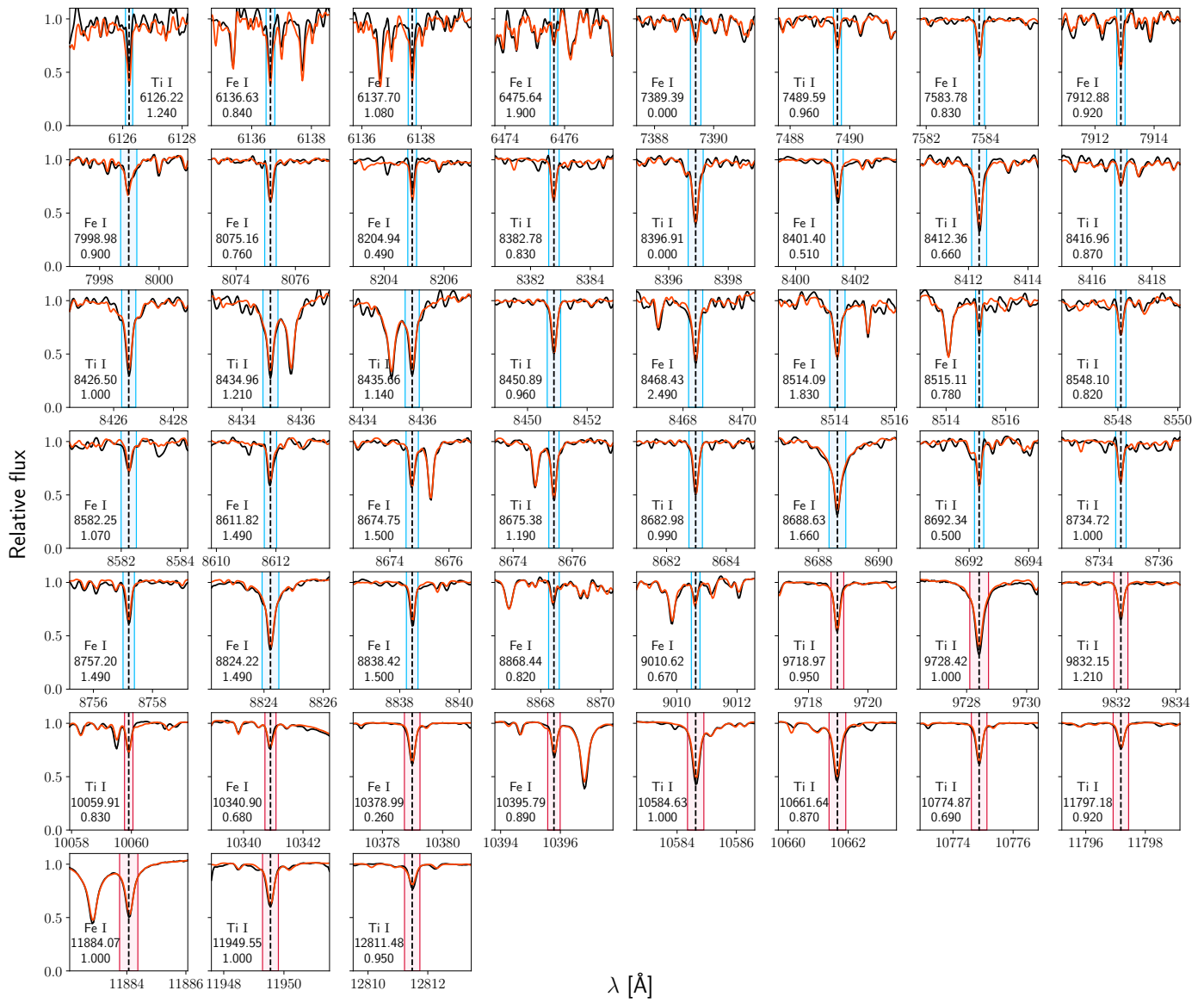
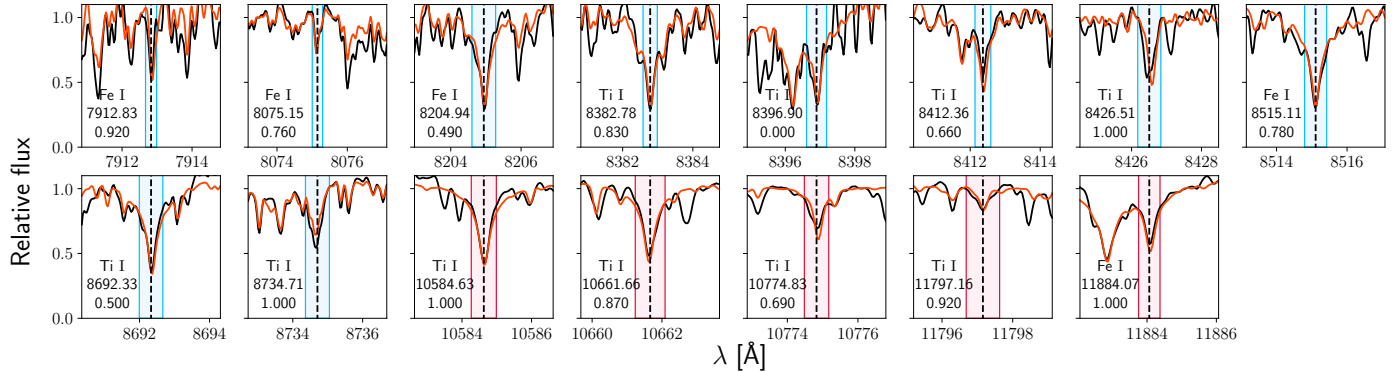
Figures A.1, A.2, and A.3 show the marginalised posterior distributions in  $T_{\text{eff}}$ ,  $\log g$ , and  $[\text{Fe}/\text{H}]$  for the reference stars, namely GX And, Luyten's star, and Teegarden's star, respectively (see Table 2). The best synthetic fits for the atomic lines and molecular bands for these stars can be found in Figs. A.4, A.5, A.6, A.7, A.8, and A.9.

Figures A.10, A.11, A.12, A.13, A.14, A.15, A.16, A.17, and A.18 show the comparison between our results and those of Rojas-Ayala et al. (2012), Gaidos & Mann (2014), Maldonado et al. (2015), Mann et al. (2015), Passegger et al. (2018), Rajpurohit et al. (2018a), Schweitzer et al. (2019), Maldonado et al. (2020), and Passegger et al. (2020), respectively, as discussed in Sect. 4.



**Fig. A.3.** Same as Fig. 5, but for Teegarden's star (M7.0 V, J02530+168). The retrieved parameters are  $T_{\text{eff}} = 3034 \pm 45$  K,  $\log g = 5.19 \pm 0.20$  dex, and  $[\text{Fe}/\text{H}] = -0.17 \pm 0.28$  dex.

**Fig. A.4.** Same as Fig. 6, but for GX And (M1.0 V, J00183+440).

**Fig. A.5.** Same as Fig. 6, but for Luyten's star (M3.5 V, J07274+052).**Fig. A.6.** Same as Fig. 6, but for Teegarden's star (M7.0 V, J02530+168).

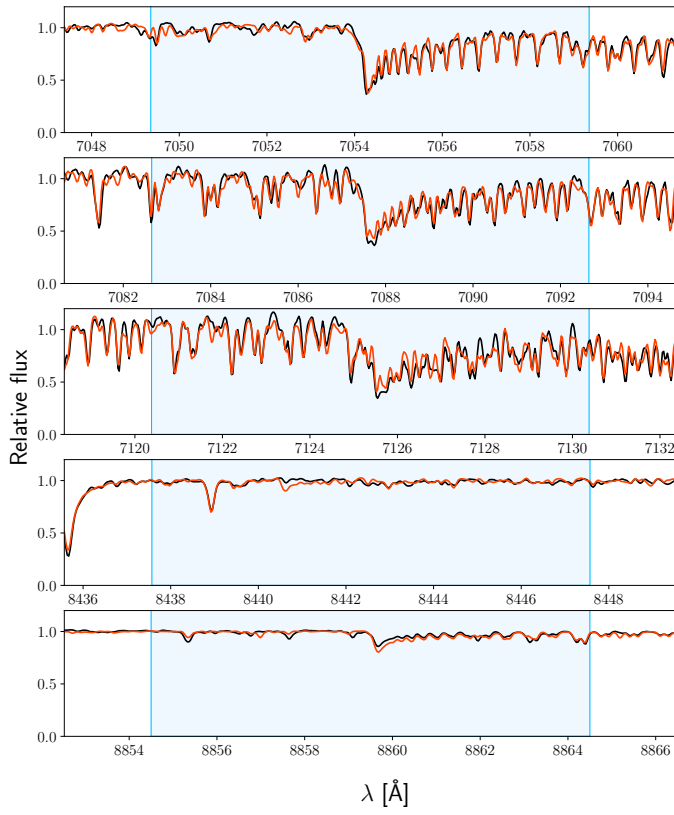


**Fig. A.7.** Same as Fig. 7, but for GX And (M1.0 V, J00183+440).

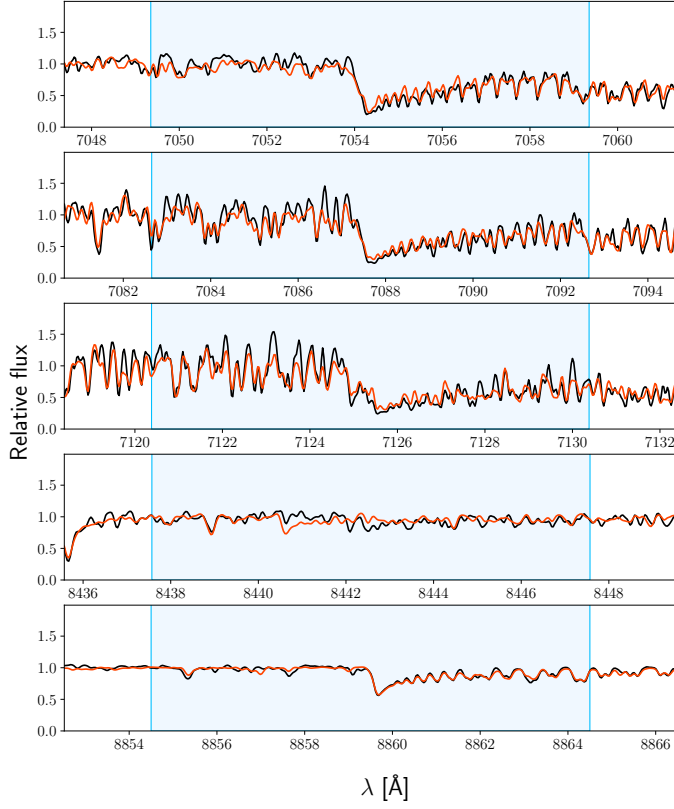


**Fig. A.8.** Same as Fig. 7, but for Luyten's star (M3.5 V, J07274+052).

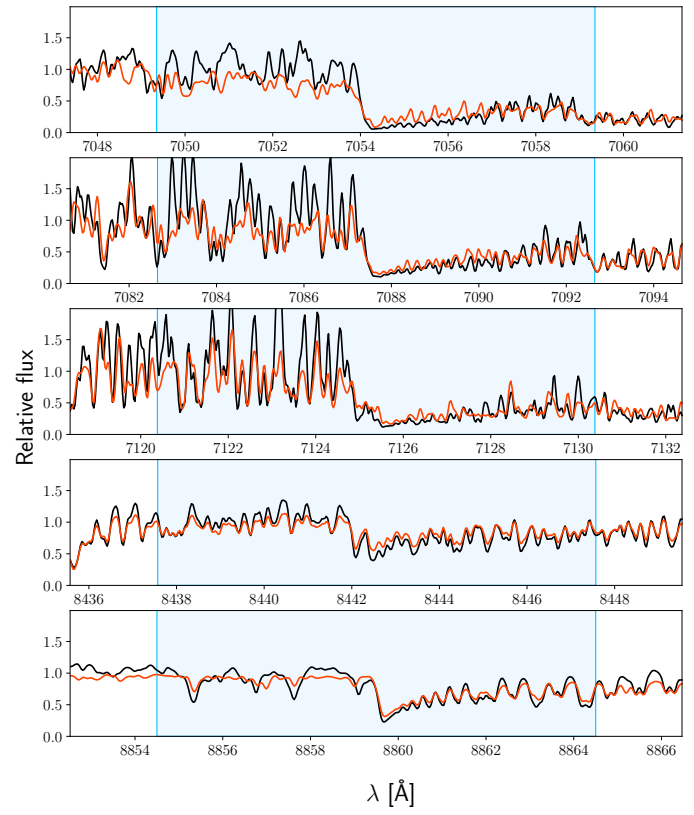


**Fig. A.9.** Same as Fig. 7, but for Teegarden's star (M7.0 V, J02530+168).

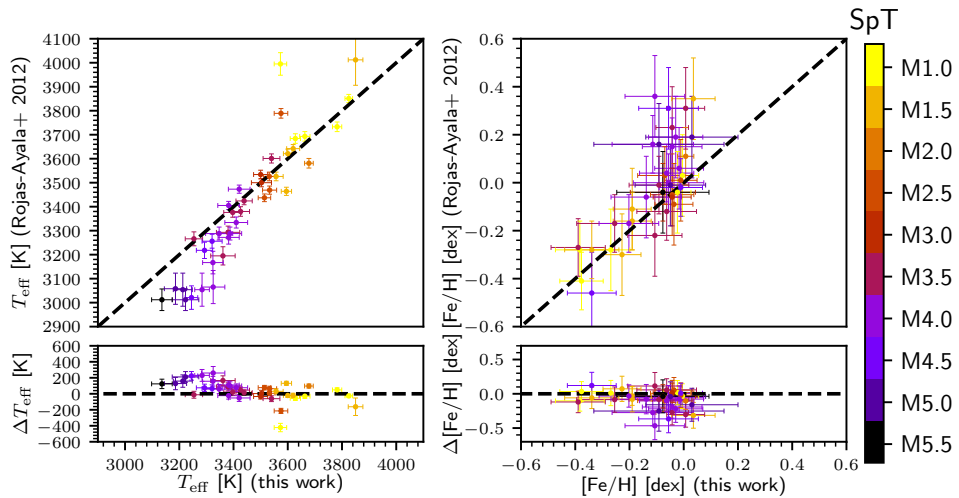


**Fig. A.10.** Comparison between this work and Rojas-Ayala et al. (2012).

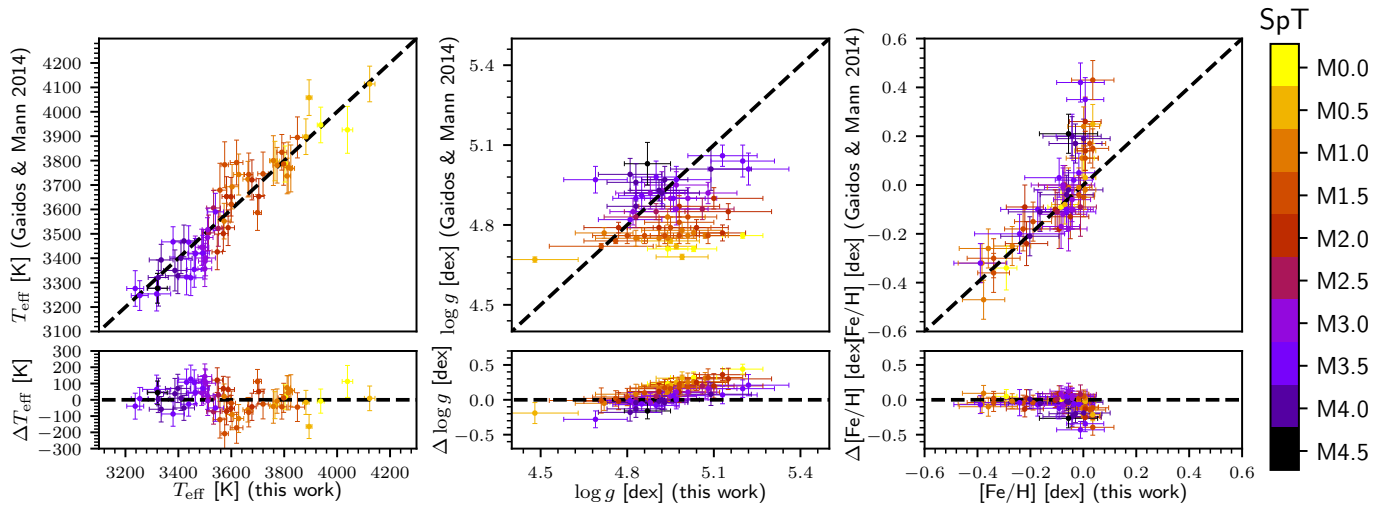


**Fig. A.11.** Comparison between this work and Gaidos & Mann (2014).

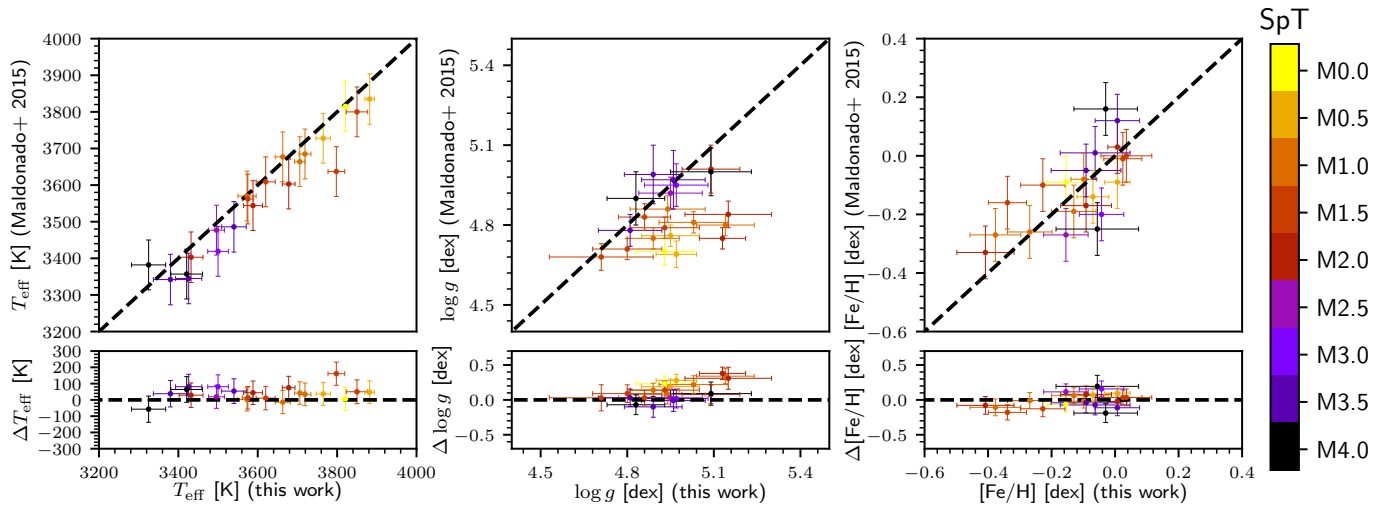


**Fig. A.12.** Comparison between this work and Maldonado et al. (2015).

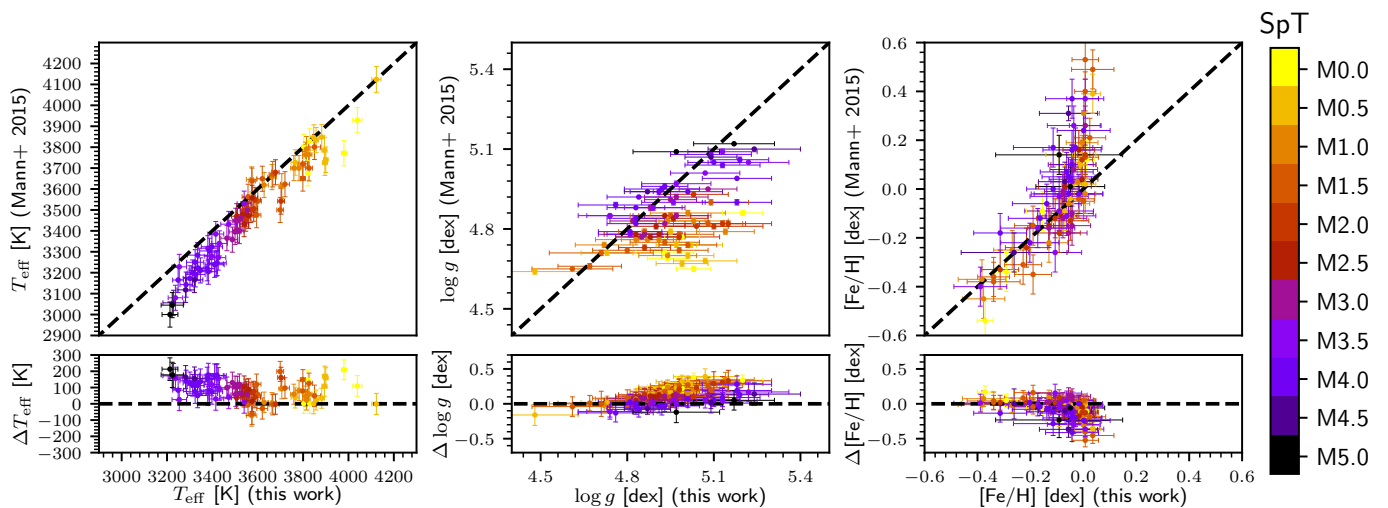


**Fig. A.13.** Comparison between this work and [Mann et al. \(2015\)](#).

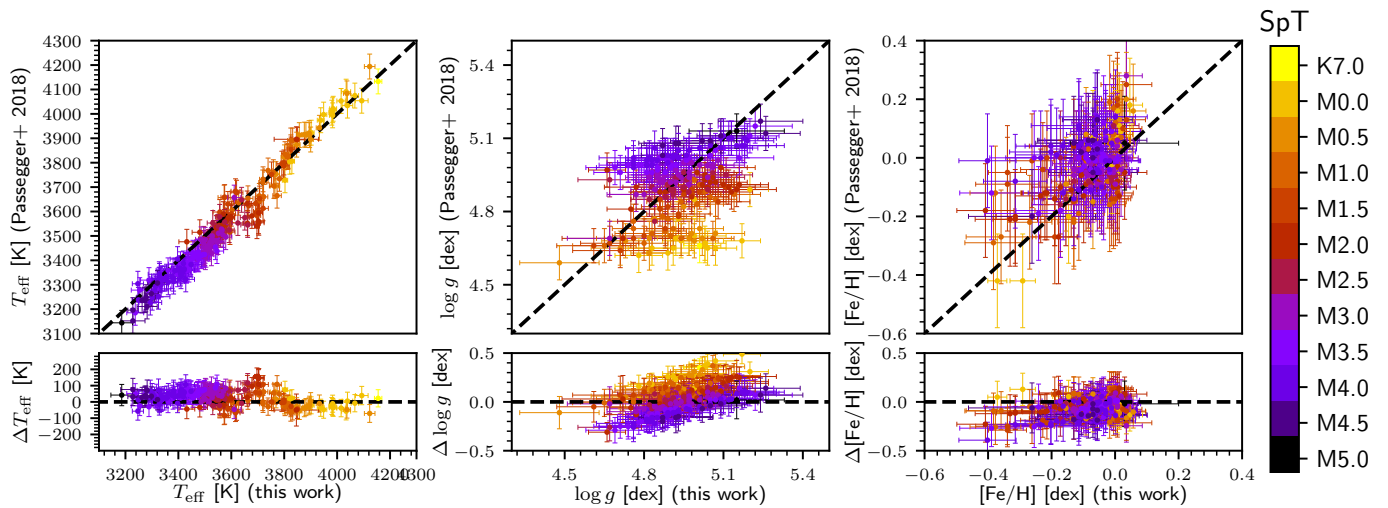


**Fig. A.14.** Comparison between this work and [Passegger et al. \(2018\)](#).

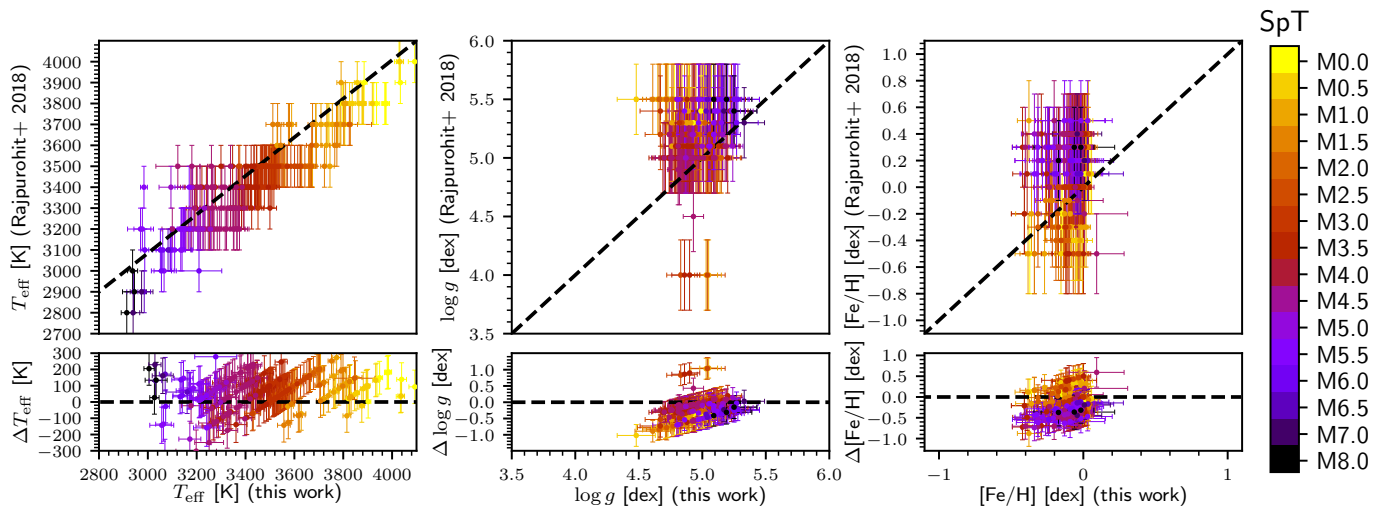


**Fig. A.15.** Comparison between this work and [Rajpurohit et al. \(2018a\)](#).

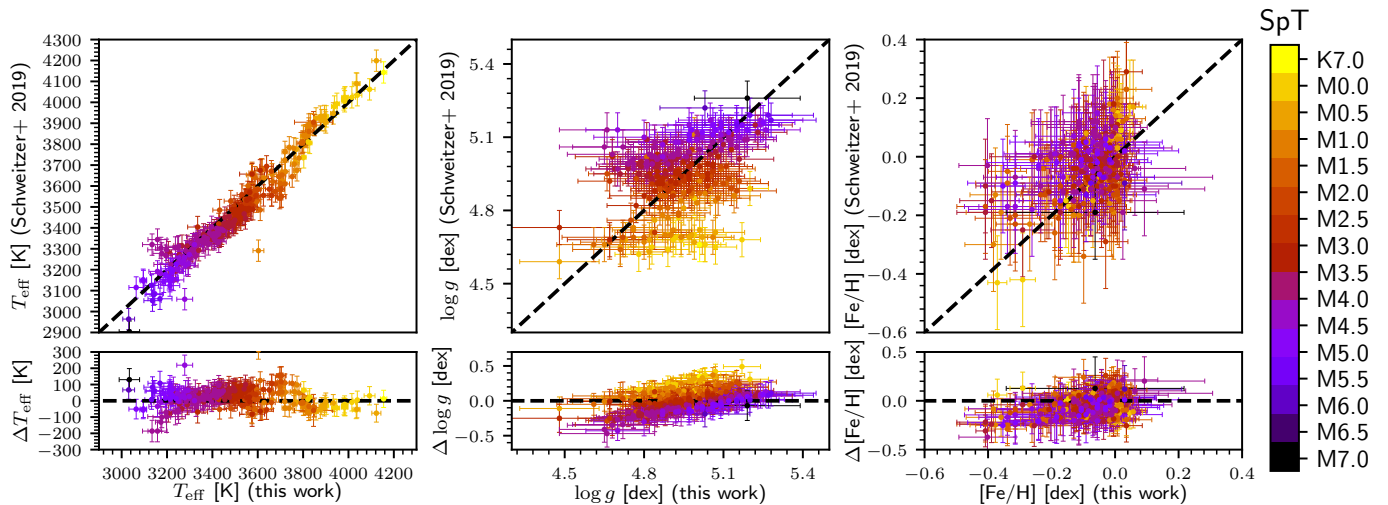


**Fig. A.16.** Comparison between this work and [Schweitzer et al. \(2019\)](#).

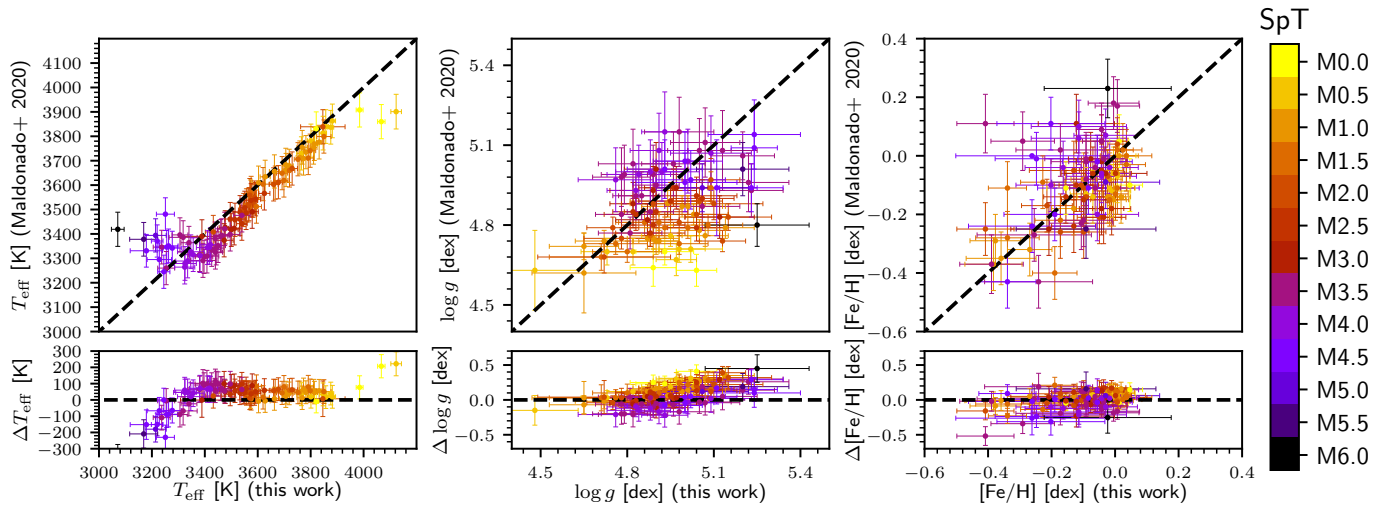


**Fig. A.17.** Comparison between this work and [Maldonado et al. \(2020\)](#).

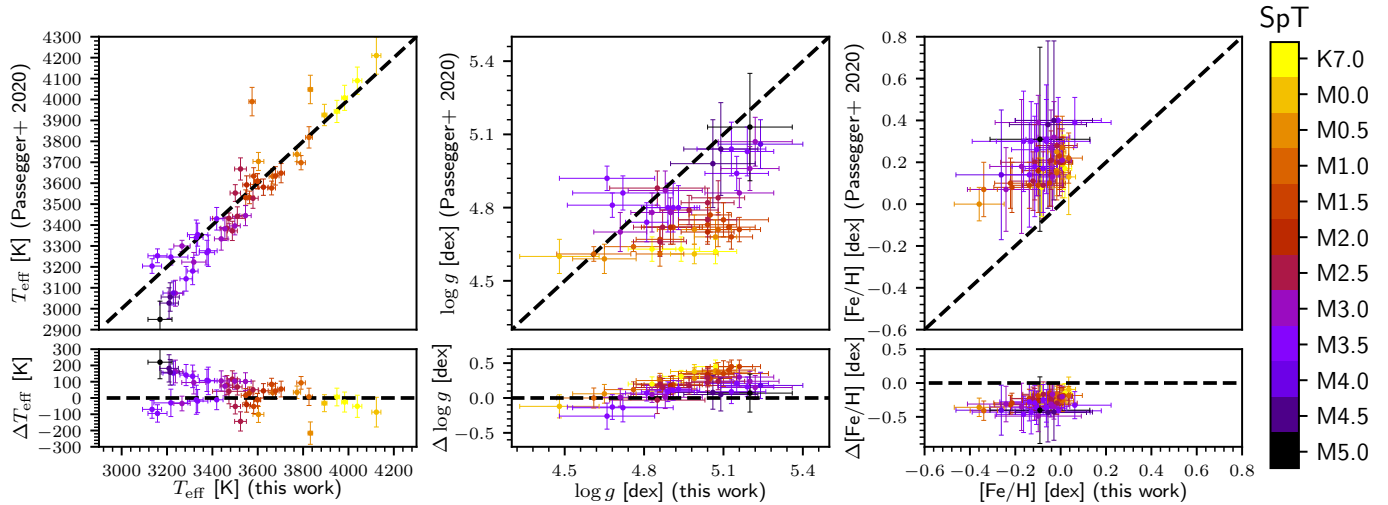


**Fig. A.18.** Comparison between this work and [Passegger et al. \(2020\)](#).

## Appendix B: Additional tables

Table B.1 contains the sample of 343 M dwarfs from the CARMENES GTO survey analysed in this work. Table B.2 displays the spectral ranges synthesised around the selected Fe I and Ti I lines according to the template spectra of GX And, Luyten's star, and Teegarden's star, as explained in Sect. 3.2. Table B.3 shows the adopted prior distributions in  $T_{\text{eff}}$  and  $\log g$  along with the stellar atmospheric parameters of the sample computed with STEPARSYN, as discussed in Sects. 3.4 and 4.

**Table B.1.** Sample of M dwarfs from the CARMENES radial velocity survey analysed in this work.

Karmn	Name	SpT <sup>(a)</sup>	$v_r$ [km s <sup>-1</sup> ]	Ref. <sup>(b)</sup>	$v \sin i$ <sup>(c)</sup> [km s <sup>-1</sup> ]	S/N	H $\alpha$ flag <sup>(d)</sup>
J04167-120	LP 714-47	K7.0 V	-7.45 ± 0.05	This work	≤ 2.0	258	0
J11110+304E	HD 97101	K7.0 V	-16.00 ± 0.03	This work	≤ 2.0	422	0
J18198-019	HD 168442	K7.0 V	-14.03 ± 0.03	Laf20	≤ 3.0	1447	0
J03463+262	HD 23453	M0.0 V	35.59 ± 0.02	Laf20	3.3 ± 4.0	728	0
J04376+528	BD+52 857	M0.0 V	33.91 ± 0.01	Laf20	3.4 ± 1.5	1167	0
J04588+498	BD+49 1280	M0.0 V	-34.35 ± 0.02	Laf20	≤ 2.0	877	0
J05365+113	V2689 Ori	M0.0 V	21.51 ± 0.02	Laf20	3.8 ± 1.5	1291	1
J06371+175	HD 260655	M0.0 V	-58.75 ± 0.02	Laf20	≤ 2.0	780	0
J07393+021	BD+02 1729	M0.0 V	19.53 ± 0.02	Laf20	≤ 2.0	606	0
J09143+526	HD 79210	M0.0 V	10.69 ± 0.02	Laf20	≤ 3.0	681	0
J09144+526	HD 79211	M0.0 V	11.90 ± 0.02	Laf20	2.3 ± 1.5	1237	0
J09561+627	BD+63 869	M0.0 V	14.92 ± 0.02	Laf20	≤ 2.0	789	0
J12123+544S	HD 238090	M0.0 V	-17.67 ± 0.02	Laf20	≤ 2.0	1138	0
J13255+688	2MASS J13253177+6850106	M0.0 V	-16.97 ± 0.04	This work	≤ 2.0	212	0
J13450+176	BD+18 2776	M0.0 V	20.27 ± 0.02	Laf20	2.3 ± 1.5	581	0
J14257+236W	BD+24 2733 A	M0.0 V	8.88 ± 0.02	Laf20	≤ 2.0	823	0
J16167+672S	HD 147379	M0.0 V	-19.36 ± 0.02	Laf20	2.7 ± 1.5	1611	0
J17303+055	BD+05 3409	M0.0 V	-13.03 ± 0.02	Laf20	≤ 2.0	751	0
J19346+045	BD+04 4157	M0.0 V	-58.86 ± 0.02	Laf20	3.9 ± 1.5	789	0
J21474+627	TYC 4266-736-1	M0.0 V	-61.33 ± 0.23	This work	≤ 2.0	533	0
J02222+478	BD+47 612	M0.5 V	-38.51 ± 0.02	Laf20	≤ 2.0	663	0
J04290+219	BD+21 652	M0.5 V	-35.56 ± 0.01	Laf20	3.9 ± 1.5	1341	0
J06105-218	HD 42581 A	M0.5 V	4.18 ± 0.02	Laf20	≤ 2.0	446	0
J09511-123	BD-11 2741	M0.5 V	61.85 ± 0.02	Laf20	≤ 2.0	421	0
J10088+692	TYC 4384-1735-1	M0.5 V	-27.02 ± 0.04	This work	≤ 2.0	487	0
J12312+086	BD+09 2636	M0.5 V	18.59 ± 0.02	Laf20	≤ 2.0	712	0
J13299+102	BD+11 2576	M0.5 V	14.00 ± 0.02	Laf20	≤ 2.0	1810	0
J14257+236E	BD+24 2733 B	M0.5 V	7.96 ± 0.02	Laf20	≤ 2.0	697	0
J14307-086	BD-07 3856	M0.5 V	-22.53 ± 0.02	Laf20	2.4 ± 1.5	996	0
J17355+616	BD+61 1678 C	M0.5 V	-15.44 ± 0.02	Laf20	≤ 2.0	585	0
J18353+457	BD+45 2743	M0.5 V	-32.05 ± 0.02	Laf20	≤ 2.0	454	0
J18580+059	BD+05 3993	M0.5 V	9.87 ± 0.02	Laf20	≤ 2.0	585	0
J22021+014	BD+00 4810	M0.5 V	17.82 ± 0.02	Laf20	≤ 2.0	951	0
J22503-070	BD-07 5871	M0.5 V	-6.13 ± 0.02	Laf20	≤ 2.0	512	0
J00051+457	GJ 2	M1.0 V	-0.56 ± 0.02	Laf20	≤ 2.0	774	0
J00183+440	GX And	M1.0 V	11.48 ± 0.02	Laf20	≤ 2.0	1795	0
J02565+554W	Ross 364	M1.0 V	76.31 ± 0.02	Laf20	≤ 2.0	225	0
J05415+534	HD 233153	M1.0 V	1.82 ± 0.02	Laf20	≤ 2.0	1088	0
J07361-031	BD-02 2198	M1.0 V	-17.06 ± 0.06	This work	3.1 ± 1.5	676	1
J10023+480	BD+48 1829	M1.0 V	-10.11 ± 0.02	Laf20	≤ 2.0	439	0
J10251-102	BD-09 3070	M1.0 V	21.26 ± 0.02	Laf20	≤ 2.0	456	0
J11054+435	BD+44 2051 A	M1.0 V	68.58 ± 0.02	Laf20	≤ 2.0	1013	0
J13209+342	BD+35 2439	M1.0 V	-35.76 ± 0.02	Laf20	≤ 2.0	324	0
J14010-026	HD 122303	M1.0 V	-26.14 ± 0.02	Laf20	≤ 2.0	424	0
J14082+805	BD+81 465	M1.0 V	7.06 ± 0.02	Laf20	≤ 2.0	559	0
J15598-082	BD-07 4156	M1.0 V	-17.47 ± 0.02	Laf20	≤ 2.0	382	0
J16581+257	BD+25 3173	M1.0 V	3.99 ± 0.02	Laf20	≤ 2.0	773	0
J17378+185	BD+18 3421	M1.0 V	-9.85 ± 0.02	Laf20	≤ 2.0	1131	0
J18051-030	HD 165222	M1.0 V	32.34 ± 0.02	Laf20	≤ 2.0	728	0
J18409-133	BD-13 5069	M1.0 V	-33.30 ± 0.02	Laf20	≤ 2.0	461	0
J20451-313	AU Mic	M1.0 V	-4.78 ± 0.13	This work	7.5 ± 1.5	510	1

**Table B.1.** continued.

Karmn	Name	SpT <sup>(a)</sup>	$v_r$ [km s <sup>-1</sup> ]	Ref. <sup>(b)</sup>	$v \sin i$ <sup>(c)</sup> [km s <sup>-1</sup> ]	S/N	H $\alpha$ flag <sup>(d)</sup>
J20533+621	BD+61 2068	M1.0 V	-17.49 ± 0.02	Laf20	≤ 2.0	1366	0
J21221+229	GSC 02187-00512	M1.0 V	5.35 ± 0.02	Laf20	≤ 2.0	1089	0
J22330+093	BD+08 4887	M1.0 V	-6.83 ± 0.02	Laf20	≤ 2.0	564	0
J22559+178	StkM 1-2065	M1.0 V	-32.24 ± 0.02	Laf20	≤ 2.0	295	0
J23245+578	BD+57 2735	M1.0 V	-33.52 ± 0.02	Laf20	≤ 2.0	596	0
J23492+024	BR Psc	M1.0 V	-71.47 ± 0.02	Laf20	≤ 2.0	1533	0
J01026+623	BD+61 195	M1.5 V	-6.30 ± 0.02	Laf20	≤ 2.0	904	0
J02123+035	BD+02 348	M1.5 V	-2.89 ± 0.02	Laf20	≤ 2.0	505	0
J03181+382	HD 275122	M1.5 V	-4.56 ± 0.02	Laf20	≤ 2.0	564	0
J04376-110	BD-11 916	M1.5 V	-7.11 ± 0.02	Laf20	≤ 2.0	333	0
J05314-036	HD 36395	M1.5 V	8.33 ± 0.02	Laf20	≤ 2.0	1020	0
J09163-186	LP 787-052	M1.5 V	14.57 ± 0.02	Laf20	≤ 2.0	115	1
J09411+132	Ross 85	M1.5 V	11.16 ± 0.02	Laf20	≤ 2.0	481	0
J09468+760	BD+76 3952	M1.5 V	-28.09 ± 0.02	Laf20	≤ 2.0	449	0
J10122-037	AN Sex	M1.5 V	7.60 ± 0.02	Laf20	≤ 2.0	776	0
J11033+359	Lalande 21185	M1.5 V	-85.02 ± 0.02	Laf20	≤ 2.0	1935	0
J11126+189	StkM 1-928	M1.5 V	31.22 ± 0.02	Laf20	≤ 2.0	468	0
J11511+352	BD+36 2219	M1.5 V	-0.06 ± 0.02	Laf20	≤ 2.0	1009	0
J13196+333	Ross 1007	M1.5 V	-12.03 ± 0.02	Laf20	≤ 2.0	161	0
J13457+148	HD 119850	M1.5 V	15.47 ± 0.02	Laf20	≤ 2.0	1541	0
J15218+209	OT Ser	M1.5 V	6.72 ± 0.02	Laf20	4.3 ± 1.5	678	1
J16254+543	GJ 625	M1.5 V	-13.38 ± 0.02	Laf20	≤ 2.0	526	0
J17052-050	Wolf 636	M1.5 V	34.48 ± 0.02	Laf20	≤ 2.0	574	0
J20450+444	BD+44 3567	M1.5 V	-25.03 ± 0.02	Laf20	≤ 2.0	604	0
J22057+656	G 264-018 A	M1.5 V	-46.90 ± 0.02	Laf20	≤ 2.0	839	0
J22565+165	HD 216899	M1.5 V	-27.66 ± 0.02	Laf20	≤ 2.0	2075	0
J00403+612	2MASS J00402129+6112490	M2.0 V	4.00 ± 0.07	This work	≤ 2.0	77	0
J01013+613	GJ 47	M2.0 V	7.24 ± 0.02	Laf20	≤ 2.0	255	0
J01433+043	GJ 70	M2.0 V	-26.23 ± 0.02	Laf20	≤ 2.0	391	0
J02358+202	BD+19 381	M2.0 V	0.66 ± 0.02	Laf20	≤ 2.0	359	0
J02489-145W	PM J02489-1432W	M2.0 V	32.27 ± 0.06	This work	≤ 2.0	218	1
J03213+799	GJ 133	M2.0 V	-13.59 ± 0.02	Laf20	≤ 2.0	376	0
J03217-066	G 077-046	M2.0 V	26.12 ± 0.02	Laf20	≤ 2.0	245	0
J04343+430	PM J04343+4302	M2.0 V	-43.21 ± 0.10	This work	≤ 2.0	273	0
J04429+189	HD 285968	M2.0 V	25.89 ± 0.02	Laf20	≤ 2.0	350	0
J04538-177	GJ 180	M2.0 V	-14.83 ± 0.02	Laf20	≤ 2.0	447	0
J05127+196	GJ 192	M2.0 V	-25.36 ± 0.02	Laf20	≤ 2.0	428	0
J06103+821	GJ 226	M2.0 V	-1.95 ± 0.02	Laf20	≤ 2.0	679	0
J07353+548	GJ 3452	M2.0 V	-15.27 ± 0.02	Laf20	≤ 2.0	180	0
J08161+013	GJ 2066	M2.0 V	61.87 ± 0.02	Laf20	≤ 2.0	706	0
J09425+700	GJ 360	M2.0 V	6.70 ± 0.02	Laf20	≤ 2.0	514	1
J10289+008	BD+01 2447	M2.0 V	8.01 ± 0.02	Laf20	≤ 2.0	819	0
J11026+219	DS Leo	M2.0 V	-14.24 ± 0.02	Laf20	2.6 ± 1.5	700	1
J11110+304W	HD 97101 B	M2.0 V	-15.69 ± 0.02	Laf20	≤ 2.0	641	0
J11201-104	LP 733-099	M2.0 V	12.03 ± 0.02	Laf20	3.6 ± 1.5	426	1
J12248-182	Ross 695	M2.0 V	50.85 ± 0.02	Laf20	≤ 2.0	317	0
J13119+658	PM J13119+6550	M2.0 V	-41.63 ± 0.06	This work	≤ 2.0	134	0
J14294+155	Ross 130	M2.0 V	7.51 ± 0.02	Laf20	≤ 2.0	129	0
J14524+123	G 066-037	M2.0 V	5.40 ± 0.02	Laf20	≤ 2.0	366	0
J15474-108	LP 743-031	M2.0 V	-0.88 ± 0.08	This work	3.0 ± 1.5	552	0
J17166+080	GJ 2128	M2.0 V	-30.93 ± 0.02	Laf20	≤ 2.0	193	0
J18174+483	TYC 3529-1437-1	M2.0 V	-24.24 ± 0.02	Laf20	≤ 2.0	793	1
J19070+208	Ross 730	M2.0 V	32.06 ± 0.02	Laf20	≤ 2.0	479	0
J19072+208	HD 349726	M2.0 V	31.83 ± 0.02	Laf20	≤ 2.0	526	0
J22115+184	Ross 271	M2.0 V	-51.67 ± 0.02	Laf20	≤ 2.0	876	0
J23381-162	G 273-093	M2.0 V	20.47 ± 0.02	Laf20	≤ 2.0	644	0
J00389+306	Wolf 1056	M2.5 V	-0.63 ± 0.03	Laf20	≤ 2.0	471	0
J01518+644	G 244-037	M2.5 V	-13.06 ± 0.03	Laf20	≤ 2.0	368	0
J02489-145E	PM J02489-1432E	M2.5 V	32.40 ± 0.06	This work	≤ 2.0	164	1

**Table B.1.** continued.

Karmn	Name	SpT <sup>(a)</sup>	$v_r$ [km s <sup>-1</sup> ]	Ref. <sup>(b)</sup>	$v \sin i$ <sup>(c)</sup> [km s <sup>-1</sup> ]	S/N	H $\alpha$ flag <sup>(d)</sup>
J05337+019	V371 Ori	M2.5 V	-0.88 ± 1.65	This work	9.8 ± 1.5	379	1
J08293+039	2MASS J08292191+0355092	M2.5 V	22.50 ± 0.03	Laf20	≤ 2.0	365	0
J08358+680	G 234-037	M2.5 V	18.86 ± 0.03	Laf20	≤ 2.0	264	0
J09133+688	G 234-057	M2.5 V	13.65 ± 0.03	Laf20	≤ 2.0	351	1
J09360-216	GJ 357	M2.5 V	-34.83 ± 0.03	Laf20	≤ 2.0	497	0
J10396-069	GJ 399	M2.5 V	2.97 ± 0.03	Laf20	≤ 2.0	225	0
J11000+228	Ross 104	M2.5 V	2.89 ± 0.03	Laf20	≤ 2.0	641	0
J11302+076	K2-18	M2.5 V	0.20 ± 0.03	Laf20	≤ 2.0	302	0
J11421+267	Ross 905	M2.5 V	9.34 ± 0.03	Laf20	≤ 2.0	1036	0
J12350+098	GJ 476	M2.5 V	33.01 ± 0.03	Laf20	≤ 2.0	145	0
J14251+518	θ Boo B	M2.5 V	-10.38 ± 0.03	Laf20	≤ 2.0	308	0
J16462+164	LP 446-006	M2.5 V	18.54 ± 0.03	Laf20	≤ 2.0	292	0
J17198+417	GJ 671	M2.5 V	-19.77 ± 0.03	Laf20	≤ 2.0	347	0
J17578+465	G 204-039	M2.5 V	-31.63 ± 0.03	Laf20	≤ 2.0	335	0
J18480-145	G 155-042	M2.5 V	-4.78 ± 0.03	Laf20	≤ 2.0	135	0
J19169+051N	V1428 Aql	M2.5 V	35.61 ± 0.03	Laf20	≤ 2.0	1194	0
J20305+654	GJ 793	M2.5 V	10.33 ± 0.03	Laf20	≤ 2.0	669	0
J20567-104	Wolf 896	M2.5 V	34.98 ± 0.03	Laf20	≤ 2.0	364	0
J21019-063	Wolf 906	M2.5 V	-15.23 ± 0.03	Laf20	≤ 2.0	389	0
J23340+001	GJ 899	M2.5 V	-4.84 ± 0.03	Laf20	≤ 2.0	487	0
J23556-061	GJ 912	M2.5 V	17.53 ± 0.07	This work	≤ 2.0	483	0
J00570+450	G 172-030	M3.0 V	6.27 ± 0.03	Laf20	≤ 2.0	268	0
J01025+716	BD+70 68	M3.0 V	1.25 ± 0.03	Laf20	≤ 2.0	1078	0
J01066+192	LSMP J0106+1913	M3.0 V	11.58 ± 0.07	This work	≤ 2.0	159	0
J02015+637	G 244-047	M3.0 V	-84.39 ± 0.03	Laf20	≤ 2.0	469	0
J02442+255	VX Ari	M3.0 V	30.30 ± 0.03	Laf20	≤ 2.0	613	0
J03473-019	G 080-021	M3.0 V	17.88 ± 0.02	Laf20	5.2 ± 1.5	234	1
J03531+625	Ross 567	M3.0 V	-120.32 ± 0.03	Laf20	≤ 2.0	562	0
J05033-173	LP 776-049	M3.0 V	15.19 ± 0.03	Laf20	≤ 2.0	483	0
J06548+332	Wolf 294	M3.0 V	22.65 ± 0.03	Laf20	≤ 2.0	1431	0
J07044+682	GJ 258	M3.0 V	-50.77 ± 0.03	Laf20	≤ 2.0	302	0
J07287-032	GJ 1097	M3.0 V	1.18 ± 0.03	Laf20	≤ 2.0	383	0
J07386-212	LP 763-001	M3.0 V	-29.18 ± 0.03	Laf20	≤ 2.0	146	0
J09140+196	LP 427-016	M3.0 V	12.88 ± 0.03	Laf20	≤ 2.0	330	0
J09428+700	GJ 362	M3.0 V	6.35 ± 0.03	Laf20	≤ 2.0	461	1
J10167-119	GJ 386	M3.0 V	-10.81 ± 0.03	Laf20	≤ 2.0	295	0
J10196+198	AD Leo	M3.0 V	12.29 ± 0.02	Laf20	3.2 ± 1.5	402	1
J10350-094	LP 670-017	M3.0 V	14.32 ± 0.03	Laf20	≤ 2.0	317	0
J11044+304	LSPM J1104+3027	M3.0 V	-11.78 ± 0.12	This work	≤ 2.0	36	0
J11467-140	GJ 443	M3.0 V	20.20 ± 0.03	Laf20	≤ 2.0	309	0
J12111-199	LTT 4562	M3.0 V	-9.38 ± 0.03	Laf20	≤ 2.0	322	0
J12230+640	Ross 690	M3.0 V	8.86 ± 0.03	Laf20	≤ 2.0	1308	0
J12388+116	Wolf 433	M3.0 V	-4.49 ± 0.03	Laf20	≤ 2.0	200	0
J13283-023W	Ross 486 A	M3.0 V	-39.73 ± 0.03	Laf20	≤ 2.0	248	0
J13582+125	Ross 837	M3.0 V	-10.13 ± 0.03	Laf20	≤ 2.0	105	0
J14152+450	Ross 992	M3.0 V	13.88 ± 0.03	Laf20	≤ 2.0	233	0
J15013+055	G 015-002	M3.0 V	-6.27 ± 0.03	Laf20	≤ 2.0	303	0
J15095+031	Ross 1047	M3.0 V	-32.79 ± 0.03	Laf20	≤ 2.0	261	0
J15194-077	HO Lib	M3.0 V	-9.66 ± 0.03	Laf20	≤ 2.0	654	0
J16092+093	G 137-084	M3.0 V	-45.13 ± 0.03	Laf20	≤ 2.0	185	0
J16102-193	K2-33	M3.0 V	-7.00 ± 0.03	Laf20	7.3 ± 1.5	67	1
J16167+672N	EW Dra	M3.0 V	-18.78 ± 0.03	Laf20	≤ 2.0	985	0
J16327+126	GJ 1203	M3.0 V	-33.07 ± 0.03	Laf20	≤ 2.0	183	0
J17071+215	Ross 863	M3.0 V	-51.06 ± 0.03	Laf20	≤ 2.0	302	0
J17364+683	BD+68 946	M3.0 V	-28.82 ± 0.08	This work	≤ 2.0	609	0
J18180+387E	G 204-058	M3.0 V	0.23 ± 0.03	Laf20	≤ 2.0	210	0
J18419+318	Ross 145	M3.0 V	-32.03 ± 0.03	Laf20	≤ 2.0	343	0
J18427+596N	HD 173739	M3.0 V	-0.75 ± 0.08	Laf20	≤ 2.0	781	0
J19084+322	G 207-019	M3.0 V	-1.98 ± 0.03	Laf20	≤ 2.0	407	0

**Table B.1.** continued.

Karmn	Name	SpT <sup>(a)</sup>	$v_r$ [km s <sup>-1</sup> ]	Ref. <sup>(b)</sup>	$v \sin i$ <sup>(c)</sup> [km s <sup>-1</sup> ]	S/N	H $\alpha$ flag <sup>(d)</sup>
J19251+283	Ross 164	M3.0 V	$-40.77 \pm 0.03$	Laf20	$\leq 2.0$	355	0
J21152+257	LP 397-041	M3.0 V	$-16.28 \pm 0.03$	Laf20	$\leq 2.0$	346	0
J21164+025	LSPM J2116+0234	M3.0 V	$-22.31 \pm 0.03$	Laf20	$\leq 2.0$	764	0
J21348+515	Wolf 926	M3.0 V	$-14.12 \pm 0.03$	Laf20	$\leq 2.0$	804	0
J22125+085	Wolf 1014	M3.0 V	$8.46 \pm 0.03$	Laf20	$\leq 2.0$	831	0
J22518+317	GT Peg	M3.0 V	$-2.44 \pm 0.05$	Laf20	$13.4 \pm 1.5$	368	1
J23585+076	Wolf 1051	M3.0 V	$-13.54 \pm 0.08$	This work	$\leq 2.0$	404	0
J00184+440	GQ And	M3.5 V	$10.68 \pm 0.03$	Laf20	$\leq 2.0$	1352	0
J02002+130	TZ Ari	M3.5 V	$-28.83 \pm 0.03$	Laf20	$\leq 2.0$	863	1
J02070+496	G 173-037	M3.5 V	$18.73 \pm 0.03$	Laf20	$\leq 2.0$	305	1
J02088+494	G 173-039	M3.5 V	$-9.73 \pm 0.06$	Laf20	$24.1 \pm 2.4$	633	1
J04225+105	LSPM J0422+1031	M3.5 V	$36.72 \pm 0.03$	Laf20	$\leq 2.0$	283	0
J04429+214	2MASS J04425586+2128230	M3.5 V	$2.80 \pm 0.03$	Laf20	$\leq 2.0$	205	0
J04520+064	Wolf 1539	M3.5 V	$-9.12 \pm 0.03$	Laf20	$\leq 2.0$	181	0
J05280+096	Ross 41	M3.5 V	$60.30 \pm 0.03$	Laf20	$\leq 2.0$	279	0
J05348+138	Ross 46	M3.5 V	$37.42 \pm 0.03$	Laf20	$\leq 2.0$	362	0
J06011+595	G 192-013	M3.5 V	$1.69 \pm 0.03$	Laf20	$\leq 2.0$	769	0
J06421+035	G 108-021	M3.5 V	$82.19 \pm 0.03$	Laf20	$\leq 2.0$	390	0
J07274+052	Luyten's star	M3.5 V	$17.89 \pm 0.03$	Laf20	$\leq 2.0$	678	0
J07319+362N	BL Lyn	M3.5 V	$-1.07 \pm 0.03$	Laf20	$\leq 2.0$	590	1
J07582+413	GJ 1105	M3.5 V	$-21.34 \pm 0.03$	Laf20	$\leq 2.0$	399	0
J08402+314	LSPM J0840+3127	M3.5 V	$66.69 \pm 0.03$	Laf20	$\leq 2.0$	227	0
J08409-234	LP 844-008	M3.5 V	$87.55 \pm 0.03$	Laf20	$\leq 2.0$	294	0
J09307+003	GJ 1125	M3.5 V	$45.87 \pm 0.03$	Laf20	$\leq 2.0$	390	0
J09423+559	GJ 363	M3.5 V	$15.00 \pm 0.03$	Laf20	$\leq 2.0$	230	0
J09439+269	Ross 93	M3.5 V	$34.18 \pm 0.03$	Laf20	$\leq 2.0$	168	0
J10125+570	LP 092-048	M3.5 V	$-3.78 \pm 0.03$	Laf20	$\leq 2.0$	242	0
J10360+051	RY Sex	M3.5 V	$20.81 \pm 0.03$	Laf20	$2.9 \pm 1.6$	171	1
J11289+101	Wolf 398	M3.5 V	$36.80 \pm 0.03$	Laf20	$\leq 2.0$	89	0
J11306-080	LP 672-042	M3.5 V	$16.43 \pm 0.03$	Laf20	$\leq 2.0$	289	0
J11476+786	GJ 445	M3.5 V	$-111.97 \pm 0.03$	Laf20	$\leq 2.0$	608	0
J12100-150	LP 734-032	M3.5 V	$80.21 \pm 0.03$	Laf20	$\leq 2.0$	497	0
J12479+097	Wolf 437	M3.5 V	$18.77 \pm 0.03$	Laf20	$\leq 2.0$	838	0
J13293+114	GJ 513	M3.5 V	$27.98 \pm 0.03$	Laf20	$\leq 2.0$	68	0
J13427+332	Ross 1015	M3.5 V	$6.45 \pm 0.03$	Laf20	$\leq 2.0$	339	0
J13458-179	LP 798-034	M3.5 V	$4.63 \pm 0.03$	Laf20	$\leq 2.0$	116	0
J14310-122	Wolf 1478	M3.5 V	$-2.08 \pm 0.03$	Laf20	$\leq 2.0$	175	0
J14544+355	Ross 1041	M3.5 V	$-41.06 \pm 0.03$	Laf20	$\leq 2.0$	456	0
J15583+354	G 180-018	M3.5 V	$9.54 \pm 0.10$	This work	$\leq 2.0$	328	0
J16303-126	V2306 Oph	M3.5 V	$-21.56 \pm 0.03$	Laf20	$\leq 2.0$	841	0
J16554-083N	GJ 643	M3.5 V	$15.50 \pm 0.03$	Laf20	$\leq 2.0$	433	0
J16570-043	LP 686-027	M3.5 V	$-3.96 \pm 0.05$	Laf20	$10.1 \pm 1.5$	405	1
J17115+384	Wolf 654	M3.5 V	$-44.78 \pm 0.03$	Laf20	$\leq 2.0$	653	0
J17578+046	Barnard's star	M3.5 V	$-110.57 \pm 0.02$	Laf20	$\leq 2.0$	2007	0
J18319+406	G 205-028	M3.5 V	$-19.32 \pm 0.03$	Laf20	$\leq 2.0$	307	0
J18346+401	LP 229-017	M3.5 V	$12.18 \pm 0.03$	Laf20	$\leq 2.0$	822	0
J18427+596S	HD 173740	M3.5 V	$1.02 \pm 0.08$	This work	$\leq 2.0$	817	0
J18498-238	GJ 729	M3.5 V	$-10.80 \pm 0.03$	Laf20	$3.0 \pm 1.5$	575	1
J22020-194	LP 819-017	M3.5 V	$-23.60 \pm 0.03$	Laf20	$\leq 2.0$	182	0
J22096-046	BD-05 5715	M3.5 V	$-15.59 \pm 0.03$	Laf20	$\leq 2.0$	679	0
J22468+443	EV Lac	M3.5 V	$0.35 \pm 0.03$	Laf20	$3.5 \pm 1.5$	944	1
J23113+085	NLTT 56083	M3.5 V	$-10.73 \pm 0.10$	Laf20	$\leq 2.0$	643	0
J00162+198E	LP 404-062	M4.0 V	$-1.62 \pm 0.02$	Laf20	$\leq 2.0$	224	0
J00286-066	GJ 1012	M4.0 V	$-12.71 \pm 0.02$	Laf20	$\leq 2.0$	594	0
J01339-176	LP 768-113	M4.0 V	$6.12 \pm 0.02$	Laf20	$\leq 2.0$	279	1
J01352-072	Barta 161 12	M4.0 V	$9.34 \pm 0.21$	Laf20	$59.8 \pm 6.9$	587	1
J02336+249	GJ 102	M4.0 V	$-6.66 \pm 0.02$	Laf20	$3.0 \pm 1.5$	303	1
J02362+068	BX Cet	M4.0 V	$25.97 \pm 0.02$	Laf20	$\leq 2.0$	611	0
J02519+224	RBS 365	M4.0 V	$9.14 \pm 0.08$	Laf20	$27.2 \pm 2.7$	565	1

**Table B.1.** continued.

Karmn	Name	SpT <sup>(a)</sup>	$v_r$ [km s <sup>-1</sup> ]	Ref. <sup>(b)</sup>	$v \sin i$ <sup>(c)</sup> [km s <sup>-1</sup> ]	S/N	H $\alpha$ flag <sup>(d)</sup>
J04311+589	STN 2051A	M4.0 V	28.43 ± 0.02	Laf20	≤ 2.0	248	0
J05019+011	1RXS J050156.7+010845	M4.0 V	19.71 ± 0.03	Laf20	6.5 ± 1.5	296	1
J05019-069	LP 656-038	M4.0 V	41.97 ± 0.02	Laf20	≤ 2.0	204	1
J05062+046	RX J0506.2+0439	M4.0 V	19.08 ± 0.08	Laf20	24.9 ± 2.5	417	1
J05360-076	Wolf 1457	M4.0 V	29.09 ± 0.02	Laf20	≤ 2.0	327	0
J05366+112	2MASS J05363846+1117487	M4.0 V	21.53 ± 0.02	Laf20	2.4 ± 1.5	283	1
J05421+124	V1352 Ori	M4.0 V	105.67 ± 0.02	Laf20	≤ 2.0	591	0
J06000+027	G 099-049	M4.0 V	29.90 ± 0.03	Laf20	4.9 ± 1.5	201	1
J06246+234	Ross 64	M4.0 V	-11.66 ± 0.02	Laf20	≤ 2.0	144	0
J06396-210	LP 780-032	M4.0 V	-7.43 ± 0.02	Laf20	≤ 2.0	385	0
J06574+740	2MASS J06572616+7405265	M4.0 V	-2.69 ± 0.10	Laf20	27.1 ± 2.7	463	1
J07033+346	LP 255-011	M4.0 V	2.03 ± 0.02	Laf20	≤ 2.0	258	1
J07472+503	2MASS J07471385+5020386	M4.0 V	-14.77 ± 0.05	Laf20	10.1 ± 1.5	381	1
J08023+033	G 050-016 A	M4.0 V	-1.15 ± 0.25	This work	≤ 2.0	282	0
J08126-215	GJ 300	M4.0 V	8.68 ± 0.02	Laf20	≤ 2.0	450	0
J08315+730	LP 035-219	M4.0 V	-90.84 ± 0.02	Laf20	≤ 2.0	269	0
J09028+680	LP 060-179	M4.0 V	-25.01 ± 0.02	Laf20	≤ 2.0	237	0
J09161+018	RX J0916.1+0153	M4.0 V	-12.75 ± 0.05	Laf20	10.4 ± 1.5	255	1
J09447-182	GJ 1129	M4.0 V	8.34 ± 0.02	Laf20	≤ 2.0	237	0
J10185-117	LP 729-054	M4.0 V	-0.05 ± 0.33	This work	≤ 2.0	356	0
J10504+331	G 119-037	M4.0 V	-59.65 ± 0.11	Laf20	≤ 2.0	327	0
J10508+068	EE Leo	M4.0 V	-1.34 ± 0.02	Laf20	≤ 2.0	632	0
J11417+427	Ross 1003	M4.0 V	-9.34 ± 0.02	Laf20	≤ 2.0	812	0
J11476+002	LP 613-049 A	M4.0 V	5.94 ± 0.03	Laf20	2.4 ± 1.5	122	1
J11477+008	Fl Vir	M4.0 V	-31.38 ± 0.02	Laf20	≤ 2.0	578	0
J12054+695	Ross 689	M4.0 V	5.26 ± 0.02	Laf20	≤ 2.0	59	0
J12156+526	StkM 2-809	M4.0 V	-9.55 ± 0.13	Laf20	35.3 ± 3.5	614	1
J12373-208	LP 795-038	M4.0 V	9.09 ± 0.02	Laf20	≤ 2.0	168	0
J12428+418	G 123-055	M4.0 V	-4.68 ± 0.02	Laf20	≤ 2.0	180	1
J13229+244	Ross 1020	M4.0 V	-19.56 ± 0.02	Laf20	≤ 2.0	647	0
J13536+776	RX J1353.6+7737	M4.0 V	-7.59 ± 0.02	Laf20	8.9 ± 1.5	412	1
J13591-198	LP 799-007	M4.0 V	-16.49 ± 0.03	Laf20	3.2 ± 1.5	195	1
J14342-125	HN Lib	M4.0 V	-1.74 ± 0.02	Laf20	≤ 2.0	806	0
J15369-141	Ross 802	M4.0 V	2.10 ± 0.02	Laf20	≤ 2.0	135	0
J16028+205	GJ 609	M4.0 V	6.18 ± 0.02	Laf20	≤ 2.0	320	0
J17542+073	GJ 1222	M4.0 V	-28.61 ± 0.02	Laf20	≤ 2.0	122	0
J18131+260	LP 390-016	M4.0 V	-8.61 ± 0.09	Laf20	5.9 ± 1.5	198	1
J18221+063	Ross 136	M4.0 V	-43.97 ± 0.02	Laf20	≤ 2.0	128	0
J18224+620	GJ 1227	M4.0 V	-13.97 ± 0.02	Laf20	≤ 2.0	357	0
J18363+136	Ross 149	M4.0 V	-45.32 ± 0.02	Laf20	≤ 2.0	307	1
J19206+731S	TOI-1670	M4.0 V	-34.42 ± 0.51	This work	≤ 2.0	88	0
J19511+464	G 208-042	M4.0 V	-12.94 ± 0.06	Laf20	22.5 ± 2.3	493	1
J20336+617	GJ 1254	M4.0 V	-21.18 ± 0.02	Laf20	≤ 2.0	490	0
J20525-169	LP 816-060	M4.0 V	16.00 ± 0.02	Laf20	≤ 2.0	414	0
J21463+382	LSPM J2146+3813	M4.0 V	-83.01 ± 0.02	Laf20	≤ 2.0	495	0
J21466-001	Wolf 940	M4.0 V	-28.55 ± 0.02	Laf20	≤ 2.0	319	0
J21466+668	G 264-012	M4.0 V	-9.77 ± 0.02	Laf20	≤ 2.0	761	0
J22012+283	V374 Peg	M4.0 V	-3.25 ± 0.14	Laf20	35.4 ± 3.5	618	1
J22252+594	G 232-070	M4.0 V	3.87 ± 0.02	Laf20	≤ 2.0	639	0
J22298+414	G 215-050	M4.0 V	2.11 ± 0.02	Laf20	≤ 2.0	231	0
J22532-142	IL Aqr	M4.0 V	-1.80 ± 0.03	Laf20	≤ 2.0	645	0
J23216+172	LP 462-027	M4.0 V	-6.77 ± 0.02	Laf20	≤ 2.0	775	0
J23431+365	GJ 1289	M4.0 V	-2.98 ± 0.02	Laf20	≤ 2.0	308	1
J23505-095	LP 763-012	M4.0 V	-21.87 ± 0.02	Laf20	≤ 2.0	365	0
J23548+385	RX J2354.8+3831	M4.0 V	5.37 ± 0.03	Laf20	3.6 ± 1.5	200	1
J01125-169	YZ Cet	M4.5 V	27.85 ± 0.02	Laf20	≤ 2.0	821	1
J04153-076	$\sigma^0$ Eri C	M4.5 V	-43.58 ± 0.02	Laf20	2.1 ± 1.5	477	1
J07446+035	YZ CMi	M4.5 V	26.71 ± 0.03	Laf20	4.0 ± 1.5	542	1
J07558+833	GJ 1101	M4.5 V	7.64 ± 0.05	Laf20	12.1 ± 1.5	315	1

**Table B.1.** continued.

Karmn	Name	SpT <sup>(a)</sup>	$v_r$ [km s $^{-1}$ ]	Ref. <sup>(b)</sup>	$v \sin i$ <sup>(c)</sup> [km s $^{-1}$ ]	S/N	H $\alpha$ flag <sup>(d)</sup>
J08119+087	Ross 619	M4.5 V	14.42 ± 0.02	Laf20	≤ 2.0	285	0
J08526+283	$\rho$ Cnc B	M4.5 V	27.18 ± 0.02	Laf20	≤ 2.0	223	0
J09005+465	GJ 1119	M4.5 V	1.99 ± 0.02	Laf20	≤ 2.0	49	1
J10416+376	GJ 1134	M4.5 V	-1.86 ± 0.02	Laf20	≤ 2.0	102	0
J11509+483	GJ 1151	M4.5 V	-35.61 ± 0.02	Laf20	≤ 2.0	429	0
J13005+056	FN Vir	M4.5 V	-25.33 ± 0.05	Laf20	16.4 ± 1.6	269	1
J17033+514	G 203-042	M4.5 V	37.18 ± 0.02	Laf20	≤ 2.0	330	0
J18075-159	GJ 1224	M4.5 V	-33.20 ± 0.02	Laf20	2.2 ± 1.5	144	1
J18189+661	LP 071-165	M4.5 V	5.36 ± 0.05	Laf20	15.3 ± 1.5	354	1
J19098+176	GJ 1232	M4.5 V	-14.26 ± 0.02	Laf20	≤ 2.0	256	0
J19216+208	GJ 1235	M4.5 V	4.52 ± 0.02	Laf20	≤ 2.0	256	0
J20405+154	GJ 1256	M4.5 V	-59.78 ± 0.02	Laf20	≤ 2.0	260	0
J22137-176	LP 819-052	M4.5 V	-24.48 ± 0.02	Laf20	≤ 2.0	418	0
J22231-176	LP 820-012	M4.5 V	-1.97 ± 0.02	Laf20	≤ 2.0	163	1
J01019+541	G 218-020	M5.0 V	-5.20 ± 0.13	Laf20	30.6 ± 3.1	426	1
J01033+623	V388 Cas	M5.0 V	-6.52 ± 0.08	Laf20	10.5 ± 1.5	392	1
J01048-181	GJ 1028	M5.0 V	11.37 ± 0.02	Laf20	≤ 2.0	203	0
J03133+047	CD Cet	M5.0 V	28.16 ± 0.02	Laf20	≤ 2.0	601	0
J04472+206	RX J0447.2+2038	M5.0 V	23.98 ± 0.31	Laf20	47.6 ± 26.8	429	1
J05084-210	2MASS J05082729-2101444	M5.0 V	22.21 ± 0.23	Laf20	25.2 ± 2.5	320	1
J06024+498	G 192-015	M5.0 V	20.26 ± 0.02	Laf20	≤ 2.0	260	0
J06318+414	LP 205-044	M5.0 V	4.35 ± 0.12	Laf20	58.4 ± 26.1	720	1
J06594+193	GJ 1093	M5.0 V	-29.51 ± 0.02	Laf20	≤ 2.0	263	1
J09449-123	G 161-071	M5.0 V	16.96 ± 0.36	Laf20	31.2 ± 3.1	412	1
J10584-107	LP 731-076	M5.0 V	10.78 ± 0.02	Laf20	3.2 ± 1.5	244	1
J11474+667	IRXS J114728.8+664405	M5.0 V	-9.40 ± 0.04	Laf20	2.7 ± 1.5	193	1
J12189+111	GL Vir	M5.0 V	5.68 ± 0.05	Laf20	15.5 ± 1.6	384	1
J13102+477	G 177-025	M5.0 V	-12.45 ± 0.02	Laf20	≤ 2.0	228	1
J14173+454	RX J1417.3+4525	M5.0 V	3.11 ± 0.06	Laf20	15.9 ± 1.6	242	1
J15499+796	LP 022-420	M5.0 V	-16.29 ± 0.10	Laf20	26.9 ± 2.7	286	1
J16313+408	G 180-060	M5.0 V	-23.16 ± 0.04	Laf20	7.1 ± 1.5	150	1
J18022+642	LP 071-082	M5.0 V	-1.63 ± 0.05	Laf20	11.3 ± 1.5	449	1
J18027+375	GJ 1223	M5.0 V	3.67 ± 0.02	Laf20	≤ 2.0	218	0
J18165+048	G 140-051	M5.0 V	-53.52 ± 0.02	Laf20	≤ 2.0	224	0
J18482+076	G 141-036	M5.0 V	-34.45 ± 0.02	Laf20	2.4 ± 1.5	348	1
J19422-207	2MASS J19421282-2045477	M5.1 V	-2.09 ± 0.03	Laf20	6.2 ± 1.5	118	1
J20093-012	2MASS J20091824-0113377	M5.0 V	-53.97 ± 0.02	Laf20	4.3 ± 1.5	149	1
J20260+585	Wolf 1069	M5.0 V	-60.05 ± 0.02	Laf20	≤ 2.0	817	0
J20556-140S	GJ 810 B	M5.0 V	-142.04 ± 0.02	Laf20	≤ 2.0	195	0
J23419+441	HH And	M5.0 V	-78.07 ± 0.02	Laf20	≤ 2.0	774	1
J00067-075	GJ 1002	M5.5 V	-40.12 ± 0.02	Laf20	≤ 2.0	566	0
J08413+594	LP 090-018	M5.5 V	6.12 ± 0.02	Laf20	≤ 2.0	431	1
J11055+435	WX UMa	M5.5 V	69.16 ± 0.02	Laf20	8.2 ± 2.7	428	1
J15305+094	NLTT 40406	M5.5 V	1.43 ± 0.05	Laf20	16.3 ± 1.6	233	1
J17338+169	IRXS J173353.5+165515	M5.5 V	-21.87 ± 0.29	Laf20	41.5 ± 7.7	438	1
J22114+409	IRXS J221124.3+410000	M5.5 V	-16.88 ± 0.02	Laf20	≤ 2.0	227	1
J23351-023	GJ 1286	M5.5 V	-41.06 ± 0.02	Laf20	≤ 2.0	364	1
J07403-174	LP 783-002	M6.0 V	-28.81 ± 0.03	Laf20	≤ 2.0	146	0
J10564+070	CN Leo	M6.0 V	19.44 ± 0.03	Laf20	≤ 2.0	628	1
J14321+081	LP 560-035	M6.0 V	-22.02 ± 0.03	Laf20	6.3 ± 1.5	204	1
J08298+267	DX Cnc	M6.5 V	9.94 ± 0.05	Laf20	10.5 ± 1.5	500	1
J09003+218	LP 368-128	M6.5 V	8.11 ± 0.07	Laf20	14.3 ± 1.5	173	1
J10482-113	LP 731-058	M6.5 V	1.74 ± 0.03	Laf20	2.1 ± 1.5	348	1
J02530+168	Teegarden's star	M7.0 V	68.42 ± 0.03	Laf20	≤ 2.0	903	1
J09033+056	NLTT 20861	M7.0 V	-28.12 ± 0.04	Laf20	9.7 ± 1.5	139	1
J16555-083	vB 8	M7.0 V	14.41 ± 0.03	Laf20	5.4 ± 1.5	264	1
J05394+406 <sup>(e)</sup>	LSR J0539+4038	M8.0 V	-6.34 ± 0.03	Laf20	4.1 ± 1.5	61	1
J19169+051S <sup>(e)</sup>	V1298 Aql	M8.0 V	35.73 ± 0.03	Laf20	2.7 ± 2.2	173	1
J19255+096 <sup>(e)</sup>	LSPM J1925+0938	M8.0 V	-2.47 ± 9.87	This work	34.7 ± 3.5	120	1

**Table B.1.** continued.

Karmn	Name	SpT <sup>(a)</sup>	$v_r$ [km s <sup>-1</sup> ]	Ref. <sup>(b)</sup>	$v \sin i$ <sup>(c)</sup> [km s <sup>-1</sup> ]	S/N	H $\alpha$ flag <sup>(d)</sup>
J23064–050 <sup>(e)</sup>	2MUCD 12171	M8.0 V	$-53.32 \pm 0.03$	Laf20	$\leq 2.0$	51	1
J04198+425 <sup>(e)</sup>	LSR J0419+4233	M8.5 V	$21.49 \pm 0.07$	Laf20	$3.6 \pm 2.3$	81	1
J18356+329 <sup>(e)</sup>	LSR J1835+3259	M8.5 V	$0.64 \pm 0.18$	Laf20	$49.2 \pm 4.9$	193	1
J08536–034 <sup>(e)</sup>	LP 666-009	M9.0 V	$-7.22 \pm 0.10$	Laf20	$9.3 \pm 2.8$	79	1

**Notes.** <sup>(a)</sup>Spectral types from Carmencita (Alonso-Floriano et al. 2015; Caballero et al. 2016a). <sup>(b)</sup>Radial velocities from Lafarga et al. (2020, Laf20) if available, or computed using serval (Zechmeister et al. 2018) otherwise. <sup>(c)</sup>Projected rotational velocities computed as in Reiners et al. (2018). <sup>(d)</sup>H $\alpha$ -active stars following Schöfer et al. (2019) (1 if active). <sup>(e)</sup>M8.0 V or later (see Table 1).

**Table B.2.** Selection of Ti I and Fe I lines in the spectra of GX And (M1.0 V), Luyten's star (M3.5 V), and Teegarden's star (M7.0 V).

Range		Atomic line <sup>(a)</sup>				Magnetically sensitive <sup>(b)</sup>	Ref. <sup>(c)</sup>	GX And	Luyten's star	Teegarden's star
$\lambda_{\min}$ [Å]	$\lambda_{\max}$ [Å]	$\lambda_{\text{line}}$ [Å]	Element	$\chi$ [eV]	$\log g f$	g <sub>eff</sub>				
5636.61	5651.65	5644.134	Ti I	2.2674	+0.120	1.010	This work	•		
5859.04	5874.01	5866.451	Ti I	1.0666	-0.790	1.170	This work	•		
5914.95	5929.51	5922.110	Ti I	1.0460	-1.380	0.500	This work	•		
5969.39	5985.75	5976.776	Fe I	3.9433	-1.236	1.100	This work	•		
		5978.541	Ti I	1.8732	-0.312	0.890	This work	•		
6056.60	6072.73	6064.626	Ti I	1.0460	-1.670	1.990	This work	•		
		6065.481	Fe I	2.6085	-1.530	0.680	This work	•		
6077.90	6092.38	6085.226	Ti I	1.0529	-1.331	1.750	This work	•		
6119.00	6145.00	6126.216	Ti I	1.0666	-1.206	1.240	This work	•	•	
		6136.615	Fe I	2.4534	-1.400	0.840	This work	•	•	
		6137.691	Fe I	2.5881	-1.403	1.080	This work	•	•	
6385.90	6400.63	6393.600	Fe I	2.4327	-1.432	0.910	This work	•		
6423.28	6438.23	6430.845	Fe I	2.1759	-2.006	1.240	This work	•		
6468.58	6489.05	6475.624	Fe I	2.5592	-2.942	1.900	This work	•		•
		6481.869	Fe I	2.2786	-2.984	1.500	This work	•		
6548.73	6563.37	6556.062	Ti I	1.4601	-1.060	1.250	This work	•		
6585.30	6606.47	6592.912	Fe I	2.7275	-1.473	1.000	This work	•		
		6599.105	Ti I	0.8995	-1.715	0.980	This work	•		
6937.06	6953.09	6945.204	Fe I	2.4242	-2.482	1.490	This work	•		
7208.93	7223.18	7216.184	Ti I	1.4432	-1.200	0.690	This work	•		
7382.29	7396.59	7389.398	Fe I	4.3013	-0.460	0.000	This work	•		
7404.15	7418.15	7411.153	Fe I	4.2833	-0.299	0.990	This work	•		
7482.50	7503.00	7489.578	Ti I	2.2492	-0.910	0.960	This work	•		
		7496.102	Ti I	2.2363	-1.060	0.870	This work	•		
7576.46	7591.08	7583.788	Fe I	3.0176	-1.885	0.830	This work	•		
7905.87	7920.37	7912.866	Fe I	0.8590	-4.848	0.920	•	This work	•	
7991.31	8006.60	7998.944	Fe I	4.3714	+0.151	0.900	This work	•		
8067.78	8082.27	8075.149	Fe I	0.9146	-5.062	0.760	•	This work	•	
8197.77	8212.48	8204.936	Fe I	0.9582	-5.058	0.490	•	This work	•	
8375.78	8457.72	8382.781	Ti I	0.8129	-1.710	0.830	•	This work	•	
		8396.898	Ti I	0.8129	-1.633	0.000	This work	•	•	
		8401.399	Fe I	2.4844	-3.163	0.510	This work	•	•	
		8412.358	Ti I	0.8181	-1.390	0.660	•	Pas19	•	
		8416.950	Ti I	2.2363	-1.080	0.870	This work	•	•	
		8426.507	Ti I	0.8259	-1.200	1.000	•	Pas19	•	
		8434.961	Ti I	0.8484	-0.830	1.210	•	Pas19	•	
		8435.653	Ti I	0.8360	-1.020	1.140	•	Pas19	•	
		8450.891	Ti I	2.2492	-0.800	0.960	This work	•	•	
8459.84	8476.15	8467.147	Ti I	2.1171	-1.101	1.100	Pas19	•		
		8468.406	Fe I	2.2227	-2.072	2.490	•	Pas19	•	
8506.00	8526.00	8514.071	Fe I	2.1979	-2.229	1.830	•	Pas19, Tab18	•	
		8515.108	Fe I	3.0176	-2.073	0.780	•	Tab18	•	
		8518.028	Ti I	2.1344	-0.936	1.260	Tab18	•		
		8518.353	Ti I	1.8792	-1.050	1.060	Tab18	•		
8541.09	8555.21	8548.088	Ti I	1.8732	-1.160	0.820	•	This work	•	
8574.78	8590.67	8582.257	Fe I	2.9904	-2.134	1.070	•	Tab18	•	
8604.25	8619.48	8611.803	Fe I	2.8450	-1.926	1.490	•	Tab18	•	
8667.41	8699.33	8674.746	Fe I	2.8316	-1.800	1.500	•	Pas19	•	
		8675.372	Ti I	1.0666	-1.500	1.190	•	Pas19	•	
		8682.983	Ti I	1.0529	-1.790	0.990	•	Pas19, Tab18	•	
		8688.623	Fe I	2.1759	-1.212	1.660	•	Pas19, Tab18	•	
		8692.330	Ti I	1.0460	-2.130	0.500	•	Tab18	•	
8727.71	8742.59	8734.710	Ti I	1.0529	-2.240	1.000	•	Tab18	•	
8750.26	8764.42	8757.187	Fe I	2.8450	-2.059	1.490	•	Tab18	•	

**Table B.2.** continued.

$\lambda_{\min}$ [\AA]	$\lambda_{\max}$ [\AA]	$\lambda_{\text{line}}$ [\AA]	Element	Atomic line <sup>(a)</sup>	$\chi$ [eV]	$\log g f$	$g_{\text{eff}}$	Magnetically sensitive <sup>(b)</sup>	Ref. <sup>(c)</sup>	GX And	Luyten's star	Teegarden's star
8815.71	8845.95	8824.219	Fe I	2.1979	-1.540	1.490	•	Pas19, Tab18	•	•		
		8838.428	Fe I	2.8581	-2.050	1.500	•	Tab18	•	•		
8848.87	8875.78	8868.430	Fe I	3.0176	-2.909	0.820		This work	•	•		
9003.23	9018.33	9010.592	Fe I	2.6085	-2.953	0.670		This work	•	•		
9711.21	9737.14	9718.960	Ti I	1.5025	-1.181	0.950	•	Pas19	•	•		
		9728.407	Ti I	0.8181	-1.206	1.000	•	Pas19	•	•		
9825.15	9839.50	9832.140	Ti I	1.8871	-1.130	1.210	•	Pas19	•	•		
10052.60	10067.70	10059.904	Ti I	1.4298	-2.080	0.830		This work	•	•		
10333.30	10347.90	10340.885	Fe I	2.1979	-3.577	0.680	•	This work	•	•		
10371.50	10386.70	10378.999	Fe I	2.2227	-4.148	0.260		This work	•	•		
10388.90	10403.60	10395.794	Fe I	2.1759	-3.393	0.890	•	This work	•	•		
10576.90	10592.30	10584.633	Ti I	0.8259	-1.775	1.000	•	Pas19	•	•	•	
10654.40	10669.20	10661.623	Ti I	0.8181	-1.915	0.870	•	Pas19	•	•	•	
10767.90	10781.90	10774.866	Ti I	0.8181	-2.666	0.690	•	Pas19	•	•	•	
11789.90	11804.90	11797.186	Ti I	1.4298	-2.280	0.920	•	This work	•	•	•	
11876.10	11891.90	11884.083	Fe I	2.2227	-2.083	1.000	•	This work	•	•	•	
11942.20	11957.00	11949.547	Ti I	1.4432	-1.570	1.000	•	This work	•	•		
12804.50	12818.60	12811.478	Ti I	2.1603	-1.390	0.950	•	This work	•	•		
12912.90	12926.90	12919.899	Ti I	2.1535	-1.560	0.760		This work	•			
15595.50	15610.40	15602.842	Ti I	2.2674	-1.435	1.000	•	This work	•			
15707.80	15723.50	15715.578	Ti I	1.8732	-1.200	0.750	•	This work	•			

**Notes.** The corresponding wavelength ranges synthesised in this work are listed in the first two columns.  $\chi$ ,  $\log g f$ , and  $g_{\text{eff}}$  are the excitation potential, the oscillator strength, and the effective Landé factors of the lines, respectively. <sup>(a)</sup>Atomic line data from the VALD3 database (Ryabchikova et al. 2015).

<sup>(b)</sup>Lines particularly affected by the stellar magnetic field (López-Gallifa et al. in prep.). <sup>(c)</sup>Lines employed in Tabernero et al. (2018, Tab18), and Passegger et al. (2019, Pas19).

**Table B.3.** Prior  $T_{\text{eff}}$  and  $\log g$  distributions adopted from Cifuentes et al. (2020) and stellar atmospheric parameters of the sample computed with SteParSyn.

Karmen	Prior $T_{\text{eff}}$ [K]	Prior $\log g$ [dex]	$T_{\text{eff}}$ [K]	$\log g$ [dex]	[Fe/H] [dex]	[Fe/H] <sub>corr</sub> [dex]	$T_{\text{eff, fixed}}$ [K]	[Fe/H] <sub>fixed</sub> [dex]	[Fe/H] <sub>corr, fixed</sub> [dex]	Pop. (a)
K7.0 V										
J04167-120	3700 ± 200	4.62 ± 0.20	3961 ± 13	5.01 ± 0.09	0.15 ± 0.04	0.15 ± 0.04	3922 ± 14	0.00 ± 0.02	0.00 ± 0.02	D
J11110+304E	4100 ± 200	4.60 ± 0.20	4211 ± 13	4.98 ± 0.07	0.04 ± 0.03	0.04 ± 0.03	4195 ± 15	-0.07 ± 0.02	-0.04 ± 0.02	D
J18198-019	4000 ± 200	4.64 ± 0.20	4155 ± 14	5.01 ± 0.06	-0.21 ± 0.04	-0.14 ± 0.04	4215 ± 5	-0.33 ± 0.03	-0.22 ± 0.03	YD
M0.0 V										
J03463+262	3900 ± 200	4.67 ± 0.20	3949 ± 12	4.83 ± 0.09	0.01 ± 0.04	0.01 ± 0.04	3941 ± 12	-0.08 ± 0.02	-0.04 ± 0.02	YD
J04376+528	3900 ± 200	4.66 ± 0.20	4039 ± 20	4.94 ± 0.07	-0.21 ± 0.05	-0.14 ± 0.05	4005 ± 9	-0.42 ± 0.03	-0.28 ± 0.03	D
J04588+498	3900 ± 200	4.65 ± 0.20	3983 ± 13	5.07 ± 0.08	0.02 ± 0.03	0.02 ± 0.03	3981 ± 15	-0.21 ± 0.03	-0.14 ± 0.03	D
J05365+113	3900 ± 200	4.65 ± 0.20	4067 ± 14	5.04 ± 0.07	0.01 ± 0.03	0.01 ± 0.03	4001 ± 6	-0.22 ± 0.02	-0.15 ± 0.02	YD
J06371+175	3800 ± 200	4.80 ± 0.20	3803 ± 10	5.20 ± 0.07	-0.63 ± 0.04	-0.43 ± 0.04	3820 ± 11	-0.68 ± 0.04	-0.46 ± 0.04	TD-D
J07393+021	3800 ± 200	4.64 ± 0.20	3980 ± 11	5.03 ± 0.06	0.01 ± 0.03	0.01 ± 0.03	3984 ± 10	-0.17 ± 0.03	-0.11 ± 0.03	YD
J09143+526	3900 ± 200	4.65 ± 0.20	4015 ± 16	4.91 ± 0.08	-0.19 ± 0.05	-0.12 ± 0.05	4004 ± 9	-0.35 ± 0.03	-0.23 ± 0.03	YD
J09144+526	3800 ± 200	4.64 ± 0.20	3983 ± 12	5.17 ± 0.07	-0.06 ± 0.04	-0.03 ± 0.04	3997 ± 15	-0.33 ± 0.03	-0.22 ± 0.03	YD
J09561+627	3800 ± 200	4.66 ± 0.20	3938 ± 13	5.03 ± 0.08	-0.03 ± 0.04	-0.01 ± 0.04	3943 ± 21	-0.16 ± 0.04	-0.10 ± 0.04	YD
J12123+544S	3800 ± 200	4.65 ± 0.20	3902 ± 11	4.99 ± 0.12	-0.14 ± 0.07	-0.08 ± 0.07	3889 ± 13	-0.37 ± 0.03	-0.25 ± 0.03	D
J13255+688	3900 ± 200	4.65 ± 0.20	4049 ± 41	4.96 ± 0.13	0.10 ± 0.04	0.10 ± 0.04	4016 ± 38	0.00 ± 0.06	0.00 ± 0.06	D
J13450+176	3900 ± 200	4.77 ± 0.20	3829 ± 10	4.99 ± 0.06	-0.79 ± 0.03	-0.54 ± 0.03	3849 ± 14	-0.78 ± 0.04	-0.54 ± 0.04	TD
J14257+236W	3800 ± 200	4.62 ± 0.20	3985 ± 13	4.89 ± 0.08	0.07 ± 0.04	0.07 ± 0.04	3954 ± 13	-0.05 ± 0.03	-0.02 ± 0.03	D
J16167+672S	4000 ± 200	4.64 ± 0.20	4034 ± 17	4.78 ± 0.09	0.00 ± 0.04	0.00 ± 0.04	4039 ± 12	-0.02 ± 0.03	-0.01 ± 0.03	D
J17303+055	3800 ± 200	4.72 ± 0.20	3821 ± 9	4.93 ± 0.10	-0.35 ± 0.06	-0.23 ± 0.06	3837 ± 7	-0.39 ± 0.03	-0.26 ± 0.03	YD
J19346+045	4000 ± 200	4.68 ± 0.20	4093 ± 24	4.92 ± 0.07	-0.34 ± 0.05	-0.22 ± 0.05	4165 ± 13	-0.47 ± 0.04	-0.32 ± 0.04	D
J21474+627	3900 ± 200	4.67 ± 0.20	4029 ± 13	4.98 ± 0.04	-0.03 ± 0.03	-0.01 ± 0.03	4001 ± 6	-0.25 ± 0.02	-0.17 ± 0.02	D
M0.5 V										
J02222+478	3900 ± 200	4.70 ± 0.20	3894 ± 11	4.99 ± 0.09	-0.01 ± 0.04	0.00 ± 0.04	3877 ± 10	-0.20 ± 0.03	-0.13 ± 0.03	D
J04290+219	4000 ± 200	4.59 ± 0.20	4123 ± 20	4.48 ± 0.15	0.05 ± 0.06	0.05 ± 0.03	4130 ± 21	0.06 ± 0.03	0.06 ± 0.03	D
J06105-218	3700 ± 200	4.70 ± 0.20	3801 ± 13	4.98 ± 0.09	-0.05 ± 0.05	-0.02 ± 0.05	3813 ± 11	-0.19 ± 0.04	-0.12 ± 0.04	YD
J09511-123	3700 ± 200	4.72 ± 0.20	3769 ± 13	4.84 ± 0.07	-0.34 ± 0.03	-0.23 ± 0.03	3778 ± 11	-0.37 ± 0.03	-0.25 ± 0.03	TD
J10088+692	3900 ± 200	4.63 ± 0.20	3952 ± 15	4.94 ± 0.08	-0.03 ± 0.04	-0.01 ± 0.04	3925 ± 15	-0.21 ± 0.03	-0.14 ± 0.03	D
J12312+086	3900 ± 200	4.71 ± 0.20	3896 ± 11	5.07 ± 0.11	-0.15 ± 0.05	-0.09 ± 0.05	3898 ± 14	-0.35 ± 0.03	-0.23 ± 0.03	D
J13299+102	3700 ± 200	4.75 ± 0.20	3765 ± 18	4.95 ± 0.10	-0.19 ± 0.05	-0.12 ± 0.05	3773 ± 16	-0.29 ± 0.04	-0.20 ± 0.04	D
J14257+236E	3800 ± 200	4.65 ± 0.20	3933 ± 12	4.71 ± 0.11	0.09 ± 0.04	0.09 ± 0.04	3873 ± 12	-0.08 ± 0.04	-0.04 ± 0.04	TD-D
J14307-086	4000 ± 200	4.64 ± 0.20	4037 ± 13	4.82 ± 0.07	0.01 ± 0.03	0.01 ± 0.03	4029 ± 12	-0.01 ± 0.02	0.00 ± 0.02	TD-D
J17355+616	3700 ± 200	4.68 ± 0.20	3847 ± 13	5.02 ± 0.11	-0.06 ± 0.06	-0.03 ± 0.06	3856 ± 11	-0.22 ± 0.03	-0.15 ± 0.03	D
J18353+457	3800 ± 200	4.66 ± 0.20	3876 ± 11	4.82 ± 0.09	-0.08 ± 0.08	-0.04 ± 0.08	3864 ± 8	-0.28 ± 0.02	-0.19 ± 0.02	D
J18580+059	3800 ± 200	4.68 ± 0.20	3857 ± 10	4.73 ± 0.09	-0.22 ± 0.05	-0.15 ± 0.05	3858 ± 7	-0.24 ± 0.02	-0.16 ± 0.02	D
J22021+014	3800 ± 200	4.68 ± 0.20	3882 ± 12	4.97 ± 0.07	-0.02 ± 0.04	0.00 ± 0.04	3869 ± 10	-0.29 ± 0.03	-0.20 ± 0.03	D
J22503-070	3800 ± 200	4.70 ± 0.20	3900 ± 10	5.01 ± 0.09	-0.13 ± 0.04	-0.08 ± 0.04	3904 ± 11	-0.34 ± 0.02	-0.23 ± 0.02	D
M1.0 V										
J00051+457	3600 ± 200	4.71 ± 0.20	3773 ± 16	5.07 ± 0.08	-0.07 ± 0.05	-0.04 ± 0.05	3770 ± 17	-0.23 ± 0.03	-0.15 ± 0.03	YD
J00183+440	3500 ± 200	4.79 ± 0.20	3603 ± 24	4.99 ± 0.14	-0.75 ± 0.11	-0.52 ± 0.11	3603 ± 23	-0.72 ± 0.07	-0.49 ± 0.10	D
J02565+554W	3700 ± 200	4.63 ± 0.20	3832 ± 10	4.65 ± 0.12	-0.07 ± 0.04	-0.04 ± 0.04	3830 ± 10	-0.09 ± 0.02	-0.05 ± 0.02	D

Table B.3. continued.

Karmn	Prior $T_{\text{eff}}$ [K]	Prior $\log g$ [dex]	$T_{\text{eff}}$ [K]	$\log g$ [dex]	[Fe/H] [dex]	[Fe/H] <sub>corr</sub> [dex]	$T_{\text{eff,fixed}}$ [K]	[Fe/H] <sub>fixed</sub> [dex]	[Fe/H] <sub>corr, fixed</sub> [dex]	Pop. <sup>(a)</sup>
J05415+534	3800 ± 200	4.71 ± 0.20	3825 ± 14	4.94 ± 0.10	-0.04 ± 0.06	-0.02 ± 0.06	3829 ± 14	-0.20 ± 0.04	-0.13 ± 0.04	YD
J07361-031	3700 ± 200	4.70 ± 0.20	3825 ± 12	5.06 ± 0.08	-0.07 ± 0.05	-0.04 ± 0.05	3841 ± 9	-0.30 ± 0.03	-0.20 ± 0.03	D
J10023+480	3700 ± 200	4.67 ± 0.20	3739 ± 15	4.76 ± 0.08	-0.21 ± 0.04	-0.14 ± 0.04	3744 ± 13	-0.26 ± 0.02	-0.18 ± 0.02	TD
J10251-102	3700 ± 200	4.73 ± 0.20	3759 ± 14	4.91 ± 0.07	-0.02 ± 0.04	0.00 ± 0.04	3763 ± 15	-0.13 ± 0.02	-0.08 ± 0.02	YD
J11054+435	3400 ± 200	4.83 ± 0.20	3628 ± 19	5.01 ± 0.13	-0.82 ± 0.09	-0.56 ± 0.09	3715 ± 15	-0.52 ± 0.04	-0.36 ± 0.04	TD-D
J13209+342	3700 ± 200	4.71 ± 0.20	3720 ± 13	4.76 ± 0.09	-0.22 ± 0.04	-0.15 ± 0.04	3732 ± 11	-0.28 ± 0.03	-0.19 ± 0.03	D
J14010-026	3700 ± 200	4.74 ± 0.20	3719 ± 15	4.89 ± 0.09	-0.24 ± 0.04	-0.16 ± 0.04	3726 ± 13	-0.32 ± 0.03	-0.21 ± 0.03	D
J14082+805	3700 ± 200	4.65 ± 0.20	3803 ± 12	4.80 ± 0.09	-0.04 ± 0.05	-0.02 ± 0.05	3805 ± 12	-0.11 ± 0.03	-0.06 ± 0.03	D
J15598-082	3600 ± 200	4.75 ± 0.20	3707 ± 14	5.05 ± 0.07	-0.04 ± 0.04	-0.02 ± 0.04	3731 ± 17	-0.25 ± 0.04	-0.17 ± 0.04	D
J16581+257	3600 ± 200	4.71 ± 0.20	3782 ± 17	4.87 ± 0.09	-0.09 ± 0.05	-0.05 ± 0.05	3785 ± 14	-0.20 ± 0.04	-0.13 ± 0.04	D
J17378+185	3700 ± 200	4.82 ± 0.20	3663 ± 19	5.03 ± 0.12	-0.58 ± 0.07	-0.40 ± 0.07	3710 ± 15	-0.48 ± 0.05	-0.33 ± 0.05	D
J18051-030	3700 ± 200	4.80 ± 0.20	3706 ± 13	5.14 ± 0.10	-0.30 ± 0.06	-0.20 ± 0.07	3709 ± 15	-0.41 ± 0.04	-0.28 ± 0.04	D
J18409-133	3700 ± 200	4.70 ± 0.20	3799 ± 12	4.88 ± 0.08	-0.04 ± 0.05	-0.02 ± 0.05	3801 ± 12	-0.14 ± 0.04	-0.08 ± 0.04	D
J20451-313	3600 ± 200	4.54 ± 0.20	3768 ± 20	4.65 ± 0.18	0.01 ± 0.06	0.01 ± 0.06	3799 ± 13	-0.17 ± 0.03	-0.11 ± 0.03	YD
J20533+621	3700 ± 200	4.70 ± 0.20	3815 ± 16	4.83 ± 0.14	-0.16 ± 0.08	-0.10 ± 0.08	3814 ± 15	-0.24 ± 0.04	-0.16 ± 0.04	D
J21221+229	3700 ± 200	4.75 ± 0.20	3761 ± 17	5.00 ± 0.10	-0.27 ± 0.05	-0.18 ± 0.08	3776 ± 14	-0.36 ± 0.05	-0.24 ± 0.05	D
J22330+093	3700 ± 200	4.78 ± 0.20	3722 ± 16	4.98 ± 0.11	-0.30 ± 0.05	-0.20 ± 0.05	3721 ± 14	-0.41 ± 0.04	-0.28 ± 0.04	YD
J22559+178	3700 ± 200	4.69 ± 0.20	3814 ± 12	4.90 ± 0.08	0.02 ± 0.03	0.02 ± 0.03	3813 ± 9	-0.18 ± 0.03	-0.11 ± 0.03	D
J23245+578	3600 ± 200	4.66 ± 0.20	3811 ± 13	4.72 ± 0.10	-0.03 ± 0.06	-0.01 ± 0.06	3810 ± 12	-0.13 ± 0.04	-0.08 ± 0.04	D
J23492+024	3700 ± 200	4.84 ± 0.20	3573 ± 23	4.94 ± 0.13	-0.80 ± 0.08	-0.55 ± 0.08	3562 ± 21	-0.85 ± 0.06	-0.58 ± 0.06	TD
M1.5 V										
J01026+623	3600 ± 200	4.69 ± 0.20	3791 ± 19	4.76 ± 0.11	0.05 ± 0.06	0.05 ± 0.06	3782 ± 18	-0.08 ± 0.04	-0.04 ± 0.04	YD
J02123+035	3700 ± 200	4.81 ± 0.20	3575 ± 14	4.86 ± 0.09	-0.72 ± 0.06	-0.49 ± 0.06	3571 ± 14	-0.75 ± 0.04	-0.52 ± 0.04	TD
J03181+382	3600 ± 200	4.63 ± 0.20	3826 ± 15	4.61 ± 0.14	-0.02 ± 0.05	0.00 ± 0.05	3825 ± 14	-0.01 ± 0.03	0.00 ± 0.03	D
J04376-110	3600 ± 200	4.78 ± 0.20	3666 ± 16	5.08 ± 0.12	-0.08 ± 0.06	-0.04 ± 0.06	3682 ± 17	-0.25 ± 0.04	-0.17 ± 0.04	D
J05314-036	3700 ± 200	4.66 ± 0.20	3850 ± 27	4.71 ± 0.18	0.05 ± 0.08	0.05 ± 0.08	3833 ± 17	0.02 ± 0.04	0.02 ± 0.04	D
J09163-186	3600 ± 200	4.78 ± 0.20	3697 ± 14	5.11 ± 0.16	-0.06 ± 0.06	-0.03 ± 0.06	3700 ± 13	-0.19 ± 0.04	-0.12 ± 0.04	YD
J09411+132	3600 ± 200	4.77 ± 0.20	3699 ± 15	5.01 ± 0.10	-0.03 ± 0.04	-0.01 ± 0.04	3688 ± 20	-0.20 ± 0.04	-0.13 ± 0.04	YD
J09468+760	3700 ± 200	4.75 ± 0.20	3616 ± 17	4.93 ± 0.10	-0.47 ± 0.04	-0.32 ± 0.04	3601 ± 14	-0.55 ± 0.05	-0.38 ± 0.05	TD
J10122-037	3600 ± 200	4.72 ± 0.20	3720 ± 20	4.98 ± 0.10	0.00 ± 0.05	0.00 ± 0.05	3714 ± 21	-0.12 ± 0.03	-0.07 ± 0.03	YD
J11033+359	3500 ± 200	4.86 ± 0.20	3557 ± 26	4.95 ± 0.14	-0.72 ± 0.10	-0.49 ± 0.10	3537 ± 26	-0.76 ± 0.06	-0.52 ± 0.06	TD
J11126+189	3600 ± 200	4.70 ± 0.20	3752 ± 14	4.88 ± 0.07	-0.02 ± 0.03	0.00 ± 0.03	3759 ± 15	-0.13 ± 0.02	-0.08 ± 0.02	D
J11511+352	3600 ± 200	4.78 ± 0.20	3692 ± 21	4.91 ± 0.15	-0.38 ± 0.08	-0.25 ± 0.08	3703 ± 18	-0.34 ± 0.05	-0.23 ± 0.05	D
J13196+333	3600 ± 200	4.66 ± 0.20	3799 ± 11	4.67 ± 0.11	-0.02 ± 0.04	0.00 ± 0.04	3799 ± 11	-0.03 ± 0.03	-0.01 ± 0.03	YD
J13457+148	3600 ± 200	4.74 ± 0.20	3620 ± 24	4.93 ± 0.12	-0.49 ± 0.07	-0.34 ± 0.07	3591 ± 17	-0.69 ± 0.05	-0.47 ± 0.05	D
J15218+209	3500 ± 200	4.67 ± 0.20	3611 ± 16	4.81 ± 0.11	-0.24 ± 0.09	-0.16 ± 0.09	3697 ± 9	-0.35 ± 0.03	-0.23 ± 0.03	D
J16254+543	3600 ± 200	4.94 ± 0.20	3595 ± 19	5.09 ± 0.13	-0.42 ± 0.07	-0.28 ± 0.07	3573 ± 20	-0.67 ± 0.06	-0.46 ± 0.06	YD
J17052-050	3500 ± 200	4.74 ± 0.20	3587 ± 14	4.89 ± 0.10	-0.57 ± 0.07	-0.39 ± 0.07	3583 ± 13	-0.60 ± 0.05	-0.41 ± 0.05	TD-D
J20450+444	3600 ± 200	4.83 ± 0.20	3600 ± 16	4.98 ± 0.12	-0.42 ± 0.07	-0.28 ± 0.07	3603 ± 18	-0.48 ± 0.06	-0.33 ± 0.06	YD
J22057+656	3700 ± 200	4.77 ± 0.20	3707 ± 17	4.86 ± 0.11	-0.30 ± 0.06	-0.20 ± 0.06	3715 ± 19	-0.32 ± 0.04	-0.21 ± 0.04	D
J22565+165	3600 ± 200	4.68 ± 0.20	3798 ± 21	4.80 ± 0.12	0.03 ± 0.06	0.03 ± 0.06	3799 ± 19	-0.07 ± 0.04	-0.04 ± 0.04	D
M2.0 V										

Table B.3. continued.

Karmn	Prior $T_{\text{eff}}$ [K]	Prior $\log g$ [dex]	$T_{\text{eff}}$ [K]	$\log g$ [dex]	[Fe/H] [dex]	[Fe/H] <sub>corr</sub> [dex]	$T_{\text{eff,fixed}}$ [K]	[Fe/H] <sub>fixed</sub> [dex]	[Fe/H] <sub>corr, fixed</sub> [dex]	Pop. <sup>(a)</sup>
J00403+612	3700 ± 200	4.77 ± 0.20	3709 ± 11	5.01 ± 0.09	-0.02 ± 0.03	0.00 ± 0.03	3715 ± 10	-0.18 ± 0.03	-0.11 ± 0.03	YD
J01013+613	3500 ± 200	4.84 ± 0.20	3564 ± 19	5.05 ± 0.08	-0.24 ± 0.07	-0.16 ± 0.07	3545 ± 10	-0.24 ± 0.04	-0.16 ± 0.04	D
J01433+043	3500 ± 200	4.83 ± 0.20	3547 ± 20	5.10 ± 0.17	-0.15 ± 0.07	-0.09 ± 0.07	3539 ± 13	-0.22 ± 0.04	-0.15 ± 0.04	D
J02358+202	3500 ± 200	4.70 ± 0.20	3703 ± 15	4.86 ± 0.09	-0.04 ± 0.04	-0.02 ± 0.04	3696 ± 16	-0.14 ± 0.03	-0.08 ± 0.03	YD
J02489-145W	3500 ± 200	4.74 ± 0.20	3655 ± 25	4.98 ± 0.10	0.04 ± 0.05	0.04 ± 0.05	3674 ± 20	-0.13 ± 0.04	-0.08 ± 0.04	YD
J03213+799	3500 ± 200	4.81 ± 0.20	3599 ± 14	5.12 ± 0.10	-0.32 ± 0.07	-0.21 ± 0.08	3580 ± 13	-0.41 ± 0.05	-0.28 ± 0.05	D
J03217-066	3600 ± 200	4.77 ± 0.20	3661 ± 17	5.16 ± 0.08	0.01 ± 0.04	0.01 ± 0.04	3683 ± 18	-0.19 ± 0.04	-0.12 ± 0.04	YD
J04343+430	3400 ± 200	4.74 ± 0.20	3525 ± 25	4.86 ± 0.11	-0.14 ± 0.09	-0.08 ± 0.09	3533 ± 22	-0.19 ± 0.06	-0.12 ± 0.06	D
J04429+189	3500 ± 200	4.73 ± 0.20	3678 ± 16	5.13 ± 0.08	-0.01 ± 0.03	0.00 ± 0.03	3667 ± 16	-0.18 ± 0.03	-0.11 ± 0.03	D
J04538-177	3500 ± 200	4.81 ± 0.20	3582 ± 17	5.04 ± 0.11	-0.47 ± 0.08	-0.32 ± 0.08	3569 ± 16	-0.62 ± 0.06	-0.42 ± 0.06	D
J05127+196	3500 ± 200	4.78 ± 0.20	3599 ± 13	4.91 ± 0.11	-0.48 ± 0.07	-0.33 ± 0.07	3697 ± 14	-0.22 ± 0.03	-0.15 ± 0.03	D
J06103+821	3500 ± 200	4.81 ± 0.20	3554 ± 20	4.95 ± 0.13	-0.24 ± 0.07	-0.16 ± 0.07	3547 ± 13	-0.24 ± 0.05	-0.16 ± 0.05	D
J07353+548	3500 ± 200	4.86 ± 0.20	3564 ± 17	5.03 ± 0.11	-0.42 ± 0.07	-0.28 ± 0.07	3572 ± 13	-0.42 ± 0.05	-0.28 ± 0.05	YD
J08161+013	3600 ± 200	4.81 ± 0.20	3570 ± 18	4.98 ± 0.14	-0.25 ± 0.07	-0.17 ± 0.07	3564 ± 14	-0.30 ± 0.06	-0.20 ± 0.06	D
J09425+700	3400 ± 200	4.71 ± 0.20	3547 ± 23	5.02 ± 0.12	0.00 ± 0.03	0.00 ± 0.03	3556 ± 18	-0.29 ± 0.06	-0.20 ± 0.06	YD
J10289+008	3600 ± 200	4.82 ± 0.20	3588 ± 24	5.15 ± 0.15	-0.22 ± 0.08	-0.15 ± 0.08	3578 ± 17	-0.39 ± 0.06	-0.26 ± 0.06	YD
J11026+219	3700 ± 200	4.68 ± 0.20	3846 ± 84	4.72 ± 0.23	-0.30 ± 0.14	-0.20 ± 0.14	3833 ± 8	-0.40 ± 0.03	-0.27 ± 0.03	D
J11110+304W	3600 ± 200	4.68 ± 0.20	3730 ± 20	4.78 ± 0.13	-0.09 ± 0.07	-0.05 ± 0.07	3730 ± 22	-0.13 ± 0.04	-0.08 ± 0.04	D
J11201-104	3600 ± 200	4.72 ± 0.20	3697 ± 9	4.66 ± 0.07	-0.39 ± 0.06	-0.26 ± 0.06	3697 ± 9	-0.36 ± 0.04	-0.24 ± 0.04	YD
J12248-182	3500 ± 200	5.00 ± 0.20	3432 ± 30	5.09 ± 0.10	-0.88 ± 0.09	-0.60 ± 0.09	3414 ± 17	-0.93 ± 0.05	-0.63 ± 0.05	TD
J13119+658	3600 ± 200	4.80 ± 0.20	3686 ± 16	4.83 ± 0.07	-0.43 ± 0.05	-0.29 ± 0.05	3672 ± 35	-0.36 ± 0.09	-0.24 ± 0.09	D
J14294+155	3500 ± 200	4.70 ± 0.20	3660 ± 17	4.75 ± 0.09	-0.24 ± 0.06	-0.16 ± 0.06	3687 ± 14	-0.18 ± 0.03	-0.11 ± 0.03	TD
J14524+123	3500 ± 200	4.70 ± 0.20	3703 ± 21	4.88 ± 0.13	0.04 ± 0.07	0.04 ± 0.07	3689 ± 15	-0.04 ± 0.03	-0.02 ± 0.03	D
J15474-108	3500 ± 200	4.76 ± 0.20	3481 ± 29	5.00 ± 0.14	-0.70 ± 0.11	-0.48 ± 0.11	3459 ± 21	-0.84 ± 0.06	-0.57 ± 0.06	D
J17166+080	3500 ± 200	4.82 ± 0.20	3567 ± 19	4.89 ± 0.11	-0.38 ± 0.09	-0.25 ± 0.09	3573 ± 16	-0.37 ± 0.07	-0.25 ± 0.07	YD
J18174+483	3500 ± 200	4.68 ± 0.20	3605 ± 29	4.87 ± 0.17	-0.47 ± 0.11	-0.32 ± 0.11	3633 ± 41	-0.46 ± 0.12	-0.31 ± 0.12	YD
J19070+208	3600 ± 200	4.94 ± 0.20	3543 ± 21	5.03 ± 0.12	-0.68 ± 0.07	-0.46 ± 0.07	3538 ± 20	-0.75 ± 0.06	-0.52 ± 0.06	D
J19072+208	3600 ± 200	4.94 ± 0.20	3558 ± 19	5.06 ± 0.10	-0.67 ± 0.06	-0.46 ± 0.06	3548 ± 19	-0.75 ± 0.05	-0.52 ± 0.05	D
J22115+184	3500 ± 200	4.69 ± 0.20	3704 ± 20	4.77 ± 0.12	-0.01 ± 0.06	0.00 ± 0.06	3696 ± 20	-0.05 ± 0.03	-0.02 ± 0.03	D
J23381-162	3500 ± 200	4.85 ± 0.20	3570 ± 22	5.07 ± 0.12	-0.51 ± 0.08	-0.35 ± 0.08	3557 ± 21	-0.63 ± 0.06	-0.43 ± 0.06	D
							M2.5 V			
J00389+306	3500 ± 200	4.81 ± 0.20	3551 ± 17	4.90 ± 0.11	-0.24 ± 0.07	-0.16 ± 0.07	3563 ± 15	-0.28 ± 0.06	-0.19 ± 0.06	D
J01518+644	3500 ± 200	4.75 ± 0.20	3625 ± 21	5.04 ± 0.10	-0.03 ± 0.05	-0.01 ± 0.05	3611 ± 20	-0.14 ± 0.05	-0.08 ± 0.05	YD
J02489-145E	3500 ± 200	4.79 ± 0.20	3572 ± 27	4.94 ± 0.12	0.00 ± 0.04	0.00 ± 0.04	3549 ± 24	-0.10 ± 0.03	-0.06 ± 0.03	YD
J05337+019	3400 ± 200	4.80 ± 0.20	3428 ± 32	4.98 ± 0.10	-0.10 ± 0.07	-0.06 ± 0.07	3440 ± 29	-0.16 ± 0.05	-0.10 ± 0.05	YD
J08293+039	3500 ± 200	4.73 ± 0.20	3651 ± 17	4.97 ± 0.13	-0.06 ± 0.06	-0.03 ± 0.06	3658 ± 13	-0.19 ± 0.04	-0.12 ± 0.04	YD
J08358+680	3400 ± 200	4.85 ± 0.20	3496 ± 16	5.11 ± 0.10	-0.07 ± 0.05	-0.04 ± 0.05	3480 ± 20	-0.16 ± 0.04	-0.10 ± 0.04	D
J09133+688	3500 ± 200	4.65 ± 0.20	3662 ± 26	4.67 ± 0.12	-0.38 ± 0.09	-0.25 ± 0.09	3653 ± 23	-0.35 ± 0.06	-0.23 ± 0.06	YD
J09360-216	3400 ± 200	4.87 ± 0.20	3496 ± 20	4.95 ± 0.11	-0.35 ± 0.07	-0.23 ± 0.07	3485 ± 19	-0.40 ± 0.04	-0.27 ± 0.04	D
J10396-069	3400 ± 200	4.73 ± 0.20	3592 ± 19	4.89 ± 0.11	-0.14 ± 0.07	-0.08 ± 0.07	3581 ± 17	-0.20 ± 0.03	-0.13 ± 0.03	YD
J11000+228	3400 ± 200	4.83 ± 0.20	3532 ± 21	5.04 ± 0.14	-0.12 ± 0.07	-0.07 ± 0.07	3521 ± 20	-0.18 ± 0.04	-0.11 ± 0.04	YD
J11302+076	3400 ± 200	4.76 ± 0.20	3563 ± 25	4.93 ± 0.10	-0.13 ± 0.10	-0.08 ± 0.10	3565 ± 23	-0.19 ± 0.05	-0.12 ± 0.05	D

Table B.3. continued.

Karmn	Prior $T_{\text{eff}}$ [K]	Prior $\log g$ [dex]	$T_{\text{eff}}$ [K]	$\log g$ [dex]	[Fe/H] [dex]	[Fe/H] <sub>corr</sub> [dex]	$T_{\text{eff,fixed}}$ [K]	[Fe/H] <sub>fixed</sub> [dex]	[Fe/H] <sub>corr, fixed</sub> [dex]	Pop. <sup>(a)</sup>
J11421+267	3400 ± 200	4.79 ± 0.20	3533 ± 26	4.83 ± 0.11	-0.19 ± 0.10	-0.12 ± 0.10	3507 ± 22	-0.22 ± 0.08	-0.15 ± 0.08	D
J12350+098	3500 ± 200	4.74 ± 0.20	3556 ± 16	4.82 ± 0.07	-0.28 ± 0.07	-0.19 ± 0.07	3536 ± 18	-0.31 ± 0.05	-0.21 ± 0.05	D
J14251+518	3400 ± 200	4.80 ± 0.20	3551 ± 22	4.90 ± 0.10	-0.21 ± 0.06	-0.14 ± 0.06	3550 ± 12	-0.25 ± 0.04	-0.17 ± 0.04	D
J16462+164	3400 ± 200	4.78 ± 0.20	3560 ± 21	4.90 ± 0.10	-0.15 ± 0.07	-0.09 ± 0.07	3547 ± 15	-0.20 ± 0.04	-0.13 ± 0.04	D
J17198+417	3400 ± 200	4.84 ± 0.20	3540 ± 20	4.96 ± 0.12	-0.30 ± 0.07	-0.20 ± 0.07	3540 ± 16	-0.28 ± 0.06	-0.19 ± 0.06	D
J17578+465	3300 ± 200	4.79 ± 0.20	3507 ± 23	4.93 ± 0.09	-0.04 ± 0.06	-0.02 ± 0.06	3509 ± 18	-0.11 ± 0.05	-0.06 ± 0.05	YD
J18480-145	3400 ± 200	4.83 ± 0.20	3540 ± 29	4.92 ± 0.11	-0.20 ± 0.06	-0.13 ± 0.06	3544 ± 15	-0.23 ± 0.05	-0.15 ± 0.05	D
J19169+05N	3400 ± 200	4.72 ± 0.20	3575 ± 25	4.88 ± 0.12	-0.14 ± 0.08	-0.08 ± 0.08	3597 ± 28	-0.22 ± 0.06	-0.15 ± 0.06	D
J20305+654	3400 ± 200	4.83 ± 0.20	3514 ± 23	5.06 ± 0.11	-0.06 ± 0.06	-0.03 ± 0.06	3525 ± 13	-0.15 ± 0.04	-0.09 ± 0.04	D
J20567-104	3300 ± 200	4.70 ± 0.20	3560 ± 27	4.91 ± 0.09	-0.07 ± 0.06	-0.04 ± 0.06	3547 ± 16	-0.21 ± 0.04	-0.14 ± 0.04	TD
J21019-063	3400 ± 200	4.74 ± 0.20	3568 ± 20	4.95 ± 0.10	-0.07 ± 0.06	-0.04 ± 0.06	3554 ± 18	-0.21 ± 0.04	-0.14 ± 0.04	D
J23340+001	3400 ± 200	4.77 ± 0.20	3530 ± 21	4.91 ± 0.09	-0.38 ± 0.08	-0.25 ± 0.08	3548 ± 15	-0.30 ± 0.04	-0.20 ± 0.04	D
J23556-061	3400 ± 200	4.80 ± 0.20	3639 ± 30	4.84 ± 0.14	-0.04 ± 0.08	-0.02 ± 0.08	3643 ± 23	-0.04 ± 0.05	-0.02 ± 0.05	D
M3.0V										
J00570+450	3300 ± 200	4.86 ± 0.20	3488 ± 22	5.04 ± 0.10	-0.04 ± 0.05	-0.02 ± 0.05	3491 ± 21	-0.17 ± 0.06	-0.11 ± 0.06	YD
J01025+716	3400 ± 200	4.74 ± 0.20	3524 ± 26	4.86 ± 0.10	-0.08 ± 0.07	-0.04 ± 0.09	3516 ± 21	-0.14 ± 0.06	-0.08 ± 0.06	D
J01066+192	3400 ± 200	4.88 ± 0.20	3496 ± 25	5.00 ± 0.11	-0.08 ± 0.07	-0.04 ± 0.07	3495 ± 22	-0.09 ± 0.05	-0.05 ± 0.05	YD
J02015+637	3400 ± 200	4.77 ± 0.20	3579 ± 23	4.87 ± 0.11	-0.14 ± 0.08	-0.08 ± 0.08	3549 ± 22	-0.16 ± 0.05	-0.10 ± 0.05	D
J02442+255	3400 ± 200	4.86 ± 0.20	3510 ± 21	4.97 ± 0.11	-0.14 ± 0.08	-0.08 ± 0.08	3512 ± 20	-0.18 ± 0.06	-0.11 ± 0.06	YD
J03473-019	3400 ± 200	4.73 ± 0.20	3473 ± 72	4.85 ± 0.18	-0.26 ± 0.15	-0.18 ± 0.15	3437 ± 76	-0.26 ± 0.18	-0.18 ± 0.18	YD
J03531+625	3500 ± 200	4.88 ± 0.20	3501 ± 23	5.04 ± 0.11	-0.28 ± 0.10	-0.19 ± 0.10	3506 ± 22	-0.26 ± 0.09	-0.18 ± 0.09	TD
J05033-173	3300 ± 200	4.95 ± 0.20	3464 ± 27	5.08 ± 0.10	-0.20 ± 0.09	-0.13 ± 0.09	3475 ± 26	-0.16 ± 0.06	-0.10 ± 0.06	YD
J06548+332	3400 ± 200	4.87 ± 0.20	3503 ± 37	4.88 ± 0.12	-0.20 ± 0.12	-0.13 ± 0.12	3497 ± 33	-0.16 ± 0.09	-0.10 ± 0.09	YD
J07044+682	3400 ± 200	4.81 ± 0.20	3527 ± 21	4.82 ± 0.09	-0.16 ± 0.08	-0.10 ± 0.08	3527 ± 19	-0.18 ± 0.06	-0.11 ± 0.06	D
J07287-032	3300 ± 200	4.81 ± 0.20	3511 ± 21	4.82 ± 0.08	-0.20 ± 0.07	-0.13 ± 0.07	3519 ± 18	-0.22 ± 0.06	-0.15 ± 0.06	D
J07386-212	3300 ± 200	4.92 ± 0.20	3488 ± 24	4.95 ± 0.09	-0.16 ± 0.07	-0.10 ± 0.07	3490 ± 21	-0.14 ± 0.06	-0.08 ± 0.06	D
J09140+196	3400 ± 200	4.72 ± 0.20	3561 ± 19	5.04 ± 0.11	-0.04 ± 0.05	-0.02 ± 0.05	3553 ± 17	-0.24 ± 0.04	-0.16 ± 0.04	YD
J09428+700	3400 ± 200	4.79 ± 0.20	3504 ± 30	5.06 ± 0.12	0.02 ± 0.05	0.02 ± 0.05	3503 ± 20	-0.07 ± 0.05	-0.04 ± 0.05	YD
J10167-119	3500 ± 200	4.75 ± 0.20	3552 ± 20	4.84 ± 0.09	-0.10 ± 0.06	-0.06 ± 0.06	3539 ± 15	-0.17 ± 0.04	-0.11 ± 0.04	D
J10196+198	3300 ± 200	4.77 ± 0.20	3477 ± 23	5.12 ± 0.12	-0.28 ± 0.12	-0.19 ± 0.12	3449 ± 54	-0.61 ± 0.24	-0.41 ± 0.24	YD
J10350-094	3300 ± 200	4.81 ± 0.20	3512 ± 20	4.85 ± 0.08	-0.15 ± 0.08	-0.09 ± 0.08	3514 ± 20	-0.16 ± 0.06	-0.10 ± 0.06	D
J11044+304	3200 ± 200	4.83 ± 0.20	3534 ± 97	4.84 ± 0.21	-0.72 ± 0.17	-0.49 ± 0.17	3513 ± 91	-0.76 ± 0.12	-0.52 ± 0.12	YD
J11467-140	3400 ± 200	4.69 ± 0.20	3565 ± 20	4.77 ± 0.11	-0.01 ± 0.05	0.00 ± 0.05	3597 ± 16	-0.03 ± 0.03	-0.01 ± 0.03	D
J12111-199	3400 ± 200	4.86 ± 0.20	3517 ± 18	4.92 ± 0.09	-0.19 ± 0.06	-0.12 ± 0.06	3522 ± 16	-0.19 ± 0.05	-0.12 ± 0.05	YD
J12230+640	3500 ± 200	4.74 ± 0.20	3563 ± 28	4.80 ± 0.13	-0.24 ± 0.10	-0.16 ± 0.10	3562 ± 28	-0.27 ± 0.07	-0.18 ± 0.07	D
J12388+116	3300 ± 200	4.73 ± 0.20	3525 ± 26	4.85 ± 0.09	-0.01 ± 0.06	0.00 ± 0.06	3521 ± 21	-0.06 ± 0.04	-0.03 ± 0.04	D
J13283-023W	3400 ± 200	4.77 ± 0.20	3554 ± 28	4.86 ± 0.13	-0.12 ± 0.09	-0.07 ± 0.09	3535 ± 16	-0.13 ± 0.04	-0.08 ± 0.04	D
J13582+125	3300 ± 200	5.03 ± 0.20	3442 ± 27	5.13 ± 0.13	-0.14 ± 0.09	-0.08 ± 0.09	3461 ± 29	-0.08 ± 0.06	-0.04 ± 0.06	D
J14152+450	3400 ± 200	4.77 ± 0.20	3516 ± 16	4.85 ± 0.06	-0.07 ± 0.05	-0.04 ± 0.05	3515 ± 13	-0.13 ± 0.04	-0.08 ± 0.04	D
J15013+055	3300 ± 200	4.85 ± 0.20	3502 ± 22	4.98 ± 0.09	-0.05 ± 0.05	-0.02 ± 0.05	3503 ± 18	-0.10 ± 0.04	-0.06 ± 0.04	D
J15095+031	3400 ± 200	4.78 ± 0.20	3545 ± 17	4.86 ± 0.09	-0.14 ± 0.07	-0.08 ± 0.07	3544 ± 16	-0.19 ± 0.04	-0.12 ± 0.04	D
J15194-077	3300 ± 200	4.90 ± 0.20	3500 ± 26	4.97 ± 0.11	-0.14 ± 0.07	-0.08 ± 0.07	3495 ± 26	-0.17 ± 0.08	-0.11 ± 0.08	YD

Table B.3. continued.

Karmn	Prior $T_{\text{eff}}$ [K]	Prior $\log g$ [dex]	$T_{\text{eff}}$ [K]	$\log g$ [dex]	[Fe/H] [dex]	[Fe/H] <sub>corr</sub> [dex]	$T_{\text{eff,fixed}}$ [K]	[Fe/H] <sub>fixed</sub> [dex]	[Fe/H] <sub>corr, fixed</sub> [dex]	Pop. <sup>(a)</sup>
J16092+093	3300 ± 200	4.82 ± 0.20	3517 ± 18	5.06 ± 0.10	-0.03 ± 0.04	-0.01 ± 0.04	3525 ± 11	-0.14 ± 0.03	-0.08 ± 0.03	D
J16102-193	3100 ± 200	4.41 ± 0.20	3575 ± 55	4.48 ± 0.19	-0.04 ± 0.07	-0.02 ± 0.07	3552 ± 46	-0.02 ± 0.06	0.00 ± 0.06	YD
J16167+672N	3400 ± 200	4.74 ± 0.20	3569 ± 32	4.97 ± 0.11	-0.04 ± 0.06	-0.02 ± 0.06	3532 ± 32	-0.08 ± 0.05	-0.04 ± 0.05	YD
J16327+126	3500 ± 200	4.84 ± 0.20	3486 ± 21	4.92 ± 0.09	-0.28 ± 0.07	-0.19 ± 0.07	3492 ± 18	-0.26 ± 0.06	-0.18 ± 0.06	TD-D
J17071+215	3400 ± 200	4.82 ± 0.20	3534 ± 30	4.94 ± 0.13	-0.22 ± 0.11	-0.15 ± 0.11	3545 ± 16	-0.21 ± 0.05	-0.14 ± 0.05	D
J17364+683	3300 ± 200	4.84 ± 0.20	3389 ± 81	4.89 ± 0.15	-0.10 ± 0.13	-0.06 ± 0.13	3385 ± 79	-0.14 ± 0.12	-0.08 ± 0.12	D
J18180+387E	3200 ± 200	4.87 ± 0.20	3495 ± 20	5.01 ± 0.10	-0.21 ± 0.07	-0.14 ± 0.07	3430 ± 47	-0.62 ± 0.19	-0.42 ± 0.19	D
J18419+318	3300 ± 200	4.84 ± 0.20	3519 ± 20	4.93 ± 0.10	-0.30 ± 0.08	-0.20 ± 0.08	3521 ± 16	-0.23 ± 0.06	-0.15 ± 0.06	D
J18427+596N	3300 ± 200	4.84 ± 0.20	3473 ± 34	4.90 ± 0.11	-0.46 ± 0.12	-0.31 ± 0.12	3466 ± 31	-0.44 ± 0.13	-0.30 ± 0.13	D
J19084+322	3300 ± 200	4.85 ± 0.20	3501 ± 25	4.92 ± 0.09	-0.13 ± 0.07	-0.08 ± 0.07	3503 ± 21	-0.17 ± 0.06	-0.11 ± 0.06	YD
J19251+283	3300 ± 200	4.84 ± 0.20	3472 ± 29	4.90 ± 0.08	-0.09 ± 0.07	-0.05 ± 0.07	3476 ± 26	-0.10 ± 0.05	-0.06 ± 0.05	D
J21152+257	3400 ± 200	4.65 ± 0.20	3611 ± 25	4.67 ± 0.16	0.05 ± 0.05	0.05 ± 0.05	3682 ± 18	0.08 ± 0.03	0.08 ± 0.03	D
J21164+025	3400 ± 200	4.79 ± 0.20	3550 ± 23	4.88 ± 0.11	-0.13 ± 0.09	-0.08 ± 0.09	3533 ± 21	-0.17 ± 0.06	-0.11 ± 0.06	YD
J21348+515	3400 ± 200	4.76 ± 0.20	3525 ± 23	4.87 ± 0.10	-0.15 ± 0.08	-0.09 ± 0.08	3528 ± 19	-0.22 ± 0.05	-0.15 ± 0.05	YD
J22125+085	3400 ± 200	4.84 ± 0.20	3528 ± 25	4.90 ± 0.13	-0.30 ± 0.09	-0.20 ± 0.09	3534 ± 23	-0.26 ± 0.07	-0.18 ± 0.07	D
J22518+317	3300 ± 200	4.74 ± 0.20	3335 ± 44	4.68 ± 0.14	-0.45 ± 0.18	-0.31 ± 0.18	3407 ± 20	-0.34 ± 0.13	-0.23 ± 0.13	YD
J23585+076	3300 ± 200	4.84 ± 0.20	3496 ± 20	4.97 ± 0.08	-0.10 ± 0.06	-0.06 ± 0.06	3496 ± 19	-0.16 ± 0.04	-0.10 ± 0.04	D
M3.5 V										
J00184+440	3200 ± 200	5.12 ± 0.20	3318 ± 53	5.20 ± 0.11	-0.53 ± 0.17	-0.36 ± 0.17	3302 ± 61	-0.55 ± 0.25	-0.38 ± 0.25	D
J02002+130	3100 ± 200	5.16 ± 0.20	3237 ± 32	5.22 ± 0.14	-0.38 ± 0.14	-0.25 ± 0.14	3210 ± 27	-0.51 ± 0.28	-0.35 ± 0.28	D
J02070+496	3400 ± 200	4.90 ± 0.20	3455 ± 22	5.16 ± 0.13	-0.12 ± 0.06	-0.07 ± 0.06	3471 ± 22	-0.10 ± 0.03	-0.06 ± 0.03	YD
J02088+494	3300 ± 200	4.83 ± 0.20	3266 ± 36	4.88 ± 0.14	-0.24 ± 0.19	-0.16 ± 0.19	3270 ± 37	-0.14 ± 0.18	-0.08 ± 0.18	YD
J04225+105	3300 ± 200	4.75 ± 0.20	3546 ± 25	4.71 ± 0.10	-0.10 ± 0.07	-0.06 ± 0.07	3536 ± 24	-0.07 ± 0.04	-0.04 ± 0.04	YD
J04429+214	3400 ± 200	4.85 ± 0.20	3499 ± 24	4.90 ± 0.08	-0.02 ± 0.04	0.00 ± 0.04	3495 ± 20	-0.02 ± 0.03	0.00 ± 0.03	D
J04520+064	3200 ± 200	4.82 ± 0.20	3439 ± 30	4.83 ± 0.08	-0.13 ± 0.06	-0.08 ± 0.06	3447 ± 30	-0.10 ± 0.06	-0.06 ± 0.06	D
J05280+096	3300 ± 200	5.02 ± 0.20	3440 ± 27	5.05 ± 0.11	-0.24 ± 0.09	-0.16 ± 0.09	3438 ± 23	-0.23 ± 0.08	-0.15 ± 0.08	D
J05348+138	3300 ± 200	4.85 ± 0.20	3464 ± 28	4.85 ± 0.08	-0.12 ± 0.07	-0.07 ± 0.07	3463 ± 28	-0.12 ± 0.07	-0.07 ± 0.07	YD
J06011+595	3300 ± 200	4.98 ± 0.20	3431 ± 35	4.97 ± 0.12	-0.22 ± 0.13	-0.15 ± 0.13	3389 ± 40	-0.11 ± 0.09	-0.06 ± 0.09	YD
J06421+035	3300 ± 200	4.82 ± 0.20	3475 ± 27	4.88 ± 0.08	-0.13 ± 0.08	-0.08 ± 0.08	3485 ± 26	-0.15 ± 0.07	-0.09 ± 0.07	D
J072274+052	3200 ± 200	4.91 ± 0.20	3380 ± 43	4.96 ± 0.11	-0.17 ± 0.11	-0.11 ± 0.11	3382 ± 45	-0.19 ± 0.11	-0.12 ± 0.11	D
J07319+362N	3200 ± 200	4.79 ± 0.20	3289 ± 32	5.10 ± 0.13	-0.15 ± 0.09	-0.09 ± 0.09	3248 ± 19	-0.93 ± 0.05	-0.63 ± 0.05	YD
J07582+413	3200 ± 200	4.95 ± 0.20	3431 ± 28	4.87 ± 0.10	-0.22 ± 0.08	-0.15 ± 0.08	3438 ± 26	-0.23 ± 0.10	-0.15 ± 0.10	D
J08402+314	3300 ± 200	4.94 ± 0.20	3426 ± 23	4.88 ± 0.09	-0.20 ± 0.07	-0.13 ± 0.07	3428 ± 23	-0.15 ± 0.07	-0.09 ± 0.07	TD-D
J08409-234	3300 ± 200	4.78 ± 0.20	3496 ± 37	4.78 ± 0.09	-0.05 ± 0.08	-0.02 ± 0.08	3489 ± 35	-0.05 ± 0.05	-0.02 ± 0.05	TD-D
J09307+003	3300 ± 200	4.91 ± 0.20	3460 ± 27	4.90 ± 0.08	-0.18 ± 0.08	-0.11 ± 0.08	3460 ± 26	-0.12 ± 0.07	-0.07 ± 0.07	D
J09423+559	3300 ± 200	4.83 ± 0.20	3439 ± 29	4.79 ± 0.06	-0.11 ± 0.06	-0.06 ± 0.06	3439 ± 29	-0.07 ± 0.06	-0.04 ± 0.06	D
J09439+269	3300 ± 200	4.82 ± 0.20	3492 ± 23	4.84 ± 0.06	-0.10 ± 0.05	-0.06 ± 0.05	3494 ± 21	-0.08 ± 0.04	-0.04 ± 0.04	D
J10125+570	3300 ± 200	4.91 ± 0.20	3474 ± 24	4.90 ± 0.08	-0.14 ± 0.06	-0.08 ± 0.06	3461 ± 24	-0.13 ± 0.06	-0.08 ± 0.06	YD
J10360+051	3200 ± 200	4.86 ± 0.20	3268 ± 16	5.14 ± 0.08	-0.91 ± 0.07	-0.62 ± 0.07	3323 ± 55	-0.77 ± 0.24	-0.53 ± 0.24	D
J11289+101	3300 ± 200	4.96 ± 0.20	3405 ± 33	4.86 ± 0.10	-0.27 ± 0.10	-0.18 ± 0.10	3383 ± 32	-0.32 ± 0.10	-0.21 ± 0.10	D
J11306-080	3300 ± 200	4.85 ± 0.20	3486 ± 28	4.90 ± 0.08	-0.03 ± 0.05	-0.01 ± 0.05	3469 ± 29	-0.04 ± 0.03	-0.02 ± 0.03	YD
J14476+786	3300 ± 200	4.99 ± 0.20	3361 ± 45	4.93 ± 0.12	-0.55 ± 0.14	-0.38 ± 0.14	3353 ± 40	-0.53 ± 0.14	-0.36 ± 0.14	TD

Table B.3. continued.

Karmn	Prior $T_{\text{eff}}$ [K]	Prior $\log g$ [dex]	$T_{\text{eff}}$ [K]	$\log g$ [dex]	[Fe/H] [dex]	[Fe/H] <sub>corr</sub> [dex]	$T_{\text{eff,fixed}}$ [K]	[Fe/H] <sub>fixed</sub> [dex]	[Fe/H] <sub>corr, fixed</sub> [dex]	Pop. <sup>(a)</sup>
J12100–150	3200 ± 200	4.82 ± 0.20	3415 ± 35	4.74 ± 0.11	-0.12 ± 0.10	-0.07 ± 0.10	3391 ± 31	-0.10 ± 0.10	-0.06 ± 0.10	TD
J12479+097	3200 ± 200	4.88 ± 0.20	3408 ± 45	4.82 ± 0.12	-0.23 ± 0.13	-0.15 ± 0.13	3413 ± 33	-0.23 ± 0.12	-0.15 ± 0.12	D
J13293+114	3400 ± 200	4.78 ± 0.20	3455 ± 24	4.83 ± 0.07	-0.17 ± 0.06	-0.11 ± 0.06	3458 ± 23	-0.17 ± 0.05	-0.11 ± 0.05	TD
J13427+332	3200 ± 200	4.94 ± 0.20	3430 ± 28	4.88 ± 0.09	-0.21 ± 0.09	-0.14 ± 0.09	3427 ± 33	-0.16 ± 0.07	-0.10 ± 0.07	D
J13458–179	3300 ± 200	4.88 ± 0.20	3443 ± 29	4.78 ± 0.10	-0.16 ± 0.09	-0.10 ± 0.09	3435 ± 29	-0.15 ± 0.09	-0.09 ± 0.09	D
J14310–122	3200 ± 200	4.87 ± 0.20	3450 ± 28	4.79 ± 0.08	-0.23 ± 0.07	-0.15 ± 0.07	3448 ± 30	-0.20 ± 0.08	-0.13 ± 0.08	YD
J14544+355	3300 ± 200	4.86 ± 0.20	3433 ± 29	4.82 ± 0.12	-0.13 ± 0.08	-0.08 ± 0.08	3432 ± 29	-0.09 ± 0.07	-0.05 ± 0.07	D
J15583+354	3300 ± 200	4.91 ± 0.20	3478 ± 32	4.91 ± 0.10	-0.16 ± 0.08	-0.10 ± 0.08	3472 ± 29	-0.16 ± 0.08	-0.10 ± 0.08	D
J16303–126	3300 ± 200	4.93 ± 0.20	3426 ± 33	4.89 ± 0.10	-0.22 ± 0.11	-0.15 ± 0.11	3426 ± 36	-0.21 ± 0.11	-0.14 ± 0.11	YD
J16554–083N	3300 ± 200	5.06 ± 0.20	3397 ± 33	5.07 ± 0.12	-0.25 ± 0.10	-0.17 ± 0.10	3413 ± 25	-0.27 ± 0.10	-0.18 ± 0.10	D
J16570–043	3300 ± 200	5.02 ± 0.20	3206 ± 14	4.81 ± 0.08	-0.89 ± 0.03	-0.60 ± 0.03	3204 ± 8	-0.94 ± 0.04	-0.64 ± 0.04	YD
J17115+384	3300 ± 200	4.81 ± 0.20	3472 ± 35	4.74 ± 0.08	-0.13 ± 0.08	-0.08 ± 0.08	3475 ± 32	-0.12 ± 0.07	-0.07 ± 0.07	D
J17578+046	3200 ± 200	5.12 ± 0.20	3254 ± 32	5.13 ± 0.12	-0.84 ± 0.10	-0.57 ± 0.10	3240 ± 27	-0.86 ± 0.09	-0.59 ± 0.09	TD
J18319+406	3300 ± 200	4.85 ± 0.20	3492 ± 25	4.92 ± 0.09	-0.07 ± 0.06	-0.04 ± 0.06	3489 ± 24	-0.07 ± 0.04	-0.04 ± 0.04	YD
J18346+401	3200 ± 200	4.76 ± 0.20	3447 ± 46	4.69 ± 0.11	-0.06 ± 0.09	-0.03 ± 0.09	3458 ± 47	0.02 ± 0.06	0.02 ± 0.06	D
J18427+596S	3300 ± 200	4.90 ± 0.20	3393 ± 48	4.98 ± 0.12	-0.56 ± 0.18	-0.38 ± 0.18	3440 ± 49	-0.39 ± 0.20	-0.26 ± 0.20	D
J18498–238	3200 ± 200	5.10 ± 0.20	3340 ± 30	5.23 ± 0.11	-0.63 ± 0.10	-0.43 ± 0.10	3268 ± 17	-0.97 ± 0.03	-0.66 ± 0.03	D
J22020–194	3300 ± 200	4.88 ± 0.20	3474 ± 23	4.85 ± 0.07	-0.17 ± 0.07	-0.11 ± 0.07	3471 ± 24	-0.15 ± 0.08	-0.09 ± 0.08	D
J22096–046	3400 ± 200	4.75 ± 0.20	3540 ± 31	4.81 ± 0.11	-0.02 ± 0.07	0.00 ± 0.07	3531 ± 32	-0.04 ± 0.05	-0.02 ± 0.05	YD
J22468+443	3200 ± 200	4.87 ± 0.20	3306 ± 30	5.06 ± 0.13	-0.89 ± 0.09	-0.60 ± 0.09	3342 ± 49	-0.81 ± 0.19	-0.55 ± 0.19	D
J23113+085	3300 ± 200	4.90 ± 0.20	3477 ± 38	4.81 ± 0.10	-0.12 ± 0.09	-0.07 ± 0.09	3472 ± 42	-0.09 ± 0.10	-0.05 ± 0.10	D
M4.0V										
J00162+198E	3200 ± 200	4.94 ± 0.20	3329 ± 30	4.93 ± 0.07	-0.18 ± 0.09	-0.11 ± 0.09	3327 ± 25	-0.19 ± 0.07	-0.12 ± 0.07	TD-D
J00286–066	3300 ± 200	4.86 ± 0.20	3419 ± 28	4.81 ± 0.08	-0.17 ± 0.08	-0.11 ± 0.08	3412 ± 35	-0.21 ± 0.10	-0.14 ± 0.10	D
J01339–176	3200 ± 200	4.94 ± 0.20	3376 ± 34	5.15 ± 0.12	-0.20 ± 0.08	-0.13 ± 0.08	3424 ± 19	-0.06 ± 0.03	-0.03 ± 0.03	YD
J01352–072	3200 ± 200	4.60 ± 0.20	3052 ± 12	4.73 ± 0.15	-0.04 ± 0.08	-0.02 ± 0.08	3033 ± 7	-0.12 ± 0.09	-0.07 ± 0.09	YD
J02336+249	3100 ± 200	5.01 ± 0.20	3313 ± 24	5.19 ± 0.10	-0.27 ± 0.10	-0.18 ± 0.10	3335 ± 22	-0.06 ± 0.05	-0.03 ± 0.05	D
J02362+068	3200 ± 200	4.96 ± 0.20	3335 ± 45	4.91 ± 0.10	-0.36 ± 0.12	-0.24 ± 0.12	3338 ± 40	-0.34 ± 0.11	-0.23 ± 0.11	D
J02519+224	3200 ± 200	4.71 ± 0.20	3158 ± 42	4.68 ± 0.17	-0.06 ± 0.19	-0.03 ± 0.19	3176 ± 33	-0.15 ± 0.16	-0.09 ± 0.16	YD
J04311+589	3200 ± 200	4.94 ± 0.20	3382 ± 39	4.89 ± 0.10	-0.25 ± 0.11	-0.17 ± 0.11	3365 ± 35	-0.24 ± 0.10	-0.16 ± 0.10	D
J05019+011	3200 ± 200	4.66 ± 0.20	3217 ± 75	4.66 ± 0.18	-0.29 ± 0.26	-0.20 ± 0.26	3207 ± 80	-0.30 ± 0.25	-0.20 ± 0.25	YD
J05019–069	3100 ± 200	5.09 ± 0.20	3284 ± 27	5.13 ± 0.13	-0.32 ± 0.13	-0.21 ± 0.13	3296 ± 26	-0.08 ± 0.04	-0.04 ± 0.04	D
J05062+046	3100 ± 200	4.68 ± 0.20	3134 ± 42	4.72 ± 0.19	0.10 ± 0.16	0.10 ± 0.16	3116 ± 38	0.10 ± 0.16	0.10 ± 0.16	YD
J05360–076	3200 ± 200	4.87 ± 0.20	3422 ± 29	4.81 ± 0.08	-0.19 ± 0.06	-0.12 ± 0.06	3384 ± 19	-0.29 ± 0.08	-0.20 ± 0.08	D
J05366+112	3200 ± 200	4.94 ± 0.20	3355 ± 23	5.17 ± 0.16	-0.29 ± 0.10	-0.20 ± 0.10	3411 ± 18	-0.04 ± 0.03	-0.02 ± 0.03	YD
J05421+124	3200 ± 200	5.01 ± 0.20	3324 ± 38	4.93 ± 0.08	-0.44 ± 0.11	-0.30 ± 0.11	3295 ± 35	-0.44 ± 0.10	-0.30 ± 0.10	TD
J06000+027	3200 ± 200	5.01 ± 0.20	3296 ± 19	5.12 ± 0.14	-0.29 ± 0.13	-0.20 ± 0.13	3323 ± 17	-0.04 ± 0.03	-0.02 ± 0.03	YD
J06246+234	3200 ± 200	5.14 ± 0.20	3249 ± 24	5.10 ± 0.09	-0.67 ± 0.10	-0.46 ± 0.10	3253 ± 21	-0.63 ± 0.09	-0.43 ± 0.09	D
J06396–210	3200 ± 200	4.94 ± 0.20	3428 ± 33	5.09 ± 0.12	-0.08 ± 0.07	-0.04 ± 0.07	3438 ± 27	-0.07 ± 0.06	-0.04 ± 0.06	D
J06574+740	3200 ± 200	4.94 ± 0.20	3173 ± 24	5.06 ± 0.13	-0.10 ± 0.06	-0.06 ± 0.06	3133 ± 11	-0.01 ± 0.01	0.00 ± 0.01	D
J07033+346	3200 ± 200	4.98 ± 0.20	3310 ± 26	5.13 ± 0.12	-0.36 ± 0.11	-0.24 ± 0.11	3386 ± 30	-0.03 ± 0.03	-0.01 ± 0.03	D
J07472+503	3200 ± 200	4.97 ± 0.20	3251 ± 59	4.92 ± 0.18	-0.14 ± 0.18	-0.08 ± 0.18	3255 ± 50	-0.20 ± 0.25	-0.13 ± 0.25	D

Table B.3. continued.

Karmn	Prior $T_{\text{eff}}$ [K]	Prior $\log g$ [dex]	$T_{\text{eff}}$ [K]	$\log g$ [dex]	[Fe/H] [dex]	[Fe/H] <sub>corr</sub> [dex]	$T_{\text{eff,fixed}}$ [K]	[Fe/H] <sub>fixed</sub> [dex]	[Fe/H] <sub>corr, fixed</sub> [dex]	Pop. <sup>(a)</sup>
J08023+033	3300 ± 200	4.86 ± 0.20	3422 ± 26	4.72 ± 0.09	-0.36 ± 0.09	-0.24 ± 0.09	3416 ± 27	-0.24 ± 0.08	-0.16 ± 0.08	TD
J08126-215	3100 ± 200	4.93 ± 0.20	3356 ± 44	4.88 ± 0.12	-0.26 ± 0.15	-0.18 ± 0.15	3334 ± 32	-0.22 ± 0.10	-0.15 ± 0.10	D
J08315+730	3300 ± 200	4.96 ± 0.20	3364 ± 42	4.90 ± 0.10	-0.30 ± 0.10	-0.20 ± 0.10	3358 ± 25	-0.32 ± 0.10	-0.21 ± 0.10	D
J09028+680	3300 ± 200	4.98 ± 0.20	3328 ± 42	4.96 ± 0.08	-0.40 ± 0.13	-0.27 ± 0.13	3317 ± 34	-0.45 ± 0.11	-0.31 ± 0.11	D
J09161+018	3200 ± 200	4.91 ± 0.20	3237 ± 60	4.84 ± 0.19	-0.13 ± 0.21	-0.08 ± 0.21	3251 ± 51	-0.09 ± 0.28	-0.05 ± 0.28	D
J09447-182	3200 ± 200	4.93 ± 0.20	3417 ± 31	4.84 ± 0.11	-0.14 ± 0.09	-0.08 ± 0.09	3390 ± 36	-0.15 ± 0.11	-0.09 ± 0.11	TD-D
J10185-117	3300 ± 200	4.83 ± 0.20	3434 ± 28	4.74 ± 0.10	-0.27 ± 0.10	-0.18 ± 0.10	3433 ± 29	-0.21 ± 0.10	-0.14 ± 0.10	D
J10504+331	3200 ± 200	4.78 ± 0.20	3441 ± 34	4.74 ± 0.07	-0.06 ± 0.06	-0.03 ± 0.06	3435 ± 33	-0.05 ± 0.06	-0.02 ± 0.06	TD
J10508+068	3200 ± 200	4.96 ± 0.20	3410 ± 42	4.92 ± 0.13	-0.14 ± 0.11	-0.08 ± 0.11	3372 ± 40	-0.25 ± 0.13	-0.17 ± 0.13	YD
J11417+427	3200 ± 200	4.84 ± 0.20	3387 ± 43	4.83 ± 0.10	-0.17 ± 0.10	-0.11 ± 0.10	3380 ± 41	-0.18 ± 0.11	-0.11 ± 0.11	YD
J11476+002	3200 ± 200	4.88 ± 0.20	3282 ± 19	5.16 ± 0.10	-0.51 ± 0.12	-0.35 ± 0.12	3229 ± 13	-0.98 ± 0.02	-0.67 ± 0.02	YD
J11477+008	3100 ± 200	5.08 ± 0.20	3325 ± 43	5.09 ± 0.14	-0.16 ± 0.13	-0.10 ± 0.13	3306 ± 41	-0.19 ± 0.14	-0.12 ± 0.14	D
J12054+695	3200 ± 200	4.91 ± 0.20	3339 ± 41	4.91 ± 0.10	-0.10 ± 0.11	-0.06 ± 0.11	3332 ± 34	-0.11 ± 0.09	-0.06 ± 0.09	YD
J12156+526	3300 ± 200	4.69 ± 0.20	3360 ± 43	4.65 ± 0.17	-0.28 ± 0.14	-0.19 ± 0.14	3384 ± 39	-0.19 ± 0.14	-0.12 ± 0.14	D
J12373-208	3200 ± 200	4.77 ± 0.20	3431 ± 36	4.70 ± 0.10	-0.06 ± 0.07	-0.03 ± 0.07	3434 ± 34	0.03 ± 0.05	0.03 ± 0.05	D
J12428+418	3200 ± 200	4.82 ± 0.20	3328 ± 25	5.05 ± 0.14	-0.14 ± 0.09	-0.08 ± 0.09	3250 ± 14	-0.07 ± 0.07	-0.04 ± 0.07	YD
J13229+244	3200 ± 200	4.95 ± 0.20	3327 ± 44	4.93 ± 0.09	-0.44 ± 0.13	-0.30 ± 0.13	3331 ± 37	-0.36 ± 0.10	-0.24 ± 0.10	D
J13536+776	3200 ± 200	4.94 ± 0.20	3198 ± 83	4.94 ± 0.21	-0.01 ± 0.30	0.00 ± 0.30	3192 ± 80	-0.01 ± 0.25	0.00 ± 0.25	D
J13591-198	3100 ± 200	4.95 ± 0.20	3261 ± 20	5.12 ± 0.10	-0.22 ± 0.07	-0.15 ± 0.07	3292 ± 16	-0.04 ± 0.03	-0.02 ± 0.03	YD
J14342-125	3100 ± 200	4.89 ± 0.20	3347 ± 50	4.76 ± 0.13	-0.26 ± 0.15	-0.18 ± 0.15	3330 ± 35	-0.22 ± 0.13	-0.15 ± 0.13	D
J15369-141	3200 ± 200	4.89 ± 0.20	3428 ± 33	4.75 ± 0.08	-0.11 ± 0.07	-0.06 ± 0.07	3400 ± 36	-0.10 ± 0.10	-0.06 ± 0.10	D
J16028+205	3200 ± 200	4.98 ± 0.20	3362 ± 34	4.97 ± 0.10	-0.16 ± 0.12	-0.10 ± 0.12	3346 ± 39	-0.19 ± 0.11	-0.12 ± 0.11	TD-D
J17542+073	3200 ± 200	4.92 ± 0.20	3312 ± 30	4.86 ± 0.08	-0.19 ± 0.09	-0.12 ± 0.09	3289 ± 31	-0.39 ± 0.12	-0.26 ± 0.12	D
J18131+260	3200 ± 200	4.89 ± 0.20	3271 ± 63	4.83 ± 0.16	-0.52 ± 0.13	-0.36 ± 0.13	3268 ± 53	-0.54 ± 0.13	-0.37 ± 0.13	D
J18221+063	3400 ± 200	4.96 ± 0.20	3397 ± 28	4.89 ± 0.09	-0.50 ± 0.11	-0.35 ± 0.11	3388 ± 25	-0.53 ± 0.09	-0.36 ± 0.09	TD
J18224+620	3100 ± 200	5.13 ± 0.20	3294 ± 43	5.12 ± 0.15	-0.10 ± 0.11	-0.06 ± 0.11	3278 ± 37	-0.26 ± 0.18	-0.18 ± 0.18	D
J18363+136	3200 ± 200	4.94 ± 0.20	3335 ± 28	5.18 ± 0.12	-0.15 ± 0.08	-0.09 ± 0.08	3398 ± 37	-0.04 ± 0.03	-0.02 ± 0.03	YD
J19206+73.1S	3200 ± 200	4.94 ± 0.20	3448 ± 77	4.82 ± 0.16	-0.11 ± 0.12	-0.06 ± 0.12	3447 ± 98	-0.06 ± 0.14	-0.03 ± 0.14	D
J19511+464	3200 ± 200	4.98 ± 0.20	3177 ± 39	5.00 ± 0.15	0.16 ± 0.19	0.16 ± 0.19	3213 ± 34	0.10 ± 0.14	0.10 ± 0.14	YD
J20336+617	3200 ± 200	4.80 ± 0.20	3406 ± 32	4.76 ± 0.14	-0.16 ± 0.12	-0.10 ± 0.12	3401 ± 32	-0.05 ± 0.09	-0.02 ± 0.09	D
J20525-169	3100 ± 200	4.97 ± 0.20	3382 ± 40	5.01 ± 0.12	-0.07 ± 0.09	-0.04 ± 0.09	3374 ± 41	-0.07 ± 0.08	-0.04 ± 0.08	D
J21463+382	3300 ± 200	5.10 ± 0.20	3247 ± 21	4.84 ± 0.11	-0.86 ± 0.09	-0.59 ± 0.09	3265 ± 27	-0.69 ± 0.10	-0.47 ± 0.10	TD
J21466-001	3200 ± 200	4.94 ± 0.20	3408 ± 29	4.82 ± 0.09	-0.21 ± 0.08	-0.14 ± 0.08	3381 ± 28	-0.20 ± 0.10	-0.13 ± 0.10	D
J21466+668	3200 ± 200	4.91 ± 0.20	3409 ± 38	4.85 ± 0.11	-0.15 ± 0.11	-0.09 ± 0.11	3396 ± 38	-0.20 ± 0.13	-0.13 ± 0.13	YD
J22012+283	3200 ± 200	4.92 ± 0.20	3195 ± 29	5.00 ± 0.16	0.03 ± 0.11	0.03 ± 0.11	3195 ± 29	0.00 ± 0.10	0.00 ± 0.10	YD
J22252+594	3200 ± 200	4.77 ± 0.20	3448 ± 40	4.76 ± 0.10	-0.06 ± 0.08	-0.03 ± 0.08	3446 ± 41	-0.04 ± 0.06	-0.02 ± 0.06	D
J22298+414	3200 ± 200	4.98 ± 0.20	3332 ± 32	4.88 ± 0.07	-0.26 ± 0.10	-0.18 ± 0.10	3314 ± 25	-0.30 ± 0.11	-0.20 ± 0.11	D
J22532-142	3200 ± 200	4.87 ± 0.20	3421 ± 40	4.83 ± 0.10	-0.11 ± 0.10	-0.06 ± 0.10	3409 ± 40	-0.17 ± 0.12	-0.11 ± 0.12	YD
J23216+172	3200 ± 200	4.81 ± 0.20	3398 ± 47	4.81 ± 0.11	-0.03 ± 0.10	-0.01 ± 0.10	3399 ± 39	-0.03 ± 0.08	-0.01 ± 0.08	D
J23431+365	3100 ± 200	5.01 ± 0.20	3301 ± 30	5.18 ± 0.12	-0.16 ± 0.10	-0.10 ± 0.10	3295 ± 26	-0.06 ± 0.06	-0.03 ± 0.06	YD
J23505-095	3100 ± 200	4.88 ± 0.20	3377 ± 34	4.83 ± 0.10	-0.14 ± 0.10	-0.08 ± 0.10	3366 ± 37	-0.10 ± 0.09	-0.06 ± 0.09	D
J23548+385	3200 ± 200	4.91 ± 0.20	3263 ± 16	5.13 ± 0.10	-0.81 ± 0.09	-0.55 ± 0.09	3265 ± 19	-0.91 ± 0.07	-0.62 ± 0.07	D

Table B.3. continued.

Karmn	Prior $T_{\text{eff}}$ [K]	Prior $\log g$ [dex]	$T_{\text{eff}}$ [K]	$\log g$ [dex]	[Fe/H] [dex]	[Fe/H] <sub>corr</sub> [dex]	$T_{\text{eff,fixed}}$ [K]	[Fe/H] <sub>fixed</sub> [dex]	[Fe/H] <sub>corr, fixed</sub> [dex]	Pop. <sup>(a)</sup>
M4.5 V										
J01125-169	3100 ± 200	5.18 ± 0.20	3228 ± 46	5.24 ± 0.16	-0.57 ± 0.20	-0.39 ± 0.20	3225 ± 43	-0.65 ± 0.22	-0.44 ± 0.22	D
J04153-076	3100 ± 200	4.98 ± 0.20	3179 ± 61	5.00 ± 0.18	-0.44 ± 0.17	-0.30 ± 0.17	3180 ± 69	-0.41 ± 0.18	-0.28 ± 0.18	TD-D
J07446+035	3100 ± 200	4.87 ± 0.20	3251 ± 34	5.11 ± 0.14	-0.57 ± 0.24	-0.39 ± 0.24	3248 ± 36	-0.63 ± 0.17	-0.43 ± 0.17	YD
J07558+833	3200 ± 200	4.98 ± 0.20	3252 ± 55	4.80 ± 0.19	-0.36 ± 0.21	-0.24 ± 0.21	3253 ± 50	-0.23 ± 0.19	-0.15 ± 0.19	YD
J08119+087	3200 ± 200	5.17 ± 0.20	3245 ± 23	5.24 ± 0.08	-0.72 ± 0.09	-0.49 ± 0.09	3225 ± 16	-0.80 ± 0.07	-0.55 ± 0.07	TD
J08526+283	3100 ± 200	4.94 ± 0.20	3321 ± 37	4.87 ± 0.08	-0.16 ± 0.11	-0.10 ± 0.11	3308 ± 39	-0.24 ± 0.12	-0.16 ± 0.12	YD
J09005+465	3100 ± 200	5.04 ± 0.20	3293 ± 30	5.16 ± 0.14	-0.06 ± 0.08	-0.03 ± 0.08	3286 ± 32	-0.12 ± 0.12	-0.07 ± 0.12	YD
J10416+376	3200 ± 200	5.05 ± 0.20	3298 ± 27	4.87 ± 0.08	-0.29 ± 0.12	-0.20 ± 0.12	3272 ± 31	-0.38 ± 0.14	-0.25 ± 0.14	D
J11509+483	3100 ± 200	5.11 ± 0.20	3282 ± 38	5.09 ± 0.09	-0.19 ± 0.10	-0.12 ± 0.10	3277 ± 41	-0.25 ± 0.15	-0.17 ± 0.15	D
J13005+056	3000 ± 200	5.06 ± 0.20	3158 ± 38	4.70 ± 0.12	-0.53 ± 0.11	-0.36 ± 0.11	3140 ± 39	-0.07 ± 0.17	-0.04 ± 0.17	D
J17033+514	3000 ± 200	5.04 ± 0.20	3273 ± 32	4.92 ± 0.14	-0.19 ± 0.17	-0.12 ± 0.17	3249 ± 33	-0.30 ± 0.18	-0.20 ± 0.18	D
J18075-159	3000 ± 200	5.10 ± 0.20	3220 ± 22	5.23 ± 0.11	-0.54 ± 0.13	-0.37 ± 0.13	3192 ± 19	-0.78 ± 0.06	-0.54 ± 0.06	D
J18189+661	3100 ± 200	5.17 ± 0.20	3172 ± 45	4.97 ± 0.15	-0.68 ± 0.16	-0.46 ± 0.16	3146 ± 44	-0.66 ± 0.19	-0.45 ± 0.19	D
J19098+176	3100 ± 200	5.07 ± 0.20	3277 ± 34	4.93 ± 0.13	-0.21 ± 0.16	-0.14 ± 0.16	3281 ± 53	-0.18 ± 0.19	-0.11 ± 0.19	D
J19216+208	3100 ± 200	5.05 ± 0.20	3278 ± 35	5.05 ± 0.12	-0.25 ± 0.13	-0.17 ± 0.13	3279 ± 35	-0.26 ± 0.12	-0.18 ± 0.12	D
J20405+154	3100 ± 200	5.07 ± 0.20	3263 ± 36	5.02 ± 0.12	-0.16 ± 0.11	-0.10 ± 0.11	3281 ± 37	-0.18 ± 0.15	-0.11 ± 0.15	D
J22137-176	3100 ± 200	5.09 ± 0.20	3256 ± 41	5.00 ± 0.10	-0.41 ± 0.16	-0.28 ± 0.16	3262 ± 41	-0.40 ± 0.14	-0.27 ± 0.14	D
J22231-176	3000 ± 200	5.08 ± 0.20	3228 ± 19	5.26 ± 0.13	-0.19 ± 0.10	-0.12 ± 0.14	3231 ± 19	-0.15 ± 0.10	-0.09 ± 0.10	D
M5.0 V										
J01019+541	2900 ± 200	5.15 ± 0.20	3070 ± 13	5.12 ± 0.03	-0.30 ± 0.06	-0.20 ± 0.06	3072 ± 15	-0.34 ± 0.04	-0.23 ± 0.04	D
J01033+623	3000 ± 200	5.02 ± 0.20	3057 ± 49	5.12 ± 0.18	-0.36 ± 0.24	-0.24 ± 0.24	3045 ± 58	-0.37 ± 0.13	-0.25 ± 0.13	YD
J01048-181	3000 ± 200	5.16 ± 0.20	3209 ± 41	5.09 ± 0.14	-0.16 ± 0.17	-0.10 ± 0.17	3200 ± 33	-0.22 ± 0.17	-0.15 ± 0.17	D
J03133+047	3000 ± 200	5.11 ± 0.20	3214 ± 40	5.06 ± 0.16	-0.10 ± 0.17	-0.06 ± 0.17	3208 ± 39	-0.21 ± 0.15	-0.14 ± 0.15	D
J04472+206	3000 ± 200	4.82 ± 0.20	3096 ± 14	5.12 ± 0.07	-0.11 ± 0.04	-0.06 ± 0.04	3075 ± 12	-0.59 ± 0.04	-0.40 ± 0.04	YD
J05084-210	3000 ± 200	4.59 ± 0.20	3233 ± 22	4.52 ± 0.10	-0.55 ± 0.07	-0.38 ± 0.07	3244 ± 19	-0.52 ± 0.06	-0.36 ± 0.06	YD
J06024+498	3000 ± 200	5.17 ± 0.20	3213 ± 35	5.17 ± 0.14	-0.15 ± 0.13	-0.09 ± 0.13	3201 ± 32	-0.20 ± 0.14	-0.13 ± 0.14	YD
J06318+414	3000 ± 200	4.81 ± 0.20	3084 ± 13	4.88 ± 0.07	-0.06 ± 0.05	-0.03 ± 0.05	3026 ± 12	-0.14 ± 0.05	-0.08 ± 0.05	YD
J06594+193	2800 ± 200	5.17 ± 0.20	3146 ± 38	5.09 ± 0.17	-0.16 ± 0.19	-0.10 ± 0.19	3158 ± 33	-0.10 ± 0.22	-0.06 ± 0.22	D
J09449-123	2900 ± 200	4.86 ± 0.20	3068 ± 15	5.05 ± 0.05	-0.21 ± 0.07	-0.14 ± 0.07	3032 ± 13	-0.22 ± 0.06	-0.15 ± 0.06	YD
J10584-107	3100 ± 200	5.07 ± 0.20	3218 ± 23	5.23 ± 0.11	-0.45 ± 0.17	-0.31 ± 0.17	3200 ± 39	-0.55 ± 0.15	-0.38 ± 0.15	YD
J11474+667	3000 ± 200	4.91 ± 0.20	3219 ± 35	4.98 ± 0.18	-0.62 ± 0.19	-0.42 ± 0.19	3211 ± 37	-0.73 ± 0.20	-0.50 ± 0.20	YD
J12189+111	2900 ± 200	5.14 ± 0.20	3064 ± 32	5.06 ± 0.17	-0.40 ± 0.22	-0.27 ± 0.22	3079 ± 28	-0.40 ± 0.19	-0.27 ± 0.19	YD
J13102+477	3000 ± 200	5.11 ± 0.20	3221 ± 21	5.25 ± 0.12	-0.37 ± 0.13	-0.25 ± 0.13	3226 ± 35	-0.34 ± 0.18	-0.23 ± 0.18	D
J14173+454	3100 ± 200	4.94 ± 0.20	3222 ± 24	5.19 ± 0.07	-0.74 ± 0.07	-0.51 ± 0.07	3150 ± 28	-0.10 ± 0.07	-0.06 ± 0.07	D
J15499+796	3000 ± 200	4.93 ± 0.20	3095 ± 15	5.07 ± 0.09	-0.25 ± 0.09	-0.17 ± 0.09	3066 ± 17	-0.20 ± 0.14	-0.13 ± 0.14	YD
J16313+408	2900 ± 200	5.10 ± 0.20	3170 ± 42	4.86 ± 0.13	-0.69 ± 0.11	-0.47 ± 0.11	3298 ± 49	-0.73 ± 0.12	-0.50 ± 0.12	YD
J18022+642	3000 ± 200	5.09 ± 0.20	3213 ± 43	5.15 ± 0.12	-0.67 ± 0.15	-0.46 ± 0.15	3198 ± 37	-0.69 ± 0.12	-0.47 ± 0.12	D
J18027+375	3000 ± 200	5.15 ± 0.20	3210 ± 39	5.02 ± 0.18	-0.08 ± 0.17	-0.04 ± 0.17	3186 ± 27	-0.22 ± 0.21	-0.15 ± 0.21	D
J18165+048	3000 ± 200	5.07 ± 0.20	3240 ± 36	4.97 ± 0.13	-0.26 ± 0.14	-0.18 ± 0.14	3258 ± 38	-0.22 ± 0.22	-0.15 ± 0.22	D
J18482+076	2900 ± 200	5.14 ± 0.20	3175 ± 39	5.10 ± 0.16	-0.19 ± 0.13	-0.12 ± 0.13	3169 ± 32	-0.14 ± 0.14	-0.08 ± 0.14	YD
J19422-207	3100 ± 200	5.04 ± 0.20	3241 ± 54	4.81 ± 0.15	-0.71 ± 0.10	-0.49 ± 0.10	3341 ± 41	-0.77 ± 0.09	-0.53 ± 0.09	YD

Table B.3. continued.

Karmen	Prior $T_{\text{eff}}$ [K]	Prior $\log g$ [dex]	$T_{\text{eff}}$ [K]	$\log g$ [dex]	[Fe/H] [dex]	[Fe/H] <sub>corr</sub> [dex]	$T_{\text{eff, fixed}}$ [K]	[Fe/H] <sub>fixed</sub> [dex]	[Fe/H] <sub>corr, fixed</sub> [dex]	Pop. <sup>(a)</sup>
J20093-012	3000 ± 200	5.12 ± 0.20	3301 ± 90	4.96 ± 0.17	-0.74 ± 0.15	-0.51 ± 0.15	3388 ± 79	-0.80 ± 0.13	-0.55 ± 0.13	D
J20260+585	3000 ± 200	5.11 ± 0.20	3223 ± 49	4.97 ± 0.15	-0.23 ± 0.24	-0.15 ± 0.24	3216 ± 47	-0.16 ± 0.23	-0.10 ± 0.23	D
J20556-140S	3100 ± 200	5.16 ± 0.20	3193 ± 23	4.98 ± 0.10	-0.53 ± 0.11	-0.36 ± 0.11	3205 ± 21	-0.45 ± 0.08	-0.31 ± 0.08	TD
J23419+441	3000 ± 200	5.16 ± 0.20	3186 ± 41	5.15 ± 0.18	0.04 ± 0.17	0.04 ± 0.17	3175 ± 36	0.01 ± 0.16	0.01 ± 0.16	TD-D
M5.5V										
J00067-075	2900 ± 200	5.22 ± 0.20	3169 ± 53	5.20 ± 0.16	-0.22 ± 0.22	-0.15 ± 0.22	3137 ± 36	-0.37 ± 0.18	-0.25 ± 0.18	D
J08413+594	3000 ± 200	5.23 ± 0.20	3141 ± 38	5.28 ± 0.17	-0.12 ± 0.16	-0.07 ± 0.16	3124 ± 35	-0.14 ± 0.15	-0.08 ± 0.15	D
J11055+435	2900 ± 200	5.29 ± 0.20	3278 ± 86	5.25 ± 0.20	-0.52 ± 0.25	-0.36 ± 0.25	3167 ± 56	-0.63 ± 0.21	-0.43 ± 0.21	TD-D
J15305+094	3000 ± 200	5.26 ± 0.20	3073 ± 15	5.16 ± 0.05	-0.43 ± 0.08	-0.29 ± 0.08	3085 ± 13	-0.39 ± 0.08	-0.26 ± 0.08	D
J17338+169	2900 ± 200	4.86 ± 0.20	3048 ± 11	4.95 ± 0.13	-0.05 ± 0.06	-0.02 ± 0.06	3017 ± 10	-0.09 ± 0.05	-0.05 ± 0.05	YD
J22114+409	3000 ± 200	5.14 ± 0.20	3132 ± 30	5.15 ± 0.16	-0.07 ± 0.12	-0.04 ± 0.12	3145 ± 27	-0.12 ± 0.14	-0.07 ± 0.14	YD
J23351-023	3000 ± 200	5.25 ± 0.20	3136 ± 38	5.27 ± 0.17	-0.20 ± 0.17	-0.13 ± 0.17	3149 ± 40	-0.22 ± 0.18	-0.15 ± 0.18	D
M6.0V										
J07403-174	2800 ± 200	5.29 ± 0.20	3031 ± 26	5.03 ± 0.17	0.04 ± 0.18	0.04 ± 0.18	3050 ± 22	0.20 ± 0.11	0.20 ± 0.11	D
J10564+070	2800 ± 200	5.23 ± 0.20	3071 ± 24	5.25 ± 0.18	-0.09 ± 0.20	-0.05 ± 0.20	3060 ± 18	-0.15 ± 0.18	-0.09 ± 0.18	D
J14321+081	2800 ± 200	5.14 ± 0.20	3161 ± 86	5.04 ± 0.21	-0.13 ± 0.32	-0.08 ± 0.32	3187 ± 77	-0.17 ± 0.25	-0.11 ± 0.25	YD
M6.5V										
J08298+267	2700 ± 200	5.28 ± 0.20	2997 ± 49	5.16 ± 0.18	0.01 ± 0.19	0.01 ± 0.19	3054 ± 30	-0.16 ± 0.16	-0.10 ± 0.16	YD
J09003+218	2700 ± 200	5.28 ± 0.20	3061 ± 43	5.17 ± 0.21	-0.02 ± 0.18	0.00 ± 0.18	3088 ± 36	-0.10 ± 0.15	-0.06 ± 0.15	YD
J10482-113	2700 ± 200	5.30 ± 0.20	3029 ± 25	5.33 ± 0.16	-0.13 ± 0.17	-0.08 ± 0.17	3032 ± 19	-0.19 ± 0.16	-0.12 ± 0.16	D
M7.0V										
J02530+168	2800 ± 200	5.31 ± 0.20	3034 ± 45	5.19 ± 0.20	-0.17 ± 0.28	-0.11 ± 0.28	3031 ± 34	0.01 ± 0.25	0.01 ± 0.25	TD
J09033+056	2800 ± 200	5.14 ± 0.20	3027 ± 19	5.09 ± 0.12	-0.38 ± 0.12	-0.25 ± 0.12	3001 ± 18	-0.21 ± 0.10	-0.14 ± 0.10	D
J16555-083	2600 ± 200	5.29 ± 0.20	3005 ± 21	5.25 ± 0.18	-0.08 ± 0.09	-0.04 ± 0.09	2989 ± 20	0.00 ± 0.11	0.00 ± 0.11	D
M8.0V										
J05394+406	2500 ± 200	5.27 ± 0.20	...	...	...	...	...	...	...	D
J19169+051S	2500 ± 200	5.29 ± 0.20	...	...	...	...	...	...	...	D
J19255+096	2400 ± 200	5.12 ± 0.20	...	...	...	...	...	...	...	YD
J23064-050	2500 ± 200	5.29 ± 0.20	...	...	...	...	...	...	...	D
M8.5V										
J04198+425	2400 ± 200	5.29 ± 0.20	...	...	...	...	...	...	...	D
J18356+329	2400 ± 200	5.36 ± 0.20	...	...	...	...	...	...	...	D
M9.0V										
J08536-034	2300 ± 200	5.33 ± 0.20	...	...	...	...	...	...	...	D

**Notes.** <sup>(a)</sup>Galactic populations, including the thick disc (TD), the thin disc (D), and the young disc (YD) ([Cortés-Contreras et al. in prep.](#)).